

Fall 2003

A three-level finite difference scheme for solving a dual-phase-lagging heat transport equation in spherical coordinates

Lixin Shen

Follow this and additional works at: <https://digitalcommons.latech.edu/dissertations>

Recommended Citation

Shen, Lixin, "" (2003). *Dissertation*. 663.
<https://digitalcommons.latech.edu/dissertations/663>

This Dissertation is brought to you for free and open access by the Graduate School at Louisiana Tech Digital Commons. It has been accepted for inclusion in Doctoral Dissertations by an authorized administrator of Louisiana Tech Digital Commons. For more information, please contact digitalcommons@latech.edu.

A THREE-LEVEL FINITE DIFFERENCE SCHEME FOR SOLVING A DUAL-
PHASE-LAGGING HEAT TRANSPORT EQUATION IN SPHERICAL
COORDINATES

by

Lixin Shen, B.S., M.S.

A Dissertation Presented in Partial Fulfillment
of the Requirements for the Degree
Doctor of Philosophy

COLLEGE OF ENGINEERING AND SCIENCE
LOUISIANA TECH UNIVERSITY

November 2003

UMI Number: 3103616

UMI[®]

UMI Microform 3103616

Copyright 2003 by ProQuest Information and Learning Company.

All rights reserved. This microform edition is protected against
unauthorized copying under Title 17, United States Code.

ProQuest Information and Learning Company
300 North Zeeb Road
P.O. Box 1346
Ann Arbor, MI 48106-1346

LOUISIANA TECH UNIVERSITY

THE GRADUATE SCHOOL

10/23/2003

Date

We hereby recommend that the dissertation prepared under our supervision
by Lixin Shen

entitled A Three-Level Finite Difference Scheme for Solving a Dual-Phase-Lagging Heat Transport
Equation in Spherical Coordinates

be accepted in partial fulfillment of the requirements for the Degree of
Doctor of Philosophy in Computational Analysis and Modeling

Weizhong Dai

Supervisor of Dissertation Research

Richard T. Greechie

Head of Department

Department

Recommendation concurred in:

Weizhong Dai

Raja Kumar

[Signature]

Lixin Shen

Advisory Committee

Approved:

Paul S. Sastry

Director of Graduate Studies

Stan Koppa

Dean of the College

Approved:

William M. McLaughlin

Dean of the Graduate School

GS Form 13
(5/03)

ABSTRACT

Heat transport through thin films or micro-objects is of vital importance in microtechnology applications. For instance, metal thin films are important components of microelectronic devices. The reduction of the device size to microscale has the advantage of enhancing the switching speed of the device. On the other hand, size reduction increases the rate of heat generation, which leads to a high thermal load on the microelectronic devices. Heat transfer at the microscale is also important for the thermal processing of materials with a pulsed-laser. Examples in metal processing are laser micromachining, laser patterning, laser processing of diamond films from carbon ion implanted copper substrates, and laser surface hardening. In thermal processing of materials, microvoids may be found owing to thermal expansion. When such defects begin in the workpiece, their thermal energy in the neighborhood of the defects may be amplified, resulting in severe material damage and, consequently, total failure of the thermal processing. A detailed understanding of the way in which the local defects dissipate the thermal energy is then necessary not only to avoid the damage but also to improve the efficiency of the thermal processing.

The heat transport equation at the microscale is different from the traditional heat diffusion equation because a second-order derivative of temperature with respect to time and a third-order mixed derivative of temperature with respect to space and time are introduced. In this study, we consider the heat transport equation in three-dimensional

spherical coordinates and develop a three-level finite difference scheme for solving the heat transport equation in a microsphere. Stability of the scheme is proved in this dissertation. It is shown that the scheme is unconditionally stable. The scheme is then employed to investigate the temperature rise in a gold sphere subjected to a short-pulse laser. Numerical results are obtained for the cases that the laser irradiation is symmetric on the surface of the sphere, and the laser irradiation is from the top to a portion of the surface of the sphere.

APPROVAL FOR SCHOLARLY DISSEMINATION

The author grants to the Prescott Memorial Library of Louisiana Tech University the right to reproduce, by appropriate methods, upon request, any or all portions of this Dissertation. It is understood that "proper request" consists of the agreement, on the part of the requesting party, that said reproduction is for his personal use and that subsequent reproduction will not occur without written approval of the author of this Dissertation. Further, any portions of the Dissertation used in books, papers, and other works must be appropriately referenced to this Dissertation.

Finally, the author of this Dissertation reserves the right to publish freely, in the literature, at any time, any or all portions of this Dissertation.

Author *Lixin Shen*

Date *Oct. 23, 2003*

TABLE OF CONTENTS

LIST OF TABLES	viii
LIST OF FIGURES	ix
NOMENCLATURE	xii
ACKNOWLEDGMENTS	xvi
CHAPTER 1 INTRODUCTION	1
1.1 Overview	1
1.2 Objective of the Research	2
1.3 Organization of the Dissertation	3
CHAPTER 2 BACKGROUND AND PREVIOUS WORK.....	4
2.1 Microscale Heat Transfer Model	4
2.1.1 Microscale Heat Conduction	5
2.1.2 Phonon-Electron Interaction Model	10
2.2 Dual-Phase-Lagging Behavior	19
2.2.1 Phase-Lag Concept	20
2.2.2 Internal Mechanisms	24
2.2.3 Temperature Formulation	25
2.2.4 Heat Flux Formulation	29
2.3 Previous Work	31
CHAPTER 3 MATHEMATICAL MODEL AND FINITE DIFFERENCE SCHEME..	38
3.1 Governing Equations	38
3.1.1 Problem Description	38
3.1.2 Three-Dimensional Spherical Coordinates	38
3.1.3 Governing Equations	39
3.2 Finite Difference Scheme	40
3.2.1 Notations	40
3.2.2 Finite Difference Scheme	41
3.3 Stability	42
3.4 Algorithms	49
3.4.1 Solving the Linear System	49

3.4.2	Algorithms	52
CHAPTER 4	NUMERICAL EXAMPLES	55
4.1	Description of the Examples	55
4.2	Example with Symmetric Heating	56
4.2.1	Heat Source	56
4.2.2	Result Analysis	57
4.3	Example with Semi Sphere Heating	66
4.3.1	Heat Source	66
4.3.2	Result Analysis	67
4.4	Example with Portion Heating	76
4.4.1	Heat Source	76
4.4.2	Result Analysis	77
CHAPTER 5	CONCLUSION	86
APPENDIX	SOURCE CODE OF THE FINITE DIFFERENCE SCHEME	88
REFERENCES	101

LIST OF TABLES

Table 2.1	Phonon-electron coupling factor G for some noble and transition metals [Qiu 1992]	13
Table 2.2	The equivalent thermal diffusivity (α_E), the equivalent thermal wave speed (C_E), and the phase lags of the temperature gradient and the heat flux vector (τ_T and τ_q) for typical metals ($C_e = 2.1 \times 10^4 J/m^3K$ at room temperature; ps \equiv picosecond) [Tzou 1996]	17
Table 4.1	Thermal property parameters of gold [Tzou 1996]	55

LIST OF FIGURES

Figure 2.1	Energy transport through phonon collision.....	5
Figure 2.2	Phonon interaction in a thin film of the same order of magnitude as the mean free path, illustrating the challenge of the microscale effect in space to the concept of temperature gradient	8
Figure 2.3	Transient reflectivity change at the front surface of gold films (thickness 0.05 and 0.1 μm) subjected to laser irradiation (pulse width 96 fs, energy flux 1 mJ/cm^2) [Qiu 1992] [Brorson 1987].....	15
Figure 2.4	Transient reflectivity change at the rear surface of gold films (thickness 0.05 and 0.1 μm) subjected to laser irradiation (pulse width 96 fs, energy flux 1 mJ/cm^2). [Qiu 1992] [Brorson 1987].....	16
Figure 2.5	The finite time required for the phonon-electron interaction in microscale. (a) The first stage of electron-gas heating by phonons and (b) the second stage of metal lattice heating by phonon-electron interactions.....	24
Figure 3.1	The three-dimensional spherical coordinates.....	39
Figure 4.1	The gold sphere subjected to short-pulse laser irradiation on the surface ($r = L$, $0 \leq \theta \leq \pi$, $0 \leq \varphi \leq 2\pi$) symmetrically.....	56
Figure 4.2	Temperature change with time at the surface of the sphere subjected to symmetric pulse laser irradiation.....	59
Figure 4.3	Contours of temperature distribution in the $r\theta$ cross-section of the sphere subjected to symmetric pulse laser irradiation on the surface when $t = 0.2 ps$	60
Figure 4.4	Contours of temperature distribution in the $r\theta$ cross-section of the sphere subjected to symmetric pulse laser irradiation on the surface when $t = 0.25 ps$	61
Figure 4.5	Contours of temperature distribution in the $r\theta$ cross-section of the sphere subjected to symmetric pulse laser irradiation on the surface when $t = 0.5 ps$	62

Figure 4.6	Contours of temperature distribution in the $r\theta$ cross-section of the sphere subjected to symmetric pulse laser irradiation on the surface when $t = 1.0 \text{ ps}$	63
Figure 4.7	Contours of temperature distribution in the $r\theta$ cross-section of the sphere subjected to symmetric pulse laser irradiation on the surface when $t = 2.0 \text{ ps}$	64
Figure 4.8	Temperature change along r -axis ($\theta = 0$ and π) of the sphere subjected to symmetric pulse laser irradiation on the surface	65
Figure 4.9	The gold sphere subjected to short-pulse laser irradiation on the top half of the surface ($r = L$, $0 \leq \theta \leq \frac{\pi}{2}$, $0 \leq \varphi \leq 2\pi$) in parallel	66
Figure 4.10	Temperature change with time at the top point of the sphere subjected to parallel pulse laser irradiation on the top half of the surface	69
Figure 4.11	Contours of temperature distribution in the $r\theta$ cross-section of the sphere subjected to parallel pulse laser irradiation on the top half of the surface when $t = 0.2 \text{ ps}$	70
Figure 4.12	Contours of temperature distribution in the $r\theta$ cross-section of the sphere subjected to parallel pulse laser irradiation on the top half of the surface when $t = 0.25 \text{ ps}$	71
Figure 4.13	Contours of temperature distribution in the $r\theta$ cross-section of the sphere subjected to parallel pulse laser irradiation on the top half of the surface when $t = 0.5 \text{ ps}$	72
Figure 4.14	Contours of temperature distribution in the $r\theta$ cross-section of the sphere subjected to parallel pulse laser irradiation on the top half of the surface when $t = 1.0 \text{ ps}$	73
Figure 4.15	Contours of temperature distribution in the $r\theta$ cross-section of the sphere subjected to parallel pulse laser irradiation on the top half of the surface when $t = 2.0 \text{ ps}$	74
Figure 4.16	Temperature change along r -axis ($\theta = 0$ and π) of the sphere subjected to parallel pulse laser irradiation on the top half of the surface	75

Figure 4.17	The gold sphere subjected to short-pulse laser irradiation on a portion of the surface ($r = L, 0 \leq \theta \leq \frac{\pi}{4}, 0 \leq \varphi \leq 2\pi$) in parallel.....	76
Figure 4.18	Temperature change with time at the top point of the sphere subjected to parallel pulse laser irradiation on a portion of the surface	79
Figure 4.19	Contours of temperature distribution in the $r\theta$ cross-section of the sphere subjected to parallel pulse laser irradiation on a portion of the surface when $t = 0.2 ps$	80
Figure 4.20	Contours of temperature distribution in the $r\theta$ cross-section of the sphere subjected to parallel pulse laser irradiation on a portion of the surface when $t = 0.25 ps$	81
Figure 4.21	Contours of temperature distribution in the $r\theta$ cross-section of the sphere subjected to parallel pulse laser irradiation on a portion of the surface when $t = 0.5 ps$	82
Figure 4.22	Contours of temperature distribution in the $r\theta$ cross-section of the sphere subjected to parallel pulse laser irradiation on a portion of the surface when $t = 1.0 ps$	83
Figure 4.23	Contours of temperature distribution in the $r\theta$ cross-section of the sphere subjected to parallel pulse laser irradiation on a portion of the surface when $t = 2.0 ps$	84
Figure 4.24	Temperature change along r -axis ($\theta = 0$ and π) of the sphere subjected to parallel pulse laser irradiation on a portion of the surface.....	85

NOMENCLATURE

A	constant coefficient
B	constant coefficient
C	constant coefficient
	thermal wave speed, m/s
$C_{(e,l)}$	volumetric heat capacity of electron gas (e) and metal lattice (l), $J/m^3 K$
C_p	volumetric heat capacity, $J/m^3 K$
d_i	$i = 1,2,3$. Distance traveled by phonons or electrons, nm
E	phonon/electron energy, J
$E^{\frac{1}{2}}$	finite difference operator
G	electron phonon coupling factor, $W/m^3 K$
H	constant coefficient
h	Planck constant, Js
J	laser influence, J/m^2
K	thermal conductivity of the electron gas, $W/m K$
	thermal conductivity, $W/m K$
k	thermal conductivity, $W/m K$
L	the length of radius of the sphere, μm
l	effective mean free path in phonon collision, μm

m_e	electron mass, kg
N	number of grid points
n_a	atomic number density per unit volume, $1/m^3$
n_e	number density of electrons per unit volume, $1/m^3$
P	finite difference operators
Q	volumetric heat source, W/m^2
q	heat flux, W/m^2
R	reflectivity
r	spherical coordinate position, μm
T	absolute temperature, K
T_∞	temperature
t	physical time, s
t_0	physical time, s
t_i	$i = 1,2,3$. Travel times of phonons or electrons in successive collision
t_p	laser pulse duration, fs
$u_{i,j,k}^n$	mesh function where n is the time level and i, j, k is the grid point
v_s	speed of sound, m/s

Greek Symbols

α	thermal diffusivity, m/s^2
Δr	grid size
ΔT	temperature change
Δt	time increment

$\Delta\varphi$	grid size
$\Delta\theta$	grid size
δ	penetration depth, <i>nm</i>
φ	spherical coordinate
ϕ	heat flux potential, <i>W/m</i>
η	heat flux vector
κ	Boltzmann constant, <i>J/K</i>
ν	vibration frequency of metal lattice, <i>1/s</i>
θ	spherical coordinate
ρ	mass density, <i>kg/m³</i>
τ	mean free time or relaxation time, <i>s</i>
τ_q	time lag of the heat flux
τ_T	time lag of the temperature gradient
∇_r	first order forward finite difference
$\nabla_{\bar{r}}$	first order backward finite difference
∇_θ	first order forward finite difference
$\nabla_{\bar{\theta}}$	first order backward finite difference
∇_φ	first order forward finite difference
$\nabla_{\bar{\varphi}}$	first order backward finite difference

Subscripts and Superscripts

0	initial value at $t = 0$
<i>a</i>	atom

D	diffusion
	Debye temperature
E	equivalent quantity
e	electron
i	number of terms in a series
j	number of terms in a series
k	number of terms in a series
l	metal lattice
max	maximum value
q	heat flux vector
r	spherical coordinate
T	temperature gradient
θ	spherical coordinate
φ	spherical coordinate

ACKNOWLEDGMENTS

This dissertation owes many thanks to a number of people for their assistance, patience, and kindness.

I am convinced this study would never have been completed were it not for the diligence and support of my advisor, Dr. Weizhong Dai. First and foremost, my sincere gratitude must go to him for his wise counsel, patient guidance, and financial support.

Many thanks to my committee, Dr. Raja Nassar, Dr. Chokchai Leangsuksun, and Dr. Tianhong Cui for their support, guidance and helpful suggestion.

I owe a huge debt of gratitude to my parents for their love and support throughout not only the courses of my Ph.D studies, but throughout my entire life. This dissertation is dedicated to them.

Finally, I would like to thank my wife, Yuxin. Her love and encouragement are unflinching, and her patience and understanding were unselfish and appreciated more than she knows.

CHAPTER 1

INTRODUCTION

1.1 Overview

Heat transport through thin films or micro-objects is of vital importance in microtechnology applications [Joseph 1989] [Joshi 1993]. For instance, metal thin films are important components of microelectronic devices. The reduction of the device size to microscale has the advantage of enhancing the switching speed of the device. On the other hand, size reduction increases the rate of heat generation, which leads to a high thermal load on the microelectronic devices. Heat transfer at the microscale is also important for the thermal processing of materials with a pulse laser [Qiu 1992, 1993]. Examples in metal processing are laser micromachining, laser patterning, laser processing of diamond films from carbon ion implanted copper substrates, and laser surface hardening. In thermal processing of materials, microvoids may be found owing to thermal expansion. When such defects begin in the workpiece, their thermal energy in the neighborhood of the defects may be amplified, resulting in severe material damage and, consequently, total failure of the thermal processing. A detailed understanding of the way in which the local defects dissipate the thermal energy is then necessary not only to avoid the damage but also to improve the efficiency of thermal processing.

The heat transport equation at the microscale is different from the traditional heat diffusion equation because a second-order derivative of temperature with respect to time and a third-order mixed derivative of temperature with respect to space and time are introduced.

1.2 Objective of the Research

The objective of this research is to develop a three-level finite difference scheme for solving a three-dimensional microscale heat transport equation in spherical coordinates.

To achieve this objective, the following development is pursued:

- (1) Develop a finite difference scheme with three levels in time and central finite difference in space so that the overall truncation error is second-order in time and space.
- (2) Analyze the stability of the scheme by the discrete energy method.
- (3) Apply the new scheme to the investigation of the temperature rise of a gold sphere subjected to short-pulse laser irradiation on the surface.

The outcome of this study will provide an efficient and reliable numerical method for solving microscale heat transport equations, and give us better understanding of the nature of heat transport in such a micro system. The research results have a significant impact on the development of high-power short-pulse lasers for applications in structural monitoring of thin metal films, laser micro-machining and patterning, structural tailoring of microfilms, and laser synthesis and processing in thin-film deposition, as well as in other disciplines such as physics, chemistry, biology, medicine, and optical technology where high-energy short-pulse lasers are important.

1.3 Organization of the Dissertation

The dissertation is organized as follows: in Chapter 2, we introduce the process of microscale heat transfer by phonon-electron interaction model, the dual-phase-lagging behavior, and review previous research. In Chapter 3, based on the dual-phase-lagging model, we state the microscale heat transport equation in three-dimensional spherical coordinates with the initial and the boundary conditions in a microsphere. A three-level finite difference scheme for solving the three-dimensional dual-phase-lagging heat transport equation is then developed. The stability of the scheme is proved, and an iteration algorithm is provided. To demonstrate the applicability of the scheme, three numerical examples are illustrated in Chapter 4. Temperature change and distribution in a gold microsphere subjected to a pulse laser irradiation are investigated in three different cases: (1) short-pulse laser irradiation on the surface of the sphere symmetrically; (2) short-pulse laser irradiation on the top half of the surface of the sphere in parallel; (3) short-pulse laser irradiation on a portion of the surface of the sphere in parallel. Finally, the conclusion and future work are discussed in Chapter 5.

CHAPTER 2

BACKGROUND AND PREVIOUS WORK

2.1 Microscale Heat Transfer Model

From a microscopic point of view, the process of heat transport is governed by phonon-electron interaction in metallic films. Conventional theories established on the macroscopic level, such as heat diffusion assuming Fourier's law, are not expected to be informative for microscale conditions because they describe macroscopic behavior averaged over many grains. This fact holds even truer should the transient behavior at extremely short times, say, on the order of picoseconds to femtoseconds, become major concerns. A typical example is the ultrafast laser heating in thermal processing of materials. The quasi-equilibrium concept implemented in Fourier's law further breaks down in this case, along with the termination of macroscopic behavior in heat transport.

This section provides a brief review of the microscopic two-step model (phonon-electron interaction model), which emphasizes microscale effects in space. Rather than a detailed review, however, emphasis is placed in the special behavior depicted by this model that might reveal possible lagging behavior in heat transport. The review articles by Tien and Chen [Tien 1994] and Duncan and Peterson [Duncan 1994] for a broad perspective in microscale heat transfer and those by Joseph and Preziosi [Joseph 1989, 1990], Tzou [Tzou 1992a], and Özisik and Tzou [Özisik 1994] for the wave theory in

heat conduction would be helpful in developing an overall understanding of the model's development.

2.1.1 Microscale Heat Conduction

Regardless of the type of conducting medium, heat transport requires sufficient collisions among energy carriers. In metals, such energy carriers include electrons and phonons. The phonon gas can be viewed as a group of "mass particle" that characterize the energy state of a metal lattice. For a metal lattice vibrating at a frequency ν at a certain temperature T , the energy state of the metal lattice, and hence the energy state of the phonon, is

$$E = h\nu, \quad (2.1)$$

with h being the Plank constant. The lattice frequency is of the order of tens of terahertz (10^{13} 1/s) at room temperature. It is conceivable that the lattice frequency increases with the temperature of the metal lattice. Energy transport from one lattice to the other can thus be thought of as the consequence of a series of phonon collisions in time history, as illustrated in Figure 2.1.

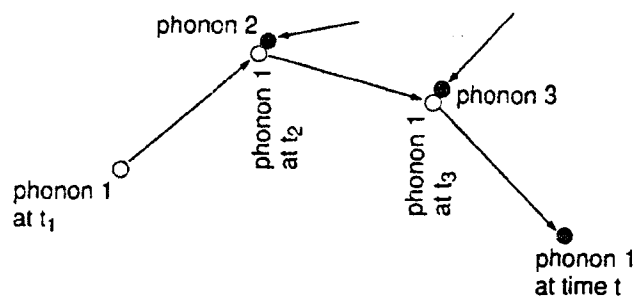


Figure 2.1 Energy transport through phonon collision.

Bearing energy $h\nu$ at time t_1 , phonon 1 collides with phonon 2 at t_2 and with phonon 3 at t_3 . In the course of such successive collisions, energy is transferred from phonon 1 to phonon 2 and 3, causing a successive change of vibrating frequency of phonon 1. For the case of illustration, the mean free path (d , in space) is defined as the algebraic mean of the distances traveled by phonon 1 between the two successive collisions with phonons 2 and 3:

$$d = \frac{d_1 + d_2 + d_3}{3}. \quad (2.2)$$

The mean free time τ , in a similar fashion, can be defined as the algebraic mean of the times traveled by phonon 1 between the two successive collisions with phonons 2 and 3:

$$\tau = \frac{(t_2 - t_1) + (t_3 - t_2) + (t - t_3)}{3} = \frac{t - t_1}{3}. \quad (2.3)$$

Two collisions for phonon 1 are used in this example for the ease of illustration. To have a meaningful statistical ensemble space, of course, a “sufficient” number of collisions must be collected for defining the mean free path and mean free time.

The macroscopic models assume the physical domain for heat transport is so large that it allows hundreds of thousands of phonon collisions to occur before an observation/description is made for the process of heat transport. Phonon collision requires a finite period of time to take place. Hundreds of thousands of such collisions also imply a sufficiently long time for the process of heat transport to occur. The macroscopic models, therefore, not only necessitate a sufficiently large physical domain for conducting heat (much larger than the mean free path) but also a sufficiently long time for heat conduction to take place (much longer than the mean free time). The

sufficiently long time for the stabilization of energy transport by phonons should not be confused with that required for the steady state to be developed. The sufficiently long time required in phonon collision is for a statistically meaningful concept in mean free path and time. The process of heat transport can still be time dependent after phonon transport becomes stabilized. In a phenomenological sense, the mean free time illustrated in Figure 2.1 is parallel to the characteristic time describing the relaxation behavior in the fast-transient process. For metals, the mean free time, or relaxation time, is of the order of picoseconds. As a rough estimate, therefore, any response time being shorter than a nanosecond should receive special attention. The fast-transient effect, such as wave behavior in heat conduction, may dramatically activate and introduce some unexpected effects in heat transport. Such a threshold value of nanoseconds, however, depends on the combined effect of geometric configuration (of the specimen) and thermal loading imposed on the system. It may vary by 1 order of magnitude should the system involve an abrupt change of geometric curvatures (such as in the vicinity of a crack or notch tips) or be subject to discontinuous thermal loading (irradiation of a short-pulse laser, for example).

The mean free path for electrons is of the order of tens of nanometers (10^{-8} m) at room temperature. The mean free path is a strong function of temperature, however. It may increase to the order of millimeters in the liquid helium temperature range, approximately 4 K. The mean free path in phonon collision (from grain boundaries) is much longer. As a rough estimate, again, the physical device with a characteristic dimension in submicrons deserves special attention. The microstructural interaction effect, such as phonon-electron interaction, may significantly enhance heat transfer in

short times. Enhancement of heat transfer enlarges the heat-affected zone and promotes the temperature level, which may thereby lead to early burnout of micro-devices if not properly prevented.

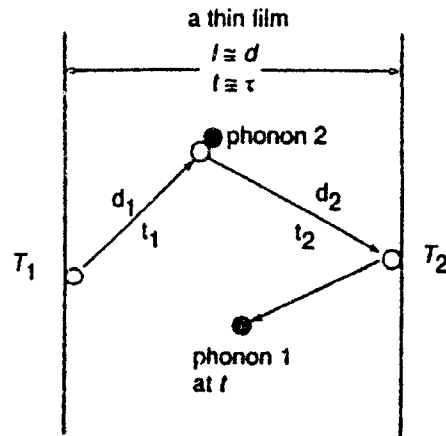


Figure 2.2 Phonon interaction in a thin film of the same order of magnitude as the mean free path, illustrating the challenge of the microscale effect in space to the concept of temperature gradient.

Because the physical dimension in microscale heat transfer is of the same order of magnitude as the mean free path and, consequently, the response time in heat transport is of the same order of magnitude as the mean free time, the quantities based on the macroscopically averaged concept must be reexamined for their true physical meanings. The temperature gradient taken for granted in macroscale heat transfer, for example, may lose its physical ground for a thin film of thickness of the same order of magnitude as the mean free path. As illustrated in Figure 2.2, it is true that we could still divide the temperature difference, $T_2 - T_1$, by the film thickness l ($\cong d$, the mean free path of phonon interaction) to obtain a “gradient-like” quantity, but the temperature gradient obtained in this manner loses its usual physical meaning because no sufficient energy carriers are between the two surfaces of the film and, consequently, the temperature field

is discontinuous across the film thickness. Should the concept of the temperature gradient fail, the conventional way of defining the heat flux vector according to Fourier's law becomes questionable. Ambiguity of the concepts in both the temperature gradient and the heat flux vector is the first challenge that the microscale effect in space has raised against conventional theories in macroscale heat transfer.

A similar situation exists in the response time for temperature. The typical response time in the thin film is of the same magnitude as the mean free time, as a result of phonons traveling in the threshold of the mean free path. If the response time of primary concern (for temperature or heat flux vector) is of the same order of magnitude as the mean free time (relaxation time), the individual effect of phonon interaction must be taken into account in the short-time transient of heat transport. It is the second challenge that the microscale effect in time has raised against conventional theories in macroscale heat transfer. From Figure 2.2, most important, it is evident that the microscale effect in space interferes with the microscale effect in time. They are not separable and must be accommodated simultaneously in the same theoretical framework. It is also clear from considering the finite speed of phonon transport in short times. Phonons propagate at the speed of sound, on average, which is of the order of 10^4 to 10^5 *m/s* at room temperature, depending on the type of solid medium. A response time of the order of picoseconds (10^{-12} *s*) thus implies a traveling distance (the penetration depth of heat by phonon transport) of the order of submicrons (10^{-8} to 10^{-7} *m*). Such a penetration depth is on the microscopic level, necessitating a simultaneous consideration of the microscale effect in space.

2.1.2 Phonon-Electron Interaction

Model

Description. Phenomenologically, the phonons illustrated in Figures 2.1 and 2.2 can be replaced phonons/electrons to depict the phonon-electron interaction for heat transport in metals. Owing to much smaller heat capacity of the electron gas, about 1 to 2 orders of magnitude smaller than that of the metal lattice, however, the heating mechanism involves, excitation of the electron gas and heating of the metal lattice through phonon-electron interaction in short times. The phonon-electron interaction model was proposed to describe this two-step process for energy transport in microscale. The early version of the two step model (phonon-electron interaction model) was proposed by Kaganov *et al.* [Kaganov 1957] and Anisimov *et al.* [Anisimov 1974] without a rigorous proof. It remained as a phenomenological model for about four decades until the recent effort by Qiu and Tien [Qiu 1993], which places the two-step model on a quantum mechanical and statistical basis. In the absence of an electrical current during short-time heating, the generalized hyperbolic constitutive equation for heat transport through the electron gas was derived from the Boltzmann transport equation. As the relaxation time of the electron gas calculated at the Fermi surface vanishes, the hyperbolic two-step model perfectly reduces to the parabolic two-step model originally proposed by Kaganov *et al.* [Kaganov 1957] and Anisimov *et al.* [Anisimov 1974].

For metals, the two-step model describes heating of the electron gas and the metal lattice by a two-step process. Mathematically,

$$C_e \frac{\partial T_e}{\partial t} = \nabla \cdot (K \nabla T_e) - G(T_e - T_l), \text{ heating of the electron gas,} \quad (2.4)$$

$$C_l \frac{\partial T_l}{\partial t} = G(T_e - T_l), \text{ heating of the metal lattice,} \quad (2.5)$$

with C denoting the volumetric heat capacity, K the thermal conductivity of electron gas, and subscripts e and l standing for electron and metal lattice, respectively. The effect of heat conduction through the metal lattice is neglected in Equation (2.5). The extremely supplied phonons, such as those from an intensified laser, first increase the temperature of the electron gas according to Equation (2.4). As clearly shown, diffusion is assumed at this stage, rendering a parabolic nature for heat transport through the electron gas. Through phonon-electron interactions, which is the second stage of heat transport and represented by Equation (2.5), the hot electron gas heats up the metal lattice by phonon-electron interaction. The energy exchange between phonons and electrons is characterized by the phonon-electron coupling factor G [Kaganov 1957]:

$$G = \frac{\pi^2}{6} \frac{m_e n_e v_s^2}{\tau_e T_e} \text{ for } T_e \gg T_l \quad (2.6)$$

where m_e represents the electron mass, n_e the number density (concentration) of electrons per unit volume, and v_s the speed of sound,

$$v_s = \frac{\kappa}{2\pi h} (6\pi^2 n_a)^{\frac{1}{3}} T_D. \quad (2.7)$$

The quantity h in Equation (2.7) stands for the Planck constant, κ the Boltzmann constant, n_a the atomic number density per unit volume, and T_D represents the Debye temperature. The electron temperature (T_e) is much higher than the lattice temperature (T_l) in the early-time response. The condition of $T_e \gg T_l$ in Equation (2.6) for the applicability of the G expression is thus valid in the fast-transient process of electron-phonon dynamics. Within the limits of Wiedemann-Frenz's law, which states that for

metals at moderate temperatures (roughly for $T_l > 0.48T_D$) the ratio of the thermal conductivity to the electrical conductivity is proportional to the temperature, and the constant of proportionality is independent of the particular metal (a metal-type-independent constant), the electronic thermal conductivity can be expressed as

$$K = \frac{\pi^2 n_e \kappa^2 \tau_e T_e}{3m_e}, \quad (2.8)$$

resulting in

$$m_e = \frac{\pi^2 n_e \kappa^2 \tau_e T_e}{3K} \quad (2.9)$$

Substituting equation (2.9) into equation (2.6) for the electron mass gives

$$G = \frac{\pi^4 (n_e v_s \kappa)^2}{18K} \quad (2.10)$$

The phonon-electron coupling factor therefore depends on the thermal conductivity (K) and the number density (v_s) of the electron gas. Through the speed of sound, in addition, the cooling factor further depends on the number density of atoms (n_a) and the Debye temperature (T_D). The coupling factor shows no strong dependence on temperature (T_e) and does not seem to be affected by electronic relaxation time (τ_e).

For us to estimate the value of G according to equation (2.10), the number density of the electron gas, n_e , is a key quantity. Qiu and Tien [Qiu 1992] assumed one free electron per atom for noble metals (silver (Ag) and gold (Au), for example) and employed the s -band approximation for the valence electrons in transition metals. Owing to the relatively heavy mass of the d -band electrons in the valence electrons, only a fraction of the s -band electrons can be viewed as free electrons. The value of n_e ,

therefore, is chosen as a fraction of the valence electrons. The phonon-electron coupling factor thus calculated, and the experimentally measured values are listed in Table 2.1 for comparison. Except for copper (Cu) and lead (Pb), which may exhibit certain ambiguous transition mechanisms, the s -band approximation seems to agree well with the experimental results. As a general trend, a higher free electron number density (n_e) and a higher Debye temperature (T_D) would result in larger values of G and smaller values of the relaxation time (τ).

Table 2.1 Phonon-electron coupling factor G for some noble and transition metals [Qiu 1992]

Metal	Calculated, $\times 10^{16} \text{ W/m}^3 \text{ K}$	Measured, $\times 10^{16} \text{ W/m}^3 \text{ K}$
Cu	14	4.8 \pm 0.7 [Brorson 1990] 10 [Elsayed-Ali 1987]
Ag	3.1	2.8 [Groeneveld 1990]
Au	2.6	2.8 \pm 0.5 [Brorson 1990]
Cr	45 ($n_e/n_a = 0.5$)	42 \pm 5 [Brorson 1990]
W	27 ($n_e/n_a = 1.0$)	26 \pm 3 [Brorson 1990]
V	648 ($n_e/n_a = 2.0$)	523 \pm 37 [Brorson 1990]
Nb	138 ($n_e/n_a = 2.0$)	387 \pm 36 [Brorson 1990]
Ti	202 ($n_e/n_a = 1.0$)	185 \pm 16 [Brorson 1990]
Pb	62	12.4 \pm 1.4 [Brorson 1990]

From a mathematical point of view, Equations (2.4) and (2.5) provide two equations for two unknowns, the electron-gas temperature (T_e) and the metal-lattice temperature (T_l). They can be solved in a coupled manner, or they can be combined to give a single energy equation describing heat transport through phonon-electron interaction in microscale. The combined energy equation, from an alternate point of view can be derived from the phase lag concept in the temporal response. Such a coincidence strongly supports the dual-phase-lag model.

Complexity of solutions for Equations (2.4) and (2.5) lies in the temperature-dependent heat capacity of the electron gas, i.e., $C_e \equiv C_e(T_e)$. For an electron-gas temperature lower than the Fermi temperature, which is of the order of 10^4 K, the electron heat capacity is proportional to the electron temperature. Such a temperature dependence makes Equations (2.4) and (2.5) nonlinear. For a gold film subjected to femtosecond laser heating, Qiu and Tien employed the Crank-Nicholson scheme of finite difference to obtain the solutions [Qiu 1992]. With regard to the comparison with the experimental result, the normalized temperature change in the electron gas is identical to the normalized reflectivity change on the film surfaces:

$$\frac{\Delta R}{(\Delta R)_{\max}} = \frac{\Delta T_e}{(\Delta T_e)_{\max}} \quad (2.11)$$

where R denotes the reflectivity and the subscript “max” refers to the maximum value occurring in the transient process. Both ratios in Equation (2.11), therefore, are less than 1. The left side of Equation (2.11) can be measured by the front-surface-pump and back-surface-probe technique [Brorson 1987] [Elsayed-Ali 1991] [Qiu 1994]. The right side of Equation (2.11), on the other hand, can be calculated by solving Equations (2.4) and (2.5) for the electron temperature and normalizing with respect to the maximum value in the transient response at various times. For a gold film subjected to irradiation of a 96 femtosecond (fs , 10^{-15} s) laser with an energy flux of 1 mJ/cm^2 , the results of reflexivity change at the front surface of the film are reproduced in Figure 2.3 from the work by Qiu and Tien [Qiu 1992]. The time delay marked on the horizontal axis is the time difference between the pump (heating) and the probe (detecting) lasers, which is equivalent to the physical time in the transient response. For both thickness of the films, 0.05 and $0.1 \text{ }\mu\text{m}$, the microscopic two-step model accommodating the phonon-electron interaction effect

nicely captures the heating ($0 \leq t \leq 0.096$ picosecond (ps)) and thermalization ($0.096 \leq t \leq 3$ ps) processes of the electron temperature. The temperature level, as respected, increases as the thickness of the film decreases. The classical theory of diffusion, which assumes an immediate equilibrium between phonons (lattice) and electrons and is called the one-step heating model by Qiu and Tien [Qiu 1992], fails to describe the fast energy transport process. Particularly in the thermalization stage, it overestimates the transient temperature by several times. The transient temperature at the front surface does not seem to depend on the film thickness according to the diffusion model. The transient temperature remains almost at the same level as the film thickness increase from 0.05 to $0.1 \mu m$.

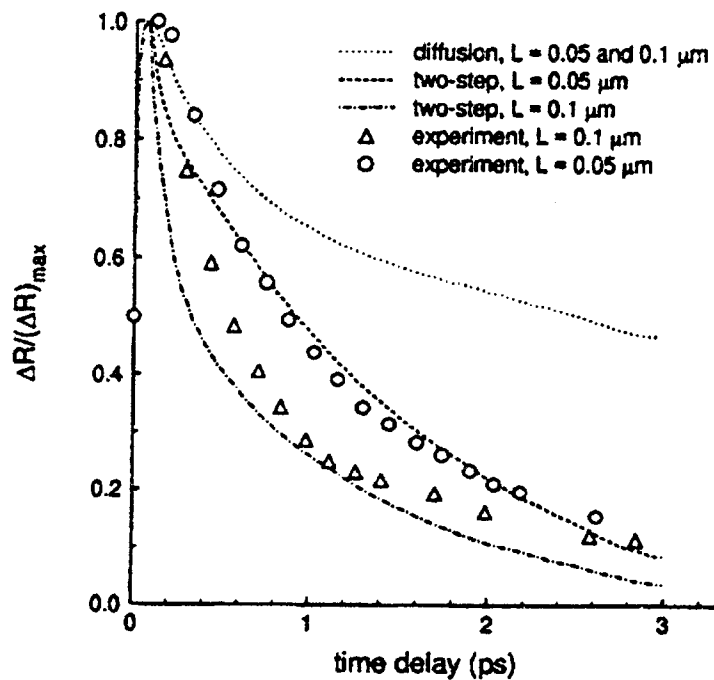


Figure 2.3 Transient reflectivity change at the front surface of gold films (thickness 0.05 and $0.1 \mu m$) subjected to laser irradiation (pulse width $96 fs$, energy flux $1 mJ/cm^2$) [Qiu 1992] [Brorson 1987].

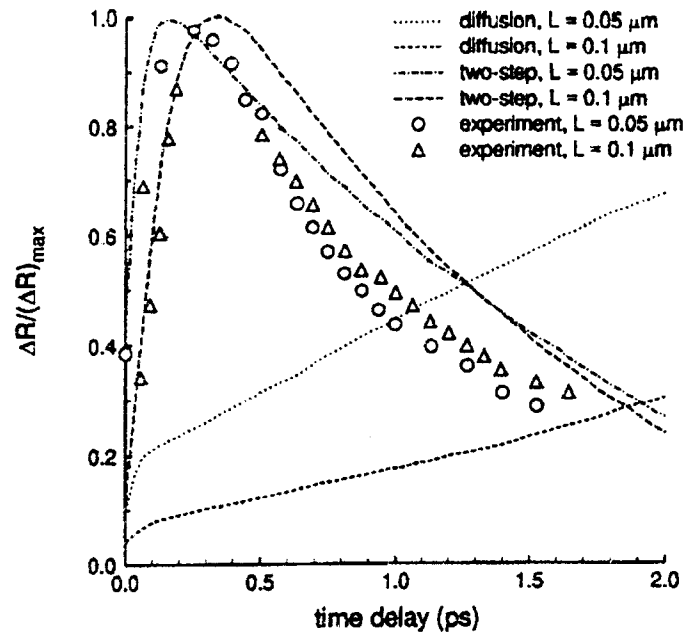


Figure 2.4 Transient reflectivity change at the rear surface of gold films (thickness 0.05 and 0.1 μm) subjected to laser irradiation (pulse width 96 fs, energy flux 1 mJ/cm^2). [Qiu 1992] [Brorson 1987].

Figure 2.4 shows the transient reflectivity change at the rear surface of the film. The heating and thermalization processes remain similar, with the response times, however, increasing. The time at which the electron temperature reaches its maximum value (the instant of time separating the heating and thermalization stages) increases with film thickness, a “wave-like” behavior even under the assumption of diffusion for heat transport through the electron gas. The one-step heating model (diffusion) completely fails to describe the thermalization process at the rear surface of the film. Unlike the situation shown in Figure 2.3 (the front surface), where at least the qualitative trend was preserved in the same domain of response times, the heating stage predicted by the diffusion model shown in Figure 2.4 (the rear surface) lasts beyond the threshold of 2 ps, resulting in a transient response of reflectivity change that significantly differs from the experimental result both quantitatively and qualitatively. From Figures 2.3 and 2.4 it is

clear that, for metals, the microscopic phonon-electron interaction is an important effect to be incorporated for an accurate description of microscale heat transport. In addition to the familiar thermal properties such as heat capacity and thermal conductivity, the phonon-electron coupling factor describing the short-time energy exchange between phonons and electrons is a dominating property in the fast-transient process of laser heating. Along with the equivalent thermal wave speed in the parabolic two-step model, typical values of the phonon-electron coupling factor (G) are listed in Table 2.2 for copper, gold, silver and lead. They are of the order of 10^{16} , in units of $W/m^3 K$, for metals.

Table 2.2 The equivalent thermal diffusivity (α_E), the equivalent thermal wave speed (C_E), and the phase lags of the temperature gradient and the heat flux vector (τ_T and τ_q) for typical metals ($C_e = 2.1 \times 10^4 J/m^3 K$ at room temperature; ps \equiv picosecond) [Tzou 1996]

	k	C_l	G	α_E	τ_T	τ_q	C_E
	$W/m K$	$J/m^3 K$ $\times 10^6$	$W/m^3 K$ $\times 10^{16}$	m^2/s $\times 10^{-4}$	ps	ps	m/s $\times 10^4$
Cu	386	3.4	4.8	1.1283	70.833	0.4348	1.6109
Ag	419	2.5	2.8	1.6620	89.286	0.7348	1.4949
Au	315	2.5	2.8	1.2495	89.286	0.7348	1.2961
Pb	35	1.5	12.4	0.2301	12.097	0.1670	1.1738

Single Energy Equation. Equations (2.4) and (2.5) can be combined to give a single energy equation governing heat transport through the metal lattice or the electron gas [Tzou 1995a, b]. Given their present forms, solving Equations (2.4) and (2.5) for T_e and T_l in a simultaneous manner may be more efficient from a numerical point of view. Combining Equations (2.4) and (2.5) together to give a single energy equation describing the electron temperature or the lattice temperature alone, however, is more indicative for the fundamental behavior in microscale heat transport. With emphasis on the

characteristics of lattice and electron temperatures, all of the thermal properties, including heat capacities of the electron gas (C_e) and the metal lattice (C_l) as well as the thermal conductivity (K) are assumed to be temperature-independent (constant).

A single energy equation governing the lattice temperature can be obtained by eliminating the electron temperature, T_e , from Equations (2.4) and (2.5). From Equation (2.5), the electron temperature can be expressed in terms of the lattice temperature and its time derivative:

$$T_e = T_l + \frac{C_l}{G} \frac{\partial T_l}{\partial t}. \quad (2.12)$$

Substituting Equation (2.12) into (2.4) and using the result of $G(T_e - T_l)$ from Equation (2.5) results in

$$\nabla^2 T_l + \left(\frac{C_l}{G} \right) \frac{\partial}{\partial t} \nabla^2 T_l = \left(\frac{C_l + C_e}{K} \right) \frac{\partial T_l}{\partial t} + \left(\frac{C_l C_e}{KG} \right) \frac{\partial^2 T_l}{\partial t^2}. \quad (2.13)$$

Equation (2.13), governing the lattice temperature alone, introduces a new type of energy equation in conductive heat transfer. It has a usual diffusion term $\left(\frac{\partial T_l}{\partial t} \right)$, a thermal wave term $\left(\frac{\partial^2 T_l}{\partial t^2} \right)$, and a mixed-derivative term $\left(\frac{\partial}{\partial t} \left[\nabla^2 T_l \right] \right)$ that reflect the combined effect of microscopic phonon-electron interaction and macroscopic diffusion. In the case that the phonon-electron coupling factor approaches infinity ($G \rightarrow \infty$), implying that energy transfer from electrons to phonons is occurring at an infinite rate, Equation (2.13) reduces to the conventional diffusion equation employing Fourier's law, with the coefficient $\frac{C_l + C_e}{K}$ appearing as the equivalent thermal diffusivity.

A single energy equation describing the electron temperature can be obtained in the same manner. From Equation (2.4),

$$T_l = T_e - \frac{k}{G} \nabla^2 T_e + \frac{C_e}{G} \frac{\partial T_e}{\partial t}. \quad (2.14)$$

Substituting Equation (2.14) into (2.5) and using the result of $G(T_e - T_l)$ from Equation (2.4) yields

$$\nabla^2 T_e + \left(\frac{C_l}{G} \right) \frac{\partial}{\partial t} \nabla^2 T_e = \left(\frac{C_l + C_e}{K} \right) \frac{\partial T_e}{\partial t} + \left(\frac{C_l C_e}{KG} \right) \frac{\partial^2 T_e}{\partial t^2}. \quad (2.15)$$

Note that Equation (2.15), governing the electron temperature, has exactly the same form as Equation (2.13), governing the lattice temperature.

2.2 Dual-Phase-Lagging Behavior

The lagging response, in general, describes the heat flux vector and the temperature gradient occurring at different instant of time in the heat transfer process. If the heat flux precedes the temperature gradient in time, the heat flux is the cause and the temperature gradient is the effect of the heat flow. If the temperature gradient precedes the heat flux, on the other hand, the temperature gradient becomes the cause and the heat flux becomes the effect. This concept of precedence does not exist in the classical theory of diffusion because the heat flux vector and the temperature gradient are assumed to occur simultaneously. In [Tzou 1996], the theoretical foundation for the lagging response in conductive heat transfer is established. It results in a new type of energy equation, capturing the classical theories of diffusion (macroscopic in both space and time), thermal waves (macroscopic in space but microscopic in time), and phonon-electron interaction model (microscopic in both space and time) in the same framework. The resulting model employing the two-phase lags in describing the transient process is called

the dual-phase-lag model. Universality of the dual-phase-lag model facilitates a consistent approach describing the intrinsic transition from one type of behavior (diffusion, for example) to another (the phonon-electron interaction) associated with shorting of the response time.

2.2.1 Phase-Lag Concept

In the classical theory of diffusion, the heat flux vector (\vec{q}) and the temperature gradient (∇T) across a material volume are assumed to occur at the same instant of time. Fourier's law of heat conduction,

$$\vec{q}(\vec{r}, t) = -k\Delta T(\vec{r}, t), \quad (2.16)$$

with \vec{r} denoting the position vector of the material volume and t the physical time, dictates such an immediate response. It results in an infinite speed of heat propagation, implying that a thermal disturbance applied at certain location in a solid medium can be sensed immediately anywhere else in the medium. Because the heat flux vector and the temperature gradient are simultaneous, there is no difference between the cause and the effect of heat flow. In the wave theory of heat conduction, on the other hand, the heat flux vector and the temperature gradient across a material volume are assumed to occur at different instants of time. In parallel to Fourier's law, the constitutive equation can be written as [Tzou 1989a, b, 1990a, b, 1992a]

$$\vec{q}(\vec{r}, t + \tau) = -k\Delta T(\vec{r}, t), \quad (2.17)$$

where τ is the time delay, called the "relaxation time" in the wave theory of heat conduction. The first-order expression of τ in Equation (2.17) with respect to t bridges all the physical quantities at the same instant of time. It results in the expression

$$\bar{q}(\bar{r}, t) + \tau \frac{\partial \bar{q}}{\partial t}(\bar{r}, t) \cong -k \Delta T(\bar{r}, t), \quad (2.18)$$

which is the *CV* wave model originated by Cattaneo [Cattaneo 1958] and Vernotte [Vernotte 1958, 1961]. The *CV* wave model removes the paradox of infinite speed of heat propagation assumed in Fourier's law. The relaxation time, instead, relates to the thermal wave speed by [Chester 1963]

$$\tau = \frac{\alpha}{C^2}, \quad (2.19)$$

where α is the thermal diffusivity and C denotes the thermal wave speed. In the case of C approaching infinity, the relaxation time decreases to zero ($\tau = 0$), and the *CV* wave model, Equations (2.17) and (2.18) reduces to Fourier's law, Equation (2.16). The thermal wave model has been one of the major research areas in conductive heat transfer. Detailed reviews can be found in the articles by Joseph and Preziosi [Joseph 1989, 1990], Tzou [Tzou 1992a] and Özisik and Tzou [Özisik 1994].

To solve for the two unknowns \bar{q} and T , Equation (2.16) (the diffusion model) or (2.18) (the thermal wave model) is combined with the energy equation established at a general time t during the transient process,

$$-\nabla \cdot \bar{q}(\bar{r}, t) + Q(\bar{r}, t) = C_p \frac{\partial T}{\partial t}(\bar{r}, t), \quad (2.20)$$

with C_p being the volumetric heat capacity, $C_p = \rho c_p$ and Q the volumetric heat source. Although allowing for a delayed response between the heat flux vector and the temperature gradient, evidently, the *CV* wave model still assumes an immediate response between the temperature gradient and the energy transport. This response occurs right after a temperature gradient is established across a material volume; in other words, the

CV wave model assumes an instantaneous heat flow. The temperature gradient is always the cause for heat transfer, and the heat flux is always the effect.

The dual-phase-lag model aims to remove the precedence assumption made in the thermal wave model. It allows either the temperature gradient (cause) to precede the heat flux vector (effect) or the heat flux vector (cause) to precede the temperature gradient (effect) in the transient process. Mathematically, it can be represented by [Tzou 1995a, b,c]

$$\bar{q}(\bar{r}, t + \tau_q) = -k \nabla T(\bar{r}, t + \tau_r), \quad (2.21)$$

where τ_r is the phase lag of the temperature gradient and τ_q is the phase lag of the heat flux vector. For the case of $\tau_r > \tau_q$, the temperature gradient established across a material volume is a result of the heat flow, implying that the heat flux vector is the cause and the temperature gradient is the effect. For $\tau_r < \tau_q$, on the other hand, heat flow is induced by the temperature gradient established at an earlier time, implying that the temperature gradient is the cause, while the heat flux vector is the effect. The first-order approximation of Equation (2.21), in a form parallel to Equation (2.18) reads

$$\bar{q}(\bar{r}, t) + \tau_q \frac{\partial \bar{q}}{\partial t}(\bar{r}, t) \cong -k \left\{ \nabla T(\bar{r}, t) + \tau_r \frac{\partial}{\partial t} [\nabla T(\bar{r}, t)] \right\}. \quad (2.22)$$

Including the cause-and-effect relationship in the transient process involves more than an addition of the phase lag into the temperature gradient. When Equation (2.22) is combined with energy Equation (2.20), the precedence switching results in capricious situations in transient conduction.

In passing, three importing characteristics in the dual-phase-lag model are noted:

1. The heat flux vector and temperature gradient shown in Equation (2.21) are the local responses within the solid medium. They must not be confused with the global quantities specified in the boundary conditions. When applying a heat flux to the boundary of a solid medium, named in a flux-specified boundary value problem, the temperature gradient established at a material point within the solid medium can still precede the heat flux vector. Application of a heat flux at the boundary does not warrant the precedence of the heat flux vector to the temperature gradient at all. In fact, whether the heat flux vector precedes the temperature gradient or not depends on the combined effect of thermal loading, geometry of the specimen, and thermal properties of the material.
2. Three characteristic times are actually involved in the dual-phase-lag model. The instant of time $(t + \tau_T)$ at which the temperature gradient is established across a material volume, $(t + \tau_q)$ for the onset of heat flow, and t for the occurrence of heat transport (at which conservation of energy is described). The constitutive equation describing the lagging behavior, Equation (2.21), differs from the *CV* wave model, Equation (2.17), by a shift in the time scale, $\tau = \tau_q - \tau_T$, which is immaterial as far as the constitutive equation itself is concerned. When combined with the energy Equation (2.20), however, such a shift in the same scale becomes nontrivial, resulting in a completely different response from that depicted by the *CV* wave model.
3. The two phase lags τ_T and τ_q , like the thermal diffusivity and thermal conductivity, are intrinsic thermal properties of the bulk material. For solids with internal structures such as interstitial gas in porous media or second-phase constituents in composites,

however, they become structural properties, which also depend on the detailed configurations of the substructures.

2.2.2 Internal Mechanisms

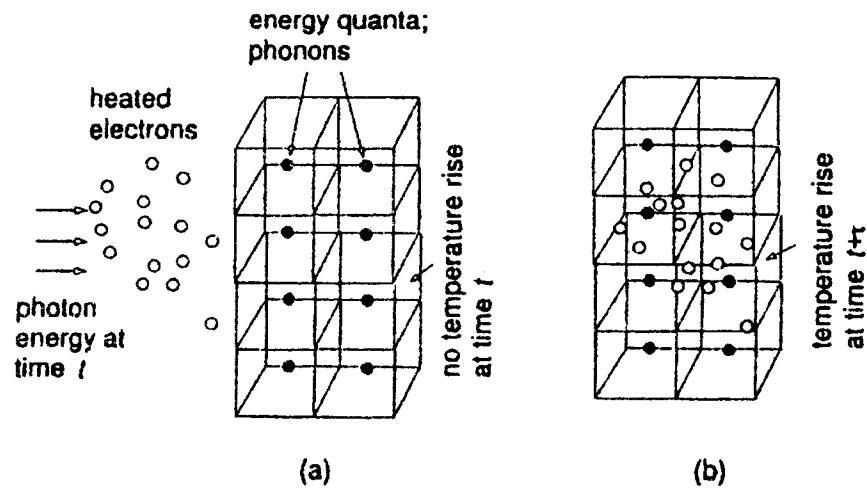


Figure 2.5 The finite time required for the phonon-electron interaction in microscale. (a) The first stage of electron-gas heating by phonons and (b) the second stage of metal lattice heating by phonon-electron interactions.

Figure 2.5 describes the delayed response caused by the phonon-electron interactions in metallic structures. The energy state of a metal lattice is discretized into quanta, called phonons in quantum mechanics. When excited by short-pulse laser, phonons from the laser beam first heat up the electron gas at a certain time t shown in Figure 2.5(a). At this moment, no appreciable temperature change in the metal lattice, distance from the heat source, can be detected. Through the phonon-electron interactions, Figure 2.5(b), energy transport from the hot electron gas to phonons follows, giving rise to an appreciable increase of temperature in the metal lattice at a later time $t + \tau$. The phonon-electron interaction requires a finite time to take place, usually of the order of picoseconds [Qiu 1992, 1993]. The resulting phase lag (τ) is thus of the same order of magnitude.

2.2.3 Temperature Formulation

Analysis in term of boundary value problems provides an efficient way to study the fundamental characteristics of lagging behavior. The energy Equation (2.20) and the constitutive Equation (2.21) depicting the lagging response are to be combined for this purpose. These two equations, generally speaking, exhibit two coupled, delayed differential equations for two unknowns, T and \bar{q} . No general solution has yet been found for this type of equation with delays. The linear version based on the first-order expansions of τ_T and τ_q , Equation (2.22), provides an approximation to describe the lagging behavior in the simplest case. It is not as general as Equation (2.21), but should reveal all the fundamental behavior in the lagging response. Such a linear approximation approaches the exact formulation when τ_T and τ_q are small, a situation existing in the phonon-electron interaction model where the values of τ_T and τ_q are of the order of picoseconds to femtoseconds. The linear expression is sufficient in this case.

At this initial stage of development, however, exploring the physical conditions under which the lagging behavior may become pronounced and searching for the appropriate experimental evidence are much more important than making a full expansion into the nonlinear regime of τ_T and τ_q . Based on the fundamental understanding thus developed, the high-order responses including the nonlinear effect of τ_T and τ_q can always be incorporated for a more refined analysis. Development of the CV wave model, in fact, bears this merit. While Equation (2.18) serves as a linear approximation of Equation (2.17), depicting a general delayed response in short times, it has been used as the basis for the hyperbolic theory of heat conduction. Finding the

physical environment in which the linear wave theory can be applied is still the most important task for researchers in this area [Özisk 1994].

In Equations (2.20) and (2.22), three characteristic times are involved in the process of heat transport: the instant of time $(t + \tau_T)$ at which the temperature gradient is established across a material volume, time $(t + \tau_q)$ at which heat flows through the material volume, and general time t at which conservation of energy is imposed. The linear expansion of τ_T and τ_q , shown by Equation (2.22) bridges all the physical quantities at the same instant of time, and Equations (2.20) and (2.22) are ready for a further combination.

The temperature representation of the energy equation results from elimination of the heat flux vector from the two equations. Assuming constant thermal properties, the divergence of Equation (2.22) gives

$$\nabla \cdot \bar{q} + \tau_q \frac{\partial}{\partial t} [\nabla \cdot \bar{q}] = -k \nabla^2 T - k \tau_T \frac{\partial}{\partial t} [\nabla^2 T]. \quad (2.23)$$

Substituting the expression of $\nabla \cdot \bar{q}$, in Equation (2.20), into Equation (2.23),

$$\nabla \cdot \bar{q} = Q - C_p \frac{\partial T}{\partial t}, \quad (2.24)$$

and introducing the thermal diffusivity $\alpha = \frac{k}{C_p}$ gives

$$\begin{aligned} & \nabla^2 T + \tau_T \frac{\partial}{\partial t} [\nabla^2 T] + \frac{1}{k} \left[Q + \tau_q \frac{\partial Q}{\partial t} \right] \\ &= \frac{1}{\alpha} \frac{\partial T}{\partial t} + \frac{\tau_q}{\alpha} \frac{\partial^2 T}{\partial t^2} \quad (T \text{ representation}) \end{aligned} \quad (2.25)$$

This equation describes the temperature response with lagging in the linearized framework accommodating the first-order effect of τ_T and τ_q . It captures several representative models in heat transfer as special cases.

In the absence of the two phase lags, $\tau_T = \tau_q = 0$, Equation (2.25) reduce to the diffusion equation employing Fourier's law. In the absence of the phase lag of the temperature gradient, $\tau_T = 0$, Equation (2.25) reduces to the *CV* wave mode. The phase lag of the heat flux vector (τ_q) reduces to the relaxation time defined by Chester [Chester 1963], Equation (2.19). The phase lag of the heat flux vector introduces an apparent heat source, $\frac{\tau_q}{k} \frac{\partial Q}{\partial t}$, in addition to the real heat source applied to the solid [Frankel 1985] [Tzou 1989a, b, 1990a, b]. The apparent heating is the physical basis for the thermal resonance phenomena explored by Tzou [Tzou 1991a, b, 1992b, c] in the wave theory of heat conduction. The two popular models for describing the macroscopic heat transfer are thus captured in the framework of the dual-phase-lag model under special cases.

Compared with the microscopic model for heat transport, the energy equation employing the dual-phase-lag model, Equation (2.25), has exactly the same form as the energy equation in the phonon-electron interaction model, Equation (2.13) or (2.15). Such perfect correlations, encouragingly, facilitate a direct determination of the two phase lags in terms of the microscopic thermal properties. Comparing Equation (2.25) with (2.13) or (2.15) for the phonon-electron interaction model, again, a perfect correlation results:

$$\alpha = \frac{K}{C_e + C_l}, \quad (2.26)$$

$$\tau_r = \frac{C_l}{G}, \quad (2.27)$$

$$\tau_q = \frac{1}{G} \left[\frac{1}{C_e} + \frac{1}{C_l} \right]^{-1}. \quad (2.28)$$

Heat capacities of the metal lattice (C_l) and the electron gas (C_e) and the phonon-electron coupling factor (G) are thus the microscopic properties determining the two phase lags. For fast-transient heat transport in metals, therefore, the dual-phase-lag model successfully captures the microscopic phonon-electron interaction model in its framework.

The perfect correlation between the dual-phase-lag model and the microscopic phonon-electron interaction model demonstrates the feasibility of modeling the microstructural interaction effect in space by its delayed response in time. Equations (2.26) ~ (2.28) explicitly indicate the microscopic properties causing such time delays in the heat flux vector and the temperature gradient.

While capturing the existing macroscopic (diffusion and wave) and microscopic (phonon-electron interaction) models in a consistent approach, the dual-phase-lag model introduces a new type of energy equation in conductive heat transfer. As shown in Equation (2.25), the mixed-derivative term, containing the first-order derivative with respect to time and the second-order derivative with respect to space, appears as the highest order differential in the equation, which will dramatically alter the fundamental characteristics of the solution for temperature. A wave term, the second-order derivative with respect to time, still exists on the right side of the energy equation, but the mixed-derivative term completely destroys the wave structure, and the energy equation is

parabolic in nature. It predicts a higher temperature level in the heat-penetration zone than diffusion but does not have a sharp wavefront in heat propagation.

2.2.4 Heat Flux Formulation

The lagging behavior depicted by Equation (2.22) makes it difficult to apply the T representation of the energy Equation (Equation (2.25)) to problems involving flux-specified boundary conditions. It can be illustrated by a direct integration of Equation (2.22) for the heat flux vector:

$$\vec{q}(\vec{r}, t) = -\left(\frac{k}{\tau_q}\right) e^{-\frac{t}{\tau_q}} \int_0^{\frac{t}{\tau_q}} e^{\frac{\eta}{\tau_q}} \left[\nabla T(\vec{r}, \eta) + \tau_T \frac{\partial}{\partial \eta} [\nabla T(\vec{r}, \eta)] \right] d\eta. \quad (2.29)$$

In the dual-phase-lag model, clearly, the heat flux vector depends not only on the temperature gradient established at the same instant of time, but also on the entire history in which the temperature gradient and its time-rate of change are established. This path dependency reveals a special behavior with “memory”, which is completely different from the pointwise relationship depicted by Fourier’s law. Should Equation (2.29) be used to specify the heat flux in a boundary condition, the T representation, Equation (2.25), will involve an integral equation in the boundary conditions. The resulting boundary value problem becomes difficult to handle, implying the need for a direct formulation in terms of the heat flux. This situation does not exist in the classical theory of diffusion. Specifying the heat flux at a boundary is equivalent to specifying the gradient of temperature according to Fourier’s law. The boundary condition switches from a Dirichlet type to a Neumann type. But no special difficulty would result.

The q representation, formulation of the energy equation in terms of heat fluxes, results from elimination of temperature from Equations (2.20) and (2.22). Taking the gradient of Equation (2.20) gives

$$C_p \frac{\partial}{\partial t}(\nabla T) = -\nabla(\nabla \cdot \bar{q}) + \nabla Q. \quad (2.30)$$

Substituting the result for $\frac{\partial}{\partial t}(\nabla T)$ from Equation (2.30) into Equation (2.22) gives

$$\bar{q} + \tau_q \frac{\partial \bar{q}}{\partial t} = -k \nabla T + \alpha \tau_r [\nabla(\nabla \cdot \bar{q}) - \nabla Q]. \quad (2.31)$$

Differentiating Equation (2.31) with respect to time and substituting Equation (2.30) for the resulting time derivative of the temperature gradient, finally, gives the result

$$\begin{aligned} & \nabla(\nabla \cdot \bar{q}) + \tau_r \frac{\partial}{\partial t} [\nabla(\nabla \cdot \bar{q})] - \left[\nabla Q + \tau_r \frac{\partial}{\partial t} (\nabla Q) \right] \\ &= \frac{1}{\alpha} \frac{\partial \bar{q}}{\partial t} + \frac{\tau_q}{\alpha} \frac{\partial^2 \bar{q}}{\partial t^2} \quad (q \text{ representation}). \end{aligned} \quad (2.32)$$

The q representation shown by Equation (2.32) has exactly the same structure in time as the T representation shown by Equation (2.25). The apparent heating, however, switches from the time derivative ($\frac{\partial Q}{\partial t}$ in Equation (2.25)) to the gradient (∇Q in Equation (2.32)) of the real heat source. Unlike the T representation, the q representation represents a set of three coupled partial differential equations to be solved for the three components of the heat flux vector.

The relationship between the T representation and the q representation can be better understood by introducing a heat flux potential,

$$\bar{q} = \nabla \phi. \quad (2.33)$$

Substituting Equation (2.33) into (2.32) gives

$$\nabla \left\{ \left[\nabla^2 \phi + \tau_r \frac{\partial}{\partial t} (\nabla^2 \phi) \right] - \left[Q + \tau_r \frac{\partial Q}{\partial t} \right] \right\} = \nabla \left\{ \frac{1}{\alpha} \frac{\partial \phi}{\partial t} + \frac{\tau_q}{\alpha} \frac{\partial^2 \phi}{\partial t^2} \right\}. \quad (2.34)$$

A general solution of Equation (2.34) is

$$\nabla^2 \phi + \tau_r \frac{\partial}{\partial t} (\nabla^2 \phi) - \left[Q + \tau_r \frac{\partial Q}{\partial t} \right] = \frac{1}{\alpha} \frac{\partial \phi}{\partial t} + \frac{\tau_q}{\alpha} \frac{\partial^2 \phi}{\partial t^2} + f(t) \quad (2.35)$$

With $f(t)$ being an arbitrary function of time. Except for a sign difference in front of the apparent heat source and the arbitrary time function, Equation (2.35) governing the heat flux potential is identical to Equation (2.25) governing the temperature. It is thus informative to conclude that the heat flux potential has a very similar behavior to temperature because the fundamental characteristics of a differential equation are dictated by the highest order differentials.

In a multidimensional problem, the heat flux potential provides a powerful transformation to solve the coupled differential equations shown by Equation (2.32). In fact, the heat flux potential is comparable with the Lamé potential in the theory of elasticity, where Navier's equation describing the conservation of momentum is decoupled in the same fashion. The q representation, especially for one-dimensional problems, is more convenient to use for problems involving a flux-specified boundary condition. It avoids the use of Equation (2.29), and hence the complicated conversion between the temperature gradient and the heat flux vector, in solving the boundary value problems.

2.3 Previous Work

The heat transport equations used to describe the thermal behavior of microstructures are expressed as [Tzou 1996] [Özsisik 1994]:

$$-\nabla \cdot \bar{q} + Q = \rho C_p \frac{\partial T}{\partial t}, \quad (2.36)$$

$$\bar{q} + \tau_q \frac{\partial \bar{q}}{\partial t} = -K \left[\nabla T + \tau_T \frac{\partial}{\partial t} [\nabla T] \right], \quad (2.37)$$

where $\bar{q} = (q_1, q_2, q_3)$ is heat flux, T is temperature, K is conductivity, C_p is specific heat, ρ is density, Q is a heat source, τ_q and τ_T are positive constants, which are the time lags of the heat flux and temperature gradient, respectively. In the classical theory of diffusion, the heat flux vector (\bar{q}) and the temperature gradient (∇T) across a material volume are assumed to occur at the same instant of time. They satisfy the Fourier's law of heat conduction:

$$\bar{q}(x, y, z, t) = -K \nabla T(x, y, z, t). \quad (2.38)$$

However, if the scale in one direction is at the sub-microscale, i.e., the order of $0.1 \mu\text{m}$, then the heat flux and temperature gradient in this direction will occur at different times, as shown in Equation (2.37) [Tzou 1996]. The significance of the heat transfer Equations (2.36) and (2.37) which is different from the classical heat transfer equations has been discussed in the previous sections.

Analytic and numerical methods for solving the above coupled Equations (2.36) and (2.37) have been widely investigated [Tzou 1995, 2001] [Özsisik 1994] [Chiffell 1994] [Wang 2000, 2001] [Antaki 1998] [Tang 1999] [Lin 1997] [Al-Nimr 2000] [Chen 2000] [Dai 1999, 2000, 2001a, b].

In [Tzou 1996] and [Özisik 1994], Equations (2.36) and (2.37) were considered in one dimension and eliminated the heat flux \bar{q} to obtain a dimensionless heat transport equation as follows:

$$A \frac{\partial T}{\partial t} + B \frac{\partial^2 T}{\partial t^2} = \frac{\partial^2 T}{\partial x^2} + C \frac{\partial^3 T}{\partial x^2 \partial t} + G, \quad (2.39)$$

where $A = \frac{\rho C_P}{K}$, $B = \frac{\tau_q \rho C_P}{K}$, $C = \tau_T$ and $G = \frac{1}{K} \left(Q + \tau_q \frac{\partial Q}{\partial t} \right)$. They studied the lagging behavior by solving the above heat transport Equation (2.39) without body heating in a semi-infinite interval, $[0, +\infty)$. The solution was obtained by using the Laplace transform method and the Riemann-sum approximation for the inversion [Chiffell 1994].

The work in [Özisik 1994] contains three major components: a thorough review of the research emphasizing engineering applications of the thermal wave theory, special features in the thermal wave propagation, and the thermal wave model in relation to the microscopic two-step model. For the sake of convenience, the research works are classified according to their individual emphases. Special features in thermal wave propagation include the sharp wavefront and rate effects, the thermal shock phenomenon, the thermal resonance phenomenon, and reflections and reflections of thermal waves across a material interface. By employing the dual-phase-lag concept, the authors show that the energy equation may be reduced to that governing the heat transport through the metal lattice in the microscopic two-step model. The dual-phase-lag concept can thus capture the microscopic mechanisms in some limiting cases.

Tzou and Chiu also studied the temperature-dependent thermal lagging in ultrafast laser heating [Tzou 2001]. Temperature-dependent phase-lags are incorporated in the

dual-phase-lag (DPL) model to fully describe the experimental data of femtosecond (f/s) laser heating on gold films of various thicknesses in the sub-micro range. An explicit finite difference algorithm is developed to perform the nonlinear analysis, which recovers the Crank-Nicholson stability criterion in the special case of Fourier diffusion. The exponents in the temperature-dependent thermal properties are determined by minimizing the mean error between the numerical and experimental results. The lagging model with temperature-dependent thermal properties enables a consistent description of all the available experimental data for ultrafast heating on gold films.

Wang and co-workers developed methods of measuring the phase-lags of the heat flux and the temperature gradient and obtained analytical solutions for 1D, 2D and 3D heat conduction domains under essentially arbitrary initial and boundary conditions. Solution structure theorems were also developed for both mixed and Cauchy problems of dual-phase-lagging heat conduction equations [Wang 2000, 2001]. In [Wang 2000], the dual-phase-lagging heat conduction equation is shown to be well-posed in a finite 1D region under Dirichlet, Neumann or Robin boundary conditions. Two solution structure theorems are developed for dual-phase-lagging heat conduction equations under linear boundary conditions. These theorems express contributions (to the temperature field) of the initial temperature distribution and the source term by that of the initial time-rate change of the temperature. It reveals the structure of the temperature field and considerably simplifies the development of solutions of dual-phase-lagging heat conduction equations. In [Wang 2001], the dual-phase-lagging heat conduction equation is shown to be a unique solution for a finite region of dimension n ($n \geq 2$) under Dirichlet, Neumann or Robin boundary conditions. The solution is also stable with respect to initial

conditions. The work is of fundamental importance in applying the dual-phase-lagging model for the microscale heat conduction of high-rate heat flux.

Tang and Araki introduce a generalized macroscopic model in treating the transient heat conduction problems in finite rigid slabs irradiated by short-pulse lasers [Tang 1999]. The analytical solution is derived by using Green's function method and finite integral transform technique. Various behaviors of conduction heat transfer-such as wave, wavelike, and diffusion-are exhibited by adjusting the relaxation parameters. Then detailed discussions have been given on the interrelations among these behaviors. The calculated temperature responses by this model are compared with two literature results measured under extremely low temperature and ultra-high speed heating, respectively. The calculations show good agreement with the experimental data.

Lin and co-workers obtained an analytic solution using the Fourier series [Lin 1997]. An exact solution, using the method of separation of variables, to the universal constitutive equation between the heat flux vector and the temperature gradient for a one-dimensional problem is addressed. Parts of the results are different from those by Tzou [Tzou 1995d]. The aim is to present a convenient approach to the short-pulse laser heating problem by virtue of the unified heat conduction equation.

Al-Nimr and Arpaci proposed a new approach, based on the physical decoupling of the hyperbolic two-step model, to describe the thermal behavior of a thin metal film exposed to picoseconds thermal pulses [Al-Nimr 2000]. The approach is based on the assumption that the metal film thermal behavior occurs in two separate stages. In the first stage, electron gas transmits its energy to the solid lattice through electron-phonon coupling and other mechanisms of energy transport are negligible. In the second stage,

electron gas and solid lattice are in thermal equilibrium, the energy transfer through electron-phonon coupling is negligible, and thermal diffusion dominates. The proposed approach eliminates the coupling between the energy equations and the reduced differential equations are easier to handle. The proposed approach applies to metal films whenever the dimensionless parameter $\frac{GL^2}{K_e}$ is much larger than one.

Chen and Beraun employed the corrective smoothed particle method to obtain a numerical solution of ultrashort laser pulse interactions with metal films [Chen 2000]. A dual-hyperbolic two-step radiation heating model is presented to investigate ultrashort laser pulse interactions with metal films. This model extends Qiu and Tien's theory by including the effect of heat conduction in the lattice. In addition, the depth distribution of laser intensity is modified by adding the ballistic range to the optical penetration depth. The effects of temperature dependence of the thermal physical properties also are examined. For comparison, the proposed model and the existing theories-the parabolic two-temperature model, Qiu and Tien's theory, and Fourier's law-are solved using a mesh-free particle method. Numerical analysis is performed with gold films; the results are compared with experimental data of Qiu, Jubhasz, Suarez, Bron, and Tien, and Wellershoff, Hohlfeld, Gudde, and Matthais. It is shown that this current model predicts more accurate thermal response than the existing theories considered in this study. It is also found that the inclusion of the ballistic effect to the depth distribution of laser intensity significantly improves the melting threshold fluence prediction.

Dai and Nassar developed a two-level finite difference scheme of the Crank-Nicholson type by introducing an intermediate function for solving Equation (2.39) in a finite interval [Dai 1999]. It is shown that the scheme is unconditionally stable by the

discrete energy method. The scheme has been generalized to a three-dimensional rectangular thin film case where the thickness is at the sub-microscale [Dai 2001a]. Further, Dai and Nassar developed high-order unconditionally stable two-level compact finite difference schemes for solving Equation (2.39) in one- and three-dimensional thin films, respectively [Dai 2001b, 2002].

CHAPTER 3

MATHEMATICAL MODEL AND FINITE

DIFFERENCE SCHEME

3.1 Governing Equations

3.1.1 Problem Description

In this chapter, we consider the case where the heat transport is in a microsphere. Microvoids may be formed in thermal processing of materials owing to thermal expansion. When such defects are initiated in the workpiece, the thermal energy in the neighborhood of the defects may be amplified, resulting in severe material damage and, consequently, total failure of the thermal processing. A detailed understanding of the way in which the local defects dissipate the thermal energy is then necessary not only to avoid the damage but also to improve the efficiency of thermal processing [Tzou 1996].

3.1.2 Three-Dimensional Spherical Coordinates

Figure 3.1 shows the three-dimensional spherical coordinates. Point P is given by spherical coordinates r, θ, φ , where r is the length of OP , ranging from 0 to ∞ ; θ is the angle between OP and the positive z -axis, ranging from 0 to π ; φ is the angle between the projection of OP on the xy -plane with the positive x -axis, ranging from 0 to 2π [Kuipers 1969].

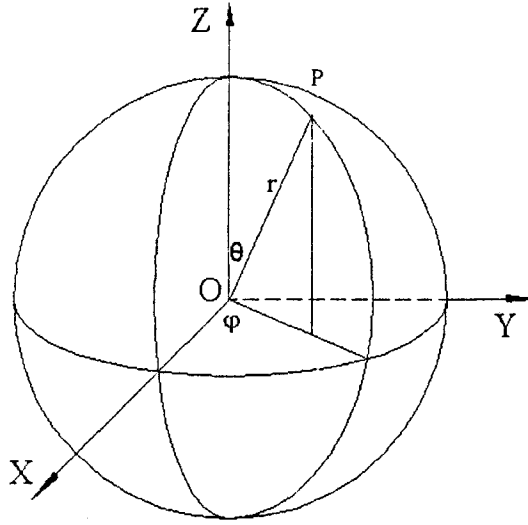


Figure 3.1 The three-dimensional spherical coordinates.

3.1.3 Governing Equations

Equation (2.39) used to describe the thermal behavior of a microsphere in three-dimensional spherical coordinates can be written as follows:

$$\begin{aligned}
 & \rho C_p \left(\frac{\partial T}{\partial t} + \tau_q \frac{\partial^2 T}{\partial t^2} \right) \\
 = & \frac{K}{r^2} \frac{\partial}{\partial r} \left(r^2 \frac{\partial T}{\partial r} \right) + \tau_r \frac{K}{r^2} \frac{\partial}{\partial r} \left(r^2 \frac{\partial^2 T}{\partial r \partial t} \right) \\
 & + \frac{K}{r^2 \sin \theta} \frac{\partial}{\partial \theta} \left(\sin \theta \frac{\partial T}{\partial \theta} \right) + \tau_r \frac{K}{r^2 \sin \theta} \frac{\partial}{\partial \theta} \left(\sin \theta \frac{\partial^2 T}{\partial \theta \partial t} \right) \\
 & + \frac{K}{r^2 \sin^2 \theta} \left(\frac{\partial^2 T}{\partial \varphi^2} \right) + \tau_r \frac{K}{r^2 \sin^2 \theta} \left(\frac{\partial^3 T}{\partial \varphi^2 \partial t} \right) \\
 & + Q, \tag{3.1}
 \end{aligned}$$

where r , θ and φ are the spherical coordinates with $0 < r < L$, $0 < \theta < \pi$, and $0 \leq \varphi \leq 2\pi$.

The initial and boundary conditions are assumed to be

$$T(r, \theta, \varphi, 0) = 0, \quad \frac{\partial T(r, \theta, \varphi, 0)}{\partial t} = 0; \quad (3.2)$$

and

$$\frac{\partial T(L, \theta, \varphi, t)}{\partial r} = 0, \quad (3.3)$$

$$\frac{\partial T(r, 0, \varphi, t)}{\partial \theta} = \frac{\partial T(r, \pi, \varphi, t)}{\partial \theta} = 0, \quad (3.4)$$

$$T(r, \theta, \varphi, t) = T(r, \theta, 2\pi + \varphi, t). \quad (3.5)$$

Such boundary conditions arise from the case where the sphere is subjected to a short-pulse laser irradiation. Hence, one may assume no heat losses from the spherical surface in the short time response [Tzou 1996]. However, other boundary conditions can be applied without difficulty. Because the well-posedness of the dual-phase-lagging heat conduction equation, Equation (2.39), has been discussed in [Wang 2001, 2002], we assume that the solution of the above initial and boundary value problem is smooth, and because the exact solution is difficult to obtain in general, our interest is in developing a finite difference scheme for solving the above initial and boundary value problem.

3.2 Finite Difference Scheme

3.2.1 Notations

We denote $T_{i,j,k}^n$ as the numerical approximation of $T(i\Delta r, j\Delta\theta, k\Delta\varphi, n\Delta t)$, where Δr , $\Delta\theta$, $\Delta\varphi$ and Δt are the r , θ , φ directional spatial and temporal mesh sizes, respectively, and $0 \leq i \leq N_r$, $0 \leq j \leq N_\theta$, $0 \leq k \leq N_\varphi$ so that $N_r\Delta r = L$, $N_\theta\Delta\theta = \pi$, and $N_\varphi\Delta\varphi = 2\pi$. We use the following difference operators:

$$\nabla_r T_{i,j,k}^n = \frac{T_{i+1,j,k}^n - T_{i,j,k}^n}{\Delta r}, \quad (3.6)$$

$$\nabla_{\bar{r}} T_{i,j,k}^n = \frac{T_{i,j,k}^n - T_{i-1,j,k}^n}{\Delta r}; \quad (3.7)$$

$$\nabla_{\theta} T_{i,j,k}^n = \frac{T_{i,j+1,k}^n - T_{i,j,k}^n}{\Delta \theta}, \quad (3.8)$$

$$\nabla_{\bar{\theta}} T_{i,j,k}^n = \frac{T_{i,j,k}^n - T_{i,j-1,k}^n}{\Delta \theta}; \quad (3.9)$$

and

$$\nabla_{\varphi} T_{i,j,k}^n = \frac{T_{i,j,k+1}^n - T_{i,j,k}^n}{\Delta \varphi}, \quad (3.10)$$

$$\nabla_{\bar{\varphi}} T_{i,j,k}^n = \frac{T_{i,j,k}^n - T_{i,j,k-1}^n}{\Delta \varphi}, \quad (3.11)$$

for r , θ , and φ coordinates, respectively.

3.2.2 Finite Difference Scheme

We develop a three-level finite difference scheme for solving the above initial and boundary problem as follows:

$$\begin{aligned} & \rho C_p \left(\frac{T_{i,j,k}^{n+1} - T_{i,j,k}^{n-1}}{2\Delta t} + \tau_q \frac{T_{i,j,k}^{n+1} - 2T_{i,j,k}^n + T_{i,j,k}^{n-1}}{(\Delta t)^2} \right) \\ &= \frac{K}{r_i^2} P_r \left(\frac{T_{i,j,k}^{n+1} + 2T_{i,j,k}^n + T_{i,j,k}^{n-1}}{4} \right) + \tau_T \frac{K}{r_i^2} P_r \left(\frac{T_{i,j,k}^{n+1} - T_{i,j,k}^{n-1}}{2\Delta t} \right) \\ &+ \frac{K}{r_i^2} \frac{1}{\sin \theta_j} P_{\theta} \left(\frac{T_{i,j,k}^{n+1} + 2T_{i,j,k}^n + T_{i,j,k}^{n-1}}{4} \right) + \frac{K}{r_i^2} \frac{\tau_T}{\sin \theta_j} P_{\theta} \left(\frac{T_{i,j,k}^{n+1} - T_{i,j,k}^{n-1}}{2\Delta t} \right) \\ &+ \frac{K}{r_i^2} \frac{1}{\sin^2 \theta_j} P_{\varphi} \left(\frac{T_{i,j,k}^{n+1} + 2T_{i,j,k}^n + T_{i,j,k}^{n-1}}{4} \right) + \frac{K}{r_i^2} \frac{\tau_T}{\sin^2 \theta_j} P_{\varphi} \left(\frac{T_{i,j,k}^{n+1} - T_{i,j,k}^{n-1}}{2\Delta t} \right) \\ &+ Q_{i,j,k}^n \end{aligned} \quad (3.12)$$

where P_r , P_θ , and P_ϕ are finite difference operators such that

$$P_r(T_{i,j,k}) \equiv r_{i+\frac{1}{2}}^2 \frac{T_{i+1,j,k} - T_{i,j,k}}{(\Delta r)^2} - r_{i-\frac{1}{2}}^2 \frac{T_{i,j,k} - T_{i-1,j,k}}{(\Delta r)^2}, \quad (3.13)$$

$$P_\theta(T_{i,j,k}) \equiv \sin \theta_{j+\frac{1}{2}} \frac{T_{i,j+1,k} - T_{i,j,k}}{(\Delta \theta)^2} - \sin \theta_{j-\frac{1}{2}} \frac{T_{i,j,k} - T_{i,j-1,k}}{(\Delta \theta)^2}, \quad (3.14)$$

and

$$P_\phi(T_{i,j,k}) \equiv \frac{T_{i,j,k+1} - 2T_{i,j,k} + T_{i,j,k-1}}{(\Delta \phi)^2}. \quad (3.15)$$

Here, $r_i = i\Delta r$ and $\theta_j = j\Delta \theta$. The initial and boundary conditions are discretized as

follows:

$$T_{i,j,k}^0 = T_{i,j,k}^1 = 0, \quad (3.16)$$

and

$$\nabla_{\bar{r}} T_{N_r,j,k}^n = 0; \quad (3.17)$$

$$\nabla_{\bar{\theta}} T_{i,1,k}^n = 0, \quad \nabla_{\bar{\theta}} T_{i,N_\theta,k}^n = 0; \quad (3.18)$$

$$T_{i,j,N_\phi+k}^n = T_{i,j,k}^n; \quad (3.19)$$

for any time level n . It should be pointed out that we use a weighted average

$$\frac{T_{i,j,k}^{n+1} + 2T_{i,j,k}^n + T_{i,j,k}^{n-1}}{4} \text{ for stability.}$$

3.3 Stability

We will employ the discrete energy method [Lees 1961, 1966] to show the stability of the scheme, Equations (3.12) ~ (3.19). To this end, we first introduce the definitions of the inner products and norms between the mesh functions $u_{i,j,k}$ and $v_{i,j,k}$.

Let S_h be a set of $\{u = \{u_{i,j,k}\} \mid 0 \leq i \leq N_r, 0 \leq j \leq N_\theta, 0 \leq k \leq N_\varphi\}$. For any $u, v \in S_h$,

the inner products and norms are defined as follows:

$$(u, v) = \Delta r \Delta \theta \Delta \varphi \sum_{i=1}^{N_r-1} \sum_{j=1}^{N_\theta-1} \sum_{k=1}^{N_\varphi} u_{i,j,k} \cdot v_{i,j,k}, \quad (3.20)$$

$$\|u\|^2 = (u, u), \quad (3.21)$$

and

$$\|\nabla_{\bar{r}} u\|_1^2 = (\nabla_{\bar{r}} u, \nabla_{\bar{r}} u)_1 = \Delta r \Delta \theta \Delta \varphi \sum_{i=1}^{N_r} \sum_{j=1}^{N_\theta-1} \sum_{k=1}^{N_\varphi} (\nabla_{\bar{r}} u_{i,j,k})^2 \quad (3.22)$$

and so on. The following lemmas 1 and 2 can be easily obtained.

LEMMA 1. For any n,

$$\begin{aligned} & \Delta r \Delta \theta \Delta \varphi \sum_{i=1}^{N_r-1} \sum_{j=1}^{N_\theta-1} \sum_{k=1}^{N_\varphi} r_i^2 \sin \theta_j (T_{i,j,k}^{n+1} - 2T_{i,j,k}^n + T_{i,j,k}^{n-1}) \cdot (T_{i,j,k}^{n+1} - T_{i,j,k}^{n-1}) \\ &= \Delta r \Delta \theta \Delta \varphi \sum_{i=1}^{N_r-1} \sum_{j=1}^{N_\theta-1} \sum_{k=1}^{N_\varphi} r_i^2 \sin \theta_j \cdot \left[(T_{i,j,k}^{n+1} - T_{i,j,k}^n)^2 - (T_{i,j,k}^n - T_{i,j,k}^{n-1})^2 \right] \\ &= \left\| r \sqrt{\sin \theta} (T^{n+1} - T^n) \right\|^2 - \left\| r \sqrt{\sin \theta} (T^n - T^{n-1}) \right\|^2. \end{aligned} \quad (3.23)$$

LEMMA 2. For any n,

$$\begin{aligned} & \Delta r \Delta \theta \Delta \varphi \sum_{i=1}^{N_r} \sum_{j=1}^{N_\theta-1} \sum_{k=1}^{N_\varphi} \sin \theta_j \left(E^{-\frac{1}{2}} r_i^2 \right) \nabla_{\bar{r}} (T_{i,j,k}^{n+1} + 2T_{i,j,k}^n + T_{i,j,k}^{n-1}) \cdot \nabla_{\bar{r}} (T_{i,j,k}^{n+1} - T_{i,j,k}^{n-1}) \\ &= \left\| \left(E^{-\frac{1}{2}} r \right) \sqrt{\sin \theta} \nabla_{\bar{r}} (T^{n+1} + T^n) \right\|_1^2 - \left\| \left(E^{-\frac{1}{2}} r \right) \sqrt{\sin \theta} \nabla_{\bar{r}} (T^n + T^{n-1}) \right\|_1^2, \end{aligned} \quad (3.24)$$

where $E^{-\frac{1}{2}}$ is a shift operator such that $E^{-\frac{1}{2}} r_i = r_{i-\frac{1}{2}}$.

LEMMA 3. For any mesh functions $T_{i,j,k}$ and $S_{i,j,k}$,

$$\begin{aligned}
\Delta r \sum_{i=1}^{N_r-1} P_r(T_{i,j,k}) \cdot S_{i,j,k} &= -\Delta r \sum_{i=1}^{N_r} r_{i-\frac{1}{2}}^2 \nabla_{\bar{r}} T_{i,j,k} \cdot \nabla_{\bar{r}} S_{i,j,k} - r_{\frac{1}{2}}^2 \nabla_{\bar{r}} T_{1,j,k} \cdot S_{0,j,k} \\
&\quad + r_{N_r-\frac{1}{2}}^2 \nabla_{\bar{r}} T_{N_r,j,k} \cdot S_{N_r,j,k}, \tag{3.25}
\end{aligned}$$

$$\begin{aligned}
\Delta \theta \sum_{j=1}^{N_\theta-1} P_\theta(T_{i,j,k}) \cdot S_{i,j,k} &= -\Delta \theta \sum_{j=1}^{N_\theta} \sin \theta_{j-\frac{1}{2}} \nabla_{\bar{\theta}} T_{i,j,k} \cdot \nabla_{\bar{\theta}} S_{i,j,k} - \sin \theta_{\frac{1}{2}} \nabla_{\bar{\theta}} T_{i,1,k} \cdot S_{i,0,k} \\
&\quad + \sin \theta_{N_\theta-\frac{1}{2}} \nabla_{\bar{\theta}} T_{i,N_\theta,k} \cdot S_{i,N_\theta,k}, \tag{3.26}
\end{aligned}$$

$$\begin{aligned}
\Delta \varphi \sum_{k=1}^{N_\varphi} P_\varphi(T_{i,j,k}) \cdot S_{i,j,k} &= -\Delta \varphi \sum_{k=1}^{N_\varphi+1} \nabla_{\bar{\varphi}} T_{i,j,k} \cdot \nabla_{\bar{\varphi}} S_{i,j,k} - \nabla_{\bar{\varphi}} T_{i,j,1} \cdot S_{i,j,0} \\
&\quad + \nabla_{\bar{\varphi}} T_{i,j,N_\varphi+1} \cdot S_{i,j,N_\varphi}. \tag{3.27}
\end{aligned}$$

Proof. One may obtain from Equation (3.13) that

$$\begin{aligned}
\Delta r \sum_{i=1}^{N_r-1} P_r(T_{i,j,k}) \cdot S_{i,j,k} &= \Delta r \sum_{i=1}^{N_r-1} r_{i+\frac{1}{2}}^2 \frac{T_{i+1,j,k} - T_{i,j,k}}{(\Delta r)^2} S_{i,j,k} - \Delta r \sum_{i=1}^{N_r-1} r_{i-\frac{1}{2}}^2 \frac{T_{i,j,k} - T_{i-1,j,k}}{(\Delta r)^2} S_{i,j,k} \\
&= \Delta r \sum_{i=2}^{N_r} r_{i-\frac{1}{2}}^2 \frac{T_{i,j,k} - T_{i-1,j,k}}{(\Delta r)^2} S_{i-1,j,k} - \Delta r \sum_{i=1}^{N_r-1} r_{i-\frac{1}{2}}^2 \frac{T_{i,j,k} - T_{i-1,j,k}}{(\Delta r)^2} S_{i,j,k} \\
&= \Delta r \sum_{i=1}^{N_r} r_{i-\frac{1}{2}}^2 \frac{T_{i,j,k} - T_{i-1,j,k}}{(\Delta r)^2} S_{i-1,j,k} - \Delta r \sum_{i=1}^{N_r} r_{i-\frac{1}{2}}^2 \frac{T_{i,j,k} - T_{i-1,j,k}}{(\Delta r)^2} S_{i,j,k} \\
&\quad - r_{\frac{1}{2}}^2 \frac{T_{1,j,k} - T_{0,j,k}}{\Delta r} S_{0,j,k} + r_{N_r-\frac{1}{2}}^2 \frac{T_{N_r,j,k} - T_{N_r-1,j,k}}{\Delta r} S_{N_r,j,k} \\
&= -\Delta r \sum_{i=1}^{N_r} r_{i-\frac{1}{2}}^2 \nabla_{\bar{r}} T_{i,j,k} \cdot \nabla_{\bar{r}} S_{i,j,k} - r_{\frac{1}{2}}^2 \frac{T_{1,j,k} - T_{0,j,k}}{\Delta r} S_{0,j,k} \\
&\quad + r_{N_r-\frac{1}{2}}^2 \frac{T_{N_r,j,k} - T_{N_r-1,j,k}}{\Delta r} S_{N_r,j,k} \\
&= -\Delta r \sum_{i=1}^{N_r} r_{i-\frac{1}{2}}^2 \nabla_{\bar{r}} T_{i,j,k} \cdot \nabla_{\bar{r}} S_{i,j,k} - r_{\frac{1}{2}}^2 \nabla_{\bar{r}} T_{1,j,k} \cdot S_{0,j,k} \\
&\quad + r_{N_r-\frac{1}{2}}^2 \nabla_{\bar{r}} T_{N_r,j,k} S_{N_r,j,k}. \tag{3.28}
\end{aligned}$$

Equations (3.14) and (3.15) can be obtained using similar arguments.

It is noted that if both $T_{i,j,k}$ and $S_{i,j,k}$ satisfy Equations (3.17) ~ (3.19), then

Equations (3.25) ~ (3.27) can be simplified as follows:

$$\Delta r \sum_{i=1}^{N_r-1} P_r(T_{i,j,k}) \cdot S_{i,j,k} = -\Delta r \sum_{i=1}^{N_r} r_{i-\frac{1}{2}}^2 \nabla_{\bar{r}} T_{i,j,k} \cdot \nabla_{\bar{r}} S_{i,j,k}, \quad (3.29)$$

$$\Delta \theta \sum_{j=1}^{N_\theta-1} P_\theta(T_{i,j,k}) \cdot S_{i,j,k} = -\Delta \theta \sum_{j=1}^{N_\theta} \sin \theta_{j-\frac{1}{2}} \nabla_{\bar{\theta}} T_{i,j,k} \cdot \nabla_{\bar{\theta}} S_{i,j,k}, \quad (3.30)$$

$$\Delta \varphi \sum_{k=1}^{N_\varphi} P_\varphi(T_{i,j,k}) \cdot S_{i,j,k} = -\Delta \varphi \sum_{k=1}^{N_\varphi+1} \nabla_{\bar{\varphi}} T_{i,j,k} \cdot \nabla_{\bar{\varphi}} S_{i,j,k}. \quad (3.31)$$

THEOREM. Assume that $T_{i,j,k}$ and $S_{i,j,k}$ satisfy Equation (3.12) and the same initial and boundary conditions, Equation (3.16) and Equations (3.17) ~ (3.19), but different source terms Q_1 and Q_2 . Let $u_{i,j,k}^n = T_{i,j,k}^n - S_{i,j,k}^n$. Then $u_{i,j,k}^n$ satisfies, for any $0 < n\Delta t \leq t_0$,

$$\begin{aligned} & 4\rho C_p \tau_q \left\| r \sqrt{\sin \theta} (u^{n+1} - u^n) \right\|_1^2 + K(\Delta t)^2 \left\| (E^{-\frac{1}{2}} r) \sqrt{\sin \theta} \nabla_{\bar{r}} (u^{n+1} + u^n) \right\|_1^2 \\ & + K(\Delta t)^2 \left\| \sqrt{E^{-\frac{1}{2}} \sin \theta} \nabla_{\bar{\theta}} (u^{n+1} + u^n) \right\|_1^2 + K(\Delta t)^2 \left\| \frac{1}{\sqrt{\sin \theta}} \nabla_{\bar{\varphi}} (u^{n+1} + u^n) \right\|_1^2 \\ & \leq 2t_0 \Delta t \max_{0 \leq m \leq n} \|g^m\|^2, \end{aligned} \quad (3.32)$$

where $g_j^n = (Q_1)_j^n - (Q_2)_j^n$. Hence, the scheme is unconditionally stable with respect to the source term.

Proof. It can be seen that $u_{i,j,k}^n$ satisfies

$$\rho C_p \left(\frac{u_{i,j,k}^{n+1} - u_{i,j,k}^{n-1}}{2\Delta t} + \tau_q \frac{u_{i,j,k}^{n+1} - 2u_{i,j,k}^n + u_{i,j,k}^{n-1}}{(\Delta t)^2} \right)$$

$$\begin{aligned}
&= \frac{K}{r_i^2} P_r \left(\frac{u_{i,j,k}^{n+1} + 2u_{i,j,k}^n + u_{i,j,k}^{n-1}}{4} \right) + \tau_T \frac{K}{r_i^2} P_r \left(\frac{u_{i,j,k}^{n+1} - u_{i,j,k}^{n-1}}{2\Delta t} \right) \\
&\quad + \frac{K}{r_i^2} \frac{1}{\sin \theta_j} P_\theta \left(\frac{u_{i,j,k}^{n+1} + 2u_{i,j,k}^n + u_{i,j,k}^{n-1}}{4} \right) + \frac{K}{r_i^2} \frac{\tau_T}{\sin \theta_j} P_\theta \left(\frac{u_{i,j,k}^{n+1} - u_{i,j,k}^{n-1}}{2\Delta t} \right) \\
&\quad + \frac{K}{r_i^2} \frac{1}{\sin^2 \theta_j} P_\varphi \left(\frac{u_{i,j,k}^{n+1} + 2u_{i,j,k}^n + u_{i,j,k}^{n-1}}{4} \right) + \frac{K}{r_i^2} \frac{\tau_T}{\sin^2 \theta_j} P_\varphi \left(\frac{u_{i,j,k}^{n+1} - u_{i,j,k}^{n-1}}{2\Delta t} \right) \\
&\quad + g_{i,j,k}^n, \tag{3.33}
\end{aligned}$$

and the initial and boundary conditions:

$$u_{i,j,k}^0 = u_{i,j,k}^1 = 0, \tag{3.34}$$

and

$$\nabla_{\bar{r}} u_{1,j,k}^n = 0, \quad \nabla_{\bar{r}} u_{N_r,j,k}^n = 0, \tag{3.35}$$

$$\nabla_{\bar{\theta}} u_{i,1,k}^n = 0, \quad \nabla_{\bar{\theta}} u_{i,N_\theta,k}^n = 0, \tag{3.36}$$

$$u_{i,j,N_\varphi+k}^n = u_{i,j,k}^n. \tag{3.37}$$

Here, it should be pointed out that we assume $\nabla_{\bar{r}} u_{1,j,k}^n = 0$ for simplicity. Multiplying Equation (3.33) by $4(\Delta t)^2 \Delta r \cdot r_i^2 \sin \theta_j (u_{i,j,k}^{n+1} - u_{i,j,k}^{n-1})$ and summing i, j, k ($1 \leq i \leq N_r - 1$, $1 \leq j \leq N_\theta - 1$, $1 \leq k \leq N_\varphi$), we obtain by Lemmas 1 ~ 3 and Equations (3.35) ~ (3.37)

$$\begin{aligned}
&2\rho C_p \Delta t \left[\left\| r \sqrt{\sin \theta} (u^{n+1} - u^{n-1}) \right\|^2 + 4\rho C_p \tau_q \left[\left\| r \sqrt{\sin \theta} (u^{n+1} - u^n) \right\|^2 \right. \right. \\
&\quad \left. \left. - \left\| r \sqrt{\sin \theta} (u^n - u^{n-1}) \right\|^2 \right] \right] \\
&= -K(\Delta t)^2 \left[\left\| \left(E^{-\frac{1}{2}} r \right) \sqrt{\sin \theta} \nabla_{\bar{r}} (u^{n+1} + u^n) \right\|_1^2 - \left\| \left(E^{-\frac{1}{2}} r \right) \sqrt{\sin \theta} \nabla_{\bar{r}} (u^n + u^{n-1}) \right\|_1^2 \right]
\end{aligned}$$

$$\begin{aligned}
& -2K\Delta t\tau_r\left\|\left(E^{-\frac{1}{2}}r\right)\sqrt{\sin\theta}\nabla_{\bar{r}}\left(u^{n+1}-u^{n-1}\right)\right\|_1^2 \\
& -K(\Delta t)^2\left[\left\|\sqrt{E^{-\frac{1}{2}}\sin\theta}\nabla_{\bar{\theta}}\left(u^{n+1}+u^n\right)\right\|_1^2-\left\|\sqrt{E^{-\frac{1}{2}}\sin\theta}\nabla_{\bar{\theta}}\left(u^n+u^{n-1}\right)\right\|_1^2\right] \\
& -2K\Delta t\tau_r\left\|\sqrt{E^{-\frac{1}{2}}\sin\theta}\nabla_{\bar{\theta}}\left(u^{n+1}-u^{n-1}\right)\right\|_1^2 \\
& -K(\Delta t)^2\left[\left\|\frac{1}{\sqrt{\sin\theta}}\nabla_{\bar{\varphi}}\left(u^{n+1}+u^n\right)\right\|_1^2-\left\|\frac{1}{\sqrt{\sin\theta}}\nabla_{\bar{\varphi}}\left(u^n+u^{n-1}\right)\right\|_1^2\right] \\
& -2K\Delta t\tau_r\left\|\frac{1}{\sqrt{\sin\theta}}\nabla_{\bar{\varphi}}\left(u^{n+1}-u^{n-1}\right)\right\|_1^2 \\
& +\left(g^n,4(\Delta t)^2r^2\sin\theta\left(u^{n+1}-u^{n-1}\right)\right). \tag{3.38}
\end{aligned}$$

By Cauchy-Schwarz's inequality, we obtain

$$\begin{aligned}
& 4(\Delta t)^2\left(g^n,r^2\sin\theta\left(u^{n+1}-u^{n-1}\right)\right) \\
& \leq 2(\Delta t)^2\left[\|g^n\|^2+\|r^2\sin\theta\left(u^{n+1}-u^{n-1}\right)\|^2\right] \\
& \leq 2(\Delta t)^2\left[\|g^n\|^2+L^2\|r\sqrt{\sin\theta}\left(u^{n+1}-u^{n-1}\right)\|^2\right]. \tag{3.39}
\end{aligned}$$

Substituting Equation (3.39) into Equation (3.38) gives

$$\begin{aligned}
& \Delta t\left(2\rho C_p-2\Delta tL^2\right)\|r\sqrt{\sin\theta}\left(u^{n+1}-u^{n-1}\right)\|^2 \\
& +4\rho C_p\tau_q\left[\|r\sqrt{\sin\theta}\left(u^{n+1}-u^n\right)\|^2-\|r\sqrt{\sin\theta}\left(u^n-u^{n-1}\right)\|^2\right] \\
& +K(\Delta t)^2\left[\left\|\left(E^{-\frac{1}{2}}r\right)\sqrt{\sin\theta}\nabla_{\bar{r}}\left(u^{n+1}+u^n\right)\right\|_1^2-\left\|\left(E^{-\frac{1}{2}}r\right)\sqrt{\sin\theta}\nabla_{\bar{r}}\left(u^n+u^{n-1}\right)\right\|_1^2\right] \\
& +2K\Delta t\tau_r\left\|\left(E^{-\frac{1}{2}}r\right)\sqrt{\sin\theta}\nabla_{\bar{r}}\left(u^{n+1}-u^{n-1}\right)\right\|_1^2
\end{aligned}$$

$$\begin{aligned}
& + K(\Delta t)^2 \left[\left\| \sqrt{E^{-\frac{1}{2}} \sin \theta} \nabla_{\bar{\theta}} (u^{n+1} + u^n) \right\|_1^2 - \left\| \sqrt{E^{-\frac{1}{2}} \sin \theta} \nabla_{\bar{\theta}} (u^n + u^{n-1}) \right\|_1^2 \right] \\
& + 2K\Delta t \tau_r \left\| \sqrt{E^{-\frac{1}{2}} \sin \theta} \nabla_{\bar{\theta}} (u^{n+1} - u^{n-1}) \right\|_1^2 \\
& + K(\Delta t)^2 \left[\left\| \frac{1}{\sqrt{\sin \theta}} \nabla_{\bar{\varphi}} (u^{n+1} + u^n) \right\|_1^2 - \left\| \frac{1}{\sqrt{\sin \theta}} \nabla_{\bar{\varphi}} (u^n + u^{n-1}) \right\|_1^2 \right] \\
& + 2K\Delta t \tau_r \left\| \frac{1}{\sqrt{\sin \theta}} \nabla_{\bar{\varphi}} (u^{n+1} - u^{n-1}) \right\|_1^2 \\
& \leq 2\Delta t^2 \|g^n\|^2. \tag{3.40}
\end{aligned}$$

Choosing Δt so that $2\rho C_p - 2\Delta t L^2 \geq 0$, dropping out the first, forth, sixth and eighth terms on the left-hand-side of Equation (3.40) and then using Equation (3.34), we obtain

$$\begin{aligned}
& 4\rho C_p \tau_q \left\| r \sqrt{\sin \theta} (u^{n+1} - u^n) \right\|_1^2 + K(\Delta t)^2 \left\| (E^{-\frac{1}{2}} r) \sqrt{\sin \theta} \nabla_{\bar{r}} (u^{n+1} + u^n) \right\|_1^2 \\
& + K(\Delta t)^2 \left\| \sqrt{E^{-\frac{1}{2}} \sin \theta} \nabla_{\bar{\theta}} (u^{n+1} + u^n) \right\|_1^2 + K(\Delta t)^2 \left\| \frac{1}{\sqrt{\sin \theta}} \nabla_{\bar{\varphi}} (u^{n+1} + u^n) \right\|_1^2 \\
& \leq 4\rho C_p \tau_q \left\| r \sqrt{\sin \theta} (u^n - u^{n-1}) \right\|_1^2 + K(\Delta t)^2 \left\| (E^{-\frac{1}{2}} r) \sqrt{\sin \theta} \nabla_{\bar{r}} (u^n + u^{n-1}) \right\|_1^2 \\
& + K(\Delta t)^2 \left\| \sqrt{E^{-\frac{1}{2}} \sin \theta} \nabla_{\bar{\theta}} (u^n + u^{n-1}) \right\|_1^2 + K(\Delta t)^2 \left\| \frac{1}{\sqrt{\sin \theta}} \nabla_{\bar{\varphi}} (u^n + u^{n-1}) \right\|_1^2 \\
& + 2(\Delta t)^2 \|g^n\|^2 \\
& \leq \dots \\
& \leq 4\rho C_p \tau_q \left\| r \sqrt{\sin \theta} (u^1 - u^0) \right\|_1^2 + K(\Delta t)^2 \left\| (E^{-\frac{1}{2}} r) \sqrt{\sin \theta} \nabla_{\bar{r}} (u^1 + u^0) \right\|_1^2
\end{aligned}$$

$$\begin{aligned}
& + K(\Delta t)^2 \left\| \sqrt{E^{-\frac{1}{2}} \sin \theta} \nabla_{\bar{\theta}} (u^1 + u^0) \right\|_1^2 + K(\Delta t)^2 \left\| \frac{1}{\sqrt{\sin \theta}} \nabla_{\bar{\theta}} (u^1 + u^0) \right\|_1^2 \\
& + 2n\Delta t^2 \max_{0 \leq m \leq n} \|g^m\|^2 \\
& \leq 2t_0\Delta t \max_{0 \leq m \leq n} \|g^m\|^2, \tag{3.41}
\end{aligned}$$

which complete the proof.

3.4 Algorithm

3.4.1 Solving the Linear System

From Equations (3.12) ~ (3.15), we have a linear system with three time levels as following:

$$A\bar{T}^{n+1} = B\bar{T}^n + C\bar{T}^{n-1} + \bar{Q}^n, \tag{3.42}$$

in which A , B , and C are coefficient matrices for the temperature vector \bar{T} on the three different time levels $n+1$, n and $n-1$, respectively. When we calculate the temperature \bar{T}^{n+1} on time level $n+1$, the temperature \bar{T}^n on time level n , \bar{T}^{n-1} on time level $n-1$, and the heat source \bar{Q}^n on time level n are known. A general equation in Equation (3.42) is given as:

$$\begin{aligned}
& a_1 T_{i,j,k}^{n+1} + a_2 T_{i-1,j,k}^{n+1} + a_3 T_{i+1,j,k}^{n+1} + a_4 T_{i,j-1,k}^{n+1} + a_5 T_{i,j+1,k}^{n+1} + a_6 T_{i,j,k-1}^{n+1} + a_7 T_{i,j,k+1}^{n+1} \\
& = b_1 T_{i,j,k}^n + b_2 T_{i-1,j,k}^n + b_3 T_{i+1,j,k}^n + b_4 T_{i,j-1,k}^n + b_5 T_{i,j+1,k}^n + b_6 T_{i,j,k-1}^n + b_7 T_{i,j,k+1}^n \\
& + c_1 T_{i,j,k}^{n-1} + c_2 T_{i-1,j,k}^{n-1} + c_3 T_{i+1,j,k}^{n-1} + c_4 T_{i,j-1,k}^{n-1} + c_5 T_{i,j+1,k}^{n-1} + c_6 T_{i,j,k-1}^{n-1} + c_7 T_{i,j,k+1}^{n-1} \\
& + 4 \frac{1}{\rho C_p} (\Delta t)^2 r_1 \theta_1^2 g_{i,j,k}^n, \tag{3.43}
\end{aligned}$$

where

$$\begin{aligned}
a_1 = & 2(\Delta t)r_1\theta_1^2 + 4\tau_q r_1\theta_1^2 + \frac{K}{\rho C_p}(\Delta t)^2 \frac{r_2 + r_3}{(\Delta r)^2} \theta_1^2 + 2\tau_T \frac{K}{\rho C_p}(\Delta t) \frac{r_2 + r_3}{(\Delta r)^2} \theta_1^2 \\
& + \frac{K}{\rho C_p}(\Delta t)^2 \frac{\theta_2 + \theta_3}{(\Delta \theta)^2} \theta_1 + 2\tau_T \frac{K}{\rho C_p}(\Delta t) \frac{\theta_2 + \theta_3}{(\Delta \theta)^2} \theta_1 \\
& + 2 \frac{K}{\rho C_p} \frac{(\Delta t)^2}{(\Delta \varphi)^2} + 4\tau_T \frac{K}{\rho C_p} \frac{\Delta t}{(\Delta \varphi)^2}, \tag{3.44}
\end{aligned}$$

$$a_2 = -\frac{K}{\rho C_p}(\Delta t)^2 \frac{r_3}{(\Delta r)^2} \theta_1^2 - 2\tau_T \frac{K}{\rho C_p}(\Delta t) \frac{r_3}{(\Delta r)^2} \theta_1^2, \tag{3.45}$$

$$a_3 = -\frac{K}{\rho C_p}(\Delta t)^2 \frac{r_2}{(\Delta r)^2} \theta_1^2 - 2\tau_T \frac{K}{\rho C_p}(\Delta t) \frac{r_2}{(\Delta r)^2} \theta_1^2, \tag{3.46}$$

$$a_4 = -\frac{K}{\rho C_p}(\Delta t)^2 \frac{\theta_3}{(\Delta \theta)^2} \theta_1 - 2\tau_T \frac{K}{\rho C_p}(\Delta t) \frac{\theta_3}{(\Delta \theta)^2} \theta_1, \tag{3.47}$$

$$a_5 = -\frac{K}{\rho C_p}(\Delta t)^2 \frac{\theta_2}{(\Delta \theta)^2} \theta_1 - 2\tau_T \frac{K}{\rho C_p}(\Delta t) \frac{\theta_2}{(\Delta \theta)^2} \theta_1, \tag{3.48}$$

$$a_6 = -\frac{K}{\rho C_p} \frac{(\Delta t)^2}{(\Delta \varphi)^2} - 2\tau_T \frac{K}{\rho C_p} \frac{\Delta t}{(\Delta \varphi)^2}, \tag{3.49}$$

$$a_7 = -\frac{K}{\rho C_p} \frac{(\Delta t)^2}{(\Delta \varphi)^2} - 2\tau_T \frac{K}{\rho C_p} \frac{\Delta t}{(\Delta \varphi)^2}, \tag{3.50}$$

$$\begin{aligned}
b_1 = & 8\tau_q r_1\theta_1^2 - 2 \frac{K}{\rho C_p}(\Delta t)^2 \frac{r_2 + r_3}{(\Delta r)^2} \theta_1^2 \\
& - 2 \frac{K}{\rho C_p}(\Delta t)^2 \frac{\theta_2 + \theta_3}{(\Delta \theta)^2} \theta_1 - 4 \frac{K}{\rho C_p} \frac{(\Delta t)^2}{(\Delta \varphi)^2}, \tag{3.51}
\end{aligned}$$

$$b_2 = 2 \frac{K}{\rho C_p}(\Delta t)^2 \frac{r_3}{(\Delta r)^2} \theta_1^2, \tag{3.52}$$

$$b_3 = 2 \frac{K}{\rho C_p}(\Delta t)^2 \frac{r_2}{(\Delta r)^2} \theta_1^2, \tag{3.53}$$

$$b_4 = 2 \frac{K}{\rho C_p} (\Delta t)^2 \frac{\theta_3}{(\Delta \theta)^2} \theta_1, \quad (3.54)$$

$$b_5 = 2 \frac{K}{\rho C_p} (\Delta t)^2 \frac{\theta_2}{(\Delta \theta)^2} \theta_1, \quad (3.55)$$

$$b_6 = 2 \frac{K}{\rho C_p} \frac{(\Delta t)^2}{(\Delta \phi)^2}, \quad (3.56)$$

$$b_7 = 2 \frac{K}{\rho C_p} \frac{(\Delta t)^2}{(\Delta \phi)^2}, \quad (3.57)$$

$$\begin{aligned} c_1 = & 2(\Delta t)r_1\theta_1^2 - 4\tau_q r_1\theta_1^2 - \frac{K}{\rho C_p} (\Delta t)^2 \frac{r_2 + r_3}{(\Delta r)^2} \theta_1^2 + 2\tau_T \frac{K}{\rho C_p} (\Delta t) \frac{r_2 + r_3}{(\Delta r)^2} \theta_1^2 \\ & - \frac{K}{\rho C_p} (\Delta t)^2 \frac{\theta_2 + \theta_3}{(\Delta \theta)^2} \theta_1 + 2\tau_T \frac{K}{\rho C_p} (\Delta t) \frac{\theta_2 + \theta_3}{(\Delta \theta)^2} \theta_1 \\ & - 2 \frac{K}{\rho C_p} \frac{(\Delta t)^2}{(\Delta \phi)^2} + 4\tau_T \frac{K}{\rho C_p} \frac{\Delta t}{(\Delta \phi)^2}, \end{aligned} \quad (3.58)$$

$$c_2 = \frac{K}{\rho C_p} (\Delta t)^2 \frac{r_3}{(\Delta r)^2} \theta_1^2 - 2\tau_T \frac{K}{\rho C_p} (\Delta t) \frac{r_3}{(\Delta r)^2} \theta_1^2 \quad (3.59)$$

$$c_3 = \frac{K}{\rho C_p} (\Delta t)^2 \frac{r_2}{(\Delta r)^2} \theta_1^2 - 2\tau_T \frac{K}{\rho C_p} (\Delta t) \frac{r_2}{(\Delta r)^2} \theta_1^2, \quad (3.60)$$

$$c_4 = \frac{K}{\rho C_p} (\Delta t)^2 \frac{\theta_3}{(\Delta \theta)^2} \theta_1 - 2\tau_T \frac{K}{\rho C_p} (\Delta t) \frac{\theta_3}{(\Delta \theta)^2} \theta_1, \quad (3.61)$$

$$c_5 = \frac{K}{\rho C_p} (\Delta t)^2 \frac{\theta_2}{(\Delta \theta)^2} \theta_1 - 2\tau_T \frac{K}{\rho C_p} (\Delta t) \frac{\theta_2}{(\Delta \theta)^2} \theta_1, \quad (3.62)$$

$$c_6 = \frac{K}{\rho C_p} \frac{(\Delta t)^2}{(\Delta \phi)^2} - 2\tau_T \frac{K}{\rho C_p} \frac{\Delta t}{(\Delta \phi)^2}, \quad (3.63)$$

$$c_7 = \frac{K}{\rho C_p} \frac{(\Delta t)^2}{(\Delta \phi)^2} - 2\tau_T \frac{K}{\rho C_p} \frac{\Delta t}{(\Delta \phi)^2}, \quad (3.64)$$

$$r_1 = (i\Delta r)^2, \quad (3.65)$$

$$r_2 = \left[\left(i + \frac{1}{2} \right) \Delta r \right]^2, \quad (3.66)$$

$$r_3 = \left[\left(i - \frac{1}{2} \right) \Delta r \right]^2, \quad (3.67)$$

$$\theta_1 = \sin \theta_j, \quad (3.68)$$

$$\theta_2 = \sin \theta_{j+\frac{1}{2}}, \quad (3.69)$$

$$\theta_3 = \sin \theta_{j-\frac{1}{2}}. \quad (3.70)$$

We rewrite Equation (3.42) as following:

$$A\vec{T}^{n+1} = \vec{H}^n, \quad (3.71)$$

in which \vec{H}^n is the result of the right hand side of Equation (3.42).

The Gauss-Seidel iteration is applied to solve the linear system:

$$T_i^{n+1} = \frac{-\sum_{j=1}^{i-1} a_{ij} T_j^{n+1} - \sum_{j=i+1}^m a_{ij} T_j^n + h_i^n}{a_{ii}}, \quad (3.72)$$

in which $m = (N_r - 1) \times (N_\theta - 1) \times (N_\phi - 1)$.

3.4.2 Algorithms

A FORTRAN-based program for solving the linear system in Equation (3.43) is developed and the source code is attached in the appendix. The main structure of the program is as follows:

Step 1 Define constants, variables, and matrixes.

Step 2 Set up initial condition.

Step 3 Calculate the coefficients of the linear system.

Step 4 Begin the loop for calculating the temperature of every mesh point for each time layer.

Step 5 Set up heat source:

(1) A short-pulse laser heating on the surface of the microsphere symmetrically ($r = L, 0 \leq \theta \leq \pi, 0 \leq \varphi \leq 2\pi$);

(2) A short-pulse laser heating on the half of the surface of the microsphere in parallel ($r = L, 0 \leq \theta \leq \frac{\pi}{2}, 0 \leq \varphi \leq 2\pi$);

(3) A short-pulse laser heating on a portion of the surface of the microsphere in parallel ($r = L, 0 \leq \theta \leq \frac{\pi}{4}, 0 \leq \varphi \leq 2\pi$).

Step 6 Calculate the left hand side of the linear system.

Step 7 Calculate the temperature of every mesh point in this time layer by Gauss-Seidel iteration.

Set tolerance TOL and maximum number of iteration N .

Step 8 Set $k=1$.

Step 9 While ($k \leq m$) do step 10 ~ 13,

where $m = (N_r - 1) \times (N_\theta - 1) \times (N_\varphi - 1)$.

Step 10 For $i = 1, \dots, m$

$$\text{Set } T_i^{n+1} = \frac{-\sum_{j=1}^{i-1} a_{ij} T_j^{n+1} - \sum_{j=i+1}^m a_{ij} T_j^n + h_i^n}{a_{ii}}.$$

Step 11 If $\|\vec{T}^{n+1} - \vec{T}^n\| < TOL$, then Step 15.

Step 12 Set $k = k + 1$.

Step 13 For $i = 1, \dots, m$ set $T_i^n = T_i^{n+1}$

Step 14 Maximum number of iterations exceeded, stop.

Step 15 Output the results:

- (1) The temperature at the top point on the surface;
- (2) The temperature distribution in the $r\theta$ cross-section;
- (3) The temperature along r -axis.

Stop.

CHAPTER 4

NUMERICAL EXAMPLES

4.1 Description of the Examples

To demonstrate the applicability of the scheme, we investigate the temperature change and distribution in a gold sphere with a short-pulse laser heating on the surface. The radius (L) of the gold sphere is $0.1 \mu m$. The thermal properties of gold are shown in Table 4.1.

Table 4.1 Thermal property parameters of gold [Tzou, 1996]

Parameters	Values
C_p	129 kJ/kg K
K	315 W/m K
ρ	19300 kg/m^3
τ_a	8.5 ps
τ_T	90 ps

The initial conditions are chosen as follows:

$$T(x, y, z, 0) = T_\infty, \quad (4.1)$$

where $T_\infty = 300 \text{ K}$,

$$\frac{\partial T}{\partial t}(x, y, z, 0) = 0. \quad (4.2)$$

The boundary conditions are assumed to be insulated:

$$\frac{\partial T(L, \theta, \varphi, t)}{\partial r} = 0, \quad (4.3)$$

$$\frac{\partial T(r,0,\varphi,t)}{\partial \theta} = \frac{\partial T(r,\pi,\varphi,t)}{\partial \theta} = 0, \quad (4.4)$$

$$T(r,\theta,\varphi,t) = T(r,\theta,2\pi + \varphi,t). \quad (4.5)$$

To apply our scheme, we choose three different meshes of $50 \times 20 \times 20$, $100 \times 20 \times 20$ and $200 \times 20 \times 20$ grid points in (r, θ, φ) coordinates. The time increment (Δt) is chosen to be 0.005 ps .

4.2 Example with Symmetric Heating

4.2.1 Heat Source

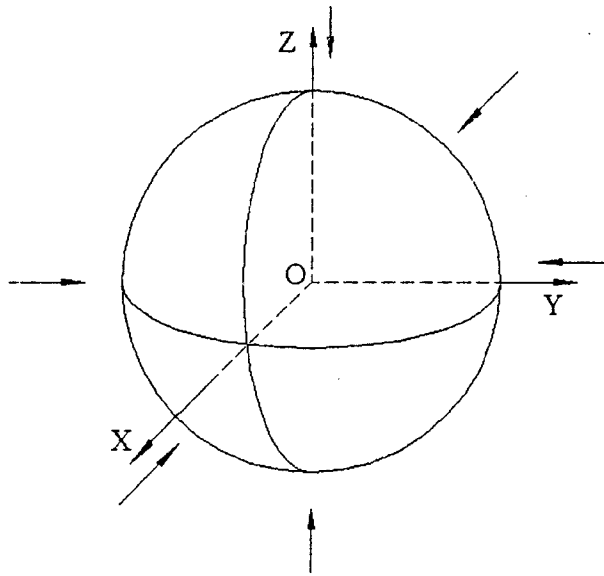


Figure 4.1 The gold sphere subjected to short-pulse laser irradiation on the surface ($r = L$, $0 \leq \theta \leq \pi$, $0 \leq \varphi \leq 2\pi$) symmetrically.

In this example, we assume that the short-pulse laser irradiation is symmetrically heating on the surface of the gold sphere, as shown in Figure 4.1. The heat source is chosen to be

$$Q(r,t) = 0.94J \left[\frac{1-R}{t_p \delta} \right] e^{-\frac{L-r}{\delta} - 2.77 \left(\frac{t-2t_p}{t_p} \right)^2}, \quad (4.6)$$

where $J = 13.4 \text{ J/m}^2$, $t_p = 100 \text{ fs}$ ($1 \text{ fs} = 10^{-15} \text{ s}$), $\delta = 15.3 \text{ nm}$ ($1 \text{ nm} = 10^{-9} \text{ m}$), and $R = 0.93$ [Tzou, 1996].

4.2.2 Result Analysis

Figure 4.2 shows the temperature change $\left(\frac{\Delta T}{(\Delta T)_{\max}} \right)$ on the surface of the gold sphere with time. The temperature rises rapidly at first and reaches the maximum temperature $(\Delta T)_{\max}$, which is about 12.36 K at time $t = 0.26 \text{ ps}$; then it goes down gradually. The plot is similar to that obtained in [Tzou, 1996]. Also, it can be seen that mesh size has no significant effect on the solution, implying that the scheme is stable.

Figures 4.3 ~ 4.7 show the contours of temperature distributions on the $r\theta$ cross-section ($0 \leq r \leq L$, $0 \leq \theta \leq \pi$) at $t = 0.2 \text{ ps}$, 0.25 ps , 0.5 ps , 1.0 ps , and 2.0 ps , respectively. It can be seen that the heat is transferred from outside to the center of the sphere. Figure 4.3 shows that at time $t = 0.2 \text{ ps}$, the heat is transferred from the surface to the near surface inner area. At time $t = 0.25 \text{ ps}$, as shown in Figure 4.4, the heat is transferred toward inside rapidly and the temperature almost reaches the maximum on the surface. Figure 4.5 shows that the heat continuously transfers to the center at time $t = 0.5 \text{ ps}$. The temperature in the area near the surface goes down. Meanwhile, the temperature in the area near the center continuously goes up. From Figure 4.6, it can be seen that at time $t = 1.0 \text{ ps}$, the temperature distribution becomes symmetric. At time $t = 2.0 \text{ ps}$, the temperature becomes equilibrium and almost reaches the average as shown in Figure 4.7.

Figure 4.8 gives the temperature rise along the r -axis of the sphere with different times ($t = 0.2 \text{ ps}$, 0.25 ps , 0.5 ps , 1.0 ps and 2.0 ps). The temperature in the area near the surface goes up rapidly at time $t = 0.2 \text{ ps}$, and almost reaches its maximum at time $t =$

0.25 ps. Then, at time $t = 0.5$ ps, 1.0 ps, 2.0 ps it goes down gradually. The temperature in the area near the center continuously goes up at time $t = 0.2$ ps, 0.25 ps, 0.5 ps, 1.0 ps and 2.0 ps. The temperature distribution becomes uniform with time.

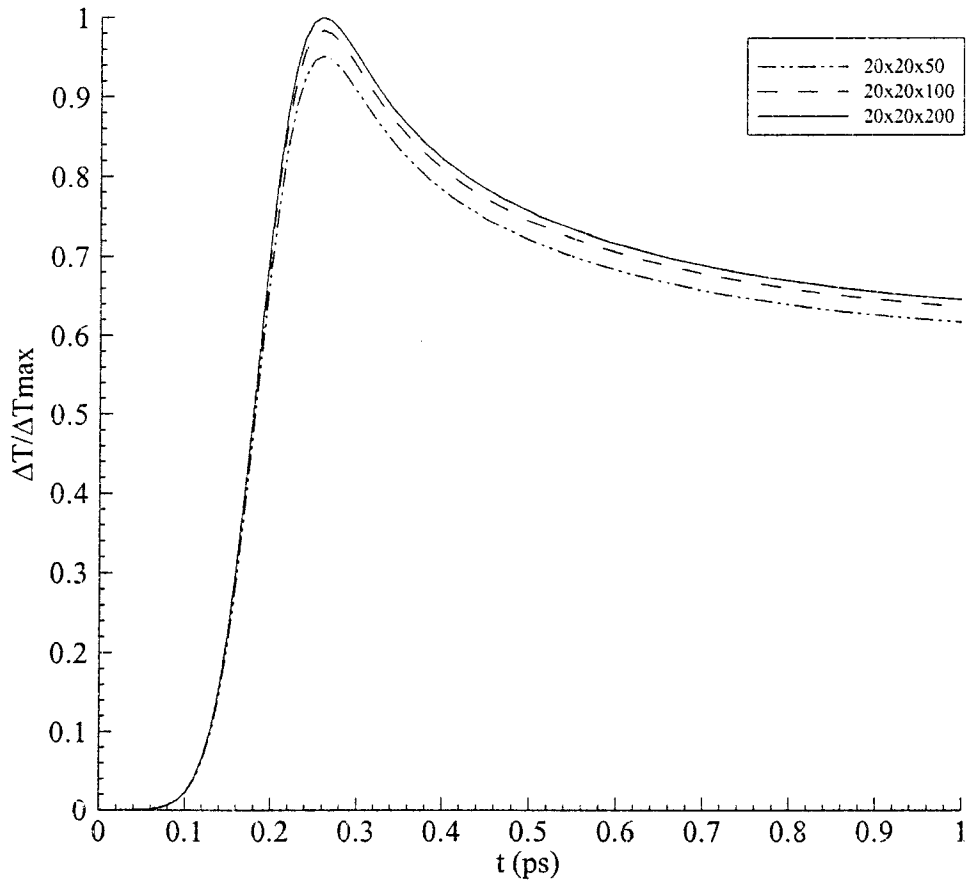


Figure 4.2 Temperature change with time at the surface of the sphere subjected to symmetric pulse laser irradiation.

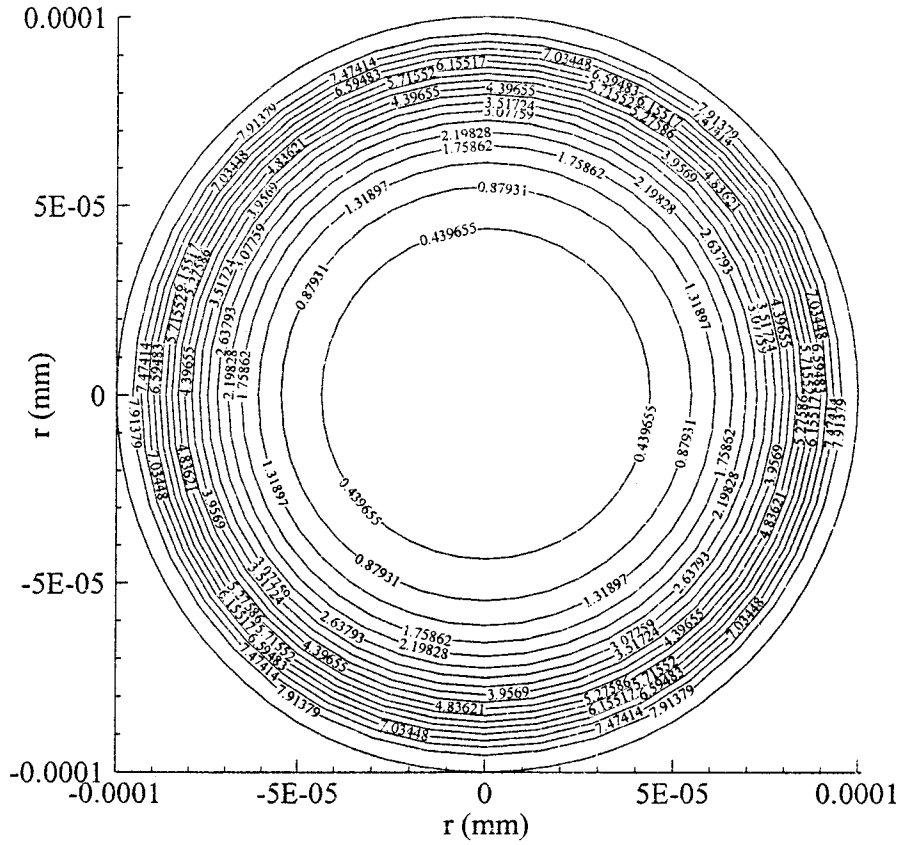


Figure 4.3 Contours of temperature distribution in the $r\theta$ cross-section of the sphere subjected to symmetric short-pulse laser irradiation on the surface when $t = 0.2 \text{ ps}$.

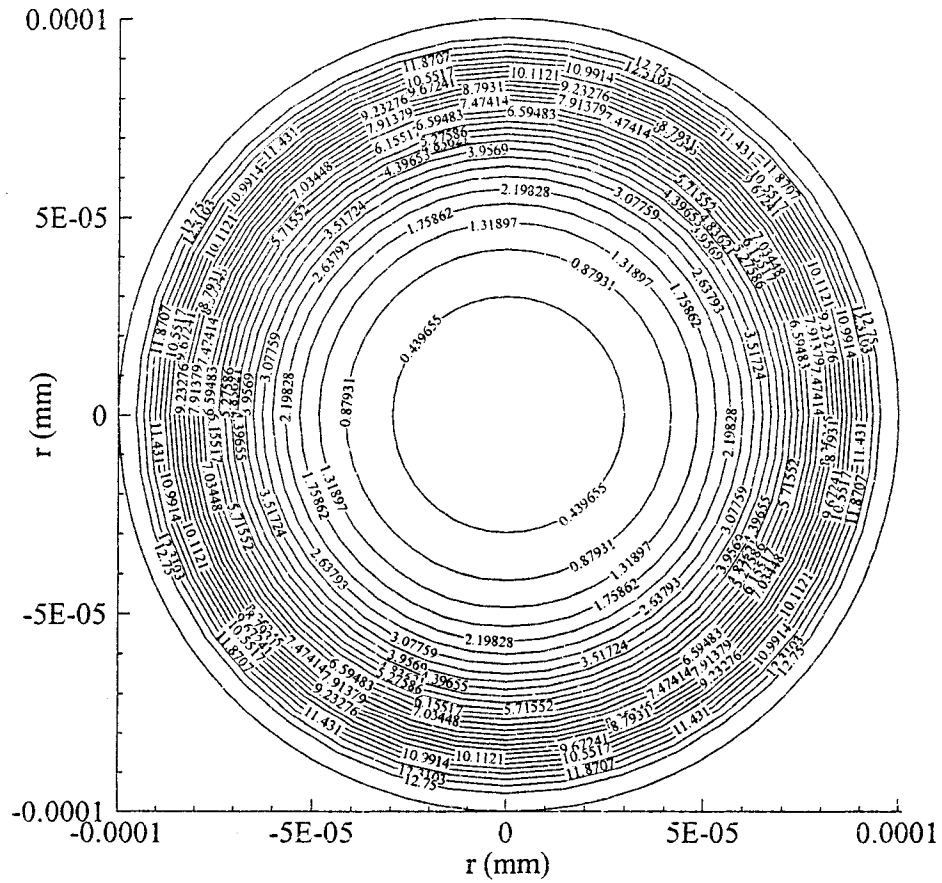


Figure 4.4 Contours of temperature distribution in the $r\theta$ cross-section of the sphere subjected to symmetric pulse laser irradiation on the surface when $t = 0.25 \text{ ps}$.

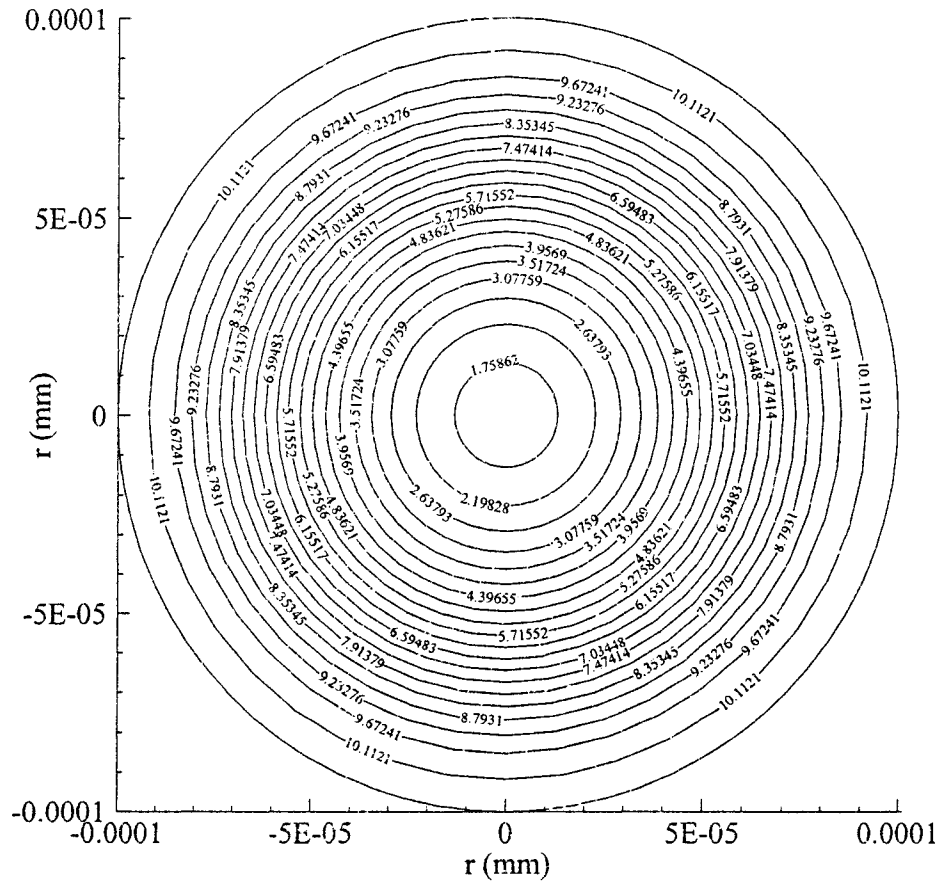


Figure 4.5 Contours of temperature distribution in the $r\theta$ cross-section of the sphere subjected to symmetric pulse laser irradiation on the surface when $t = 0.5$ ps.

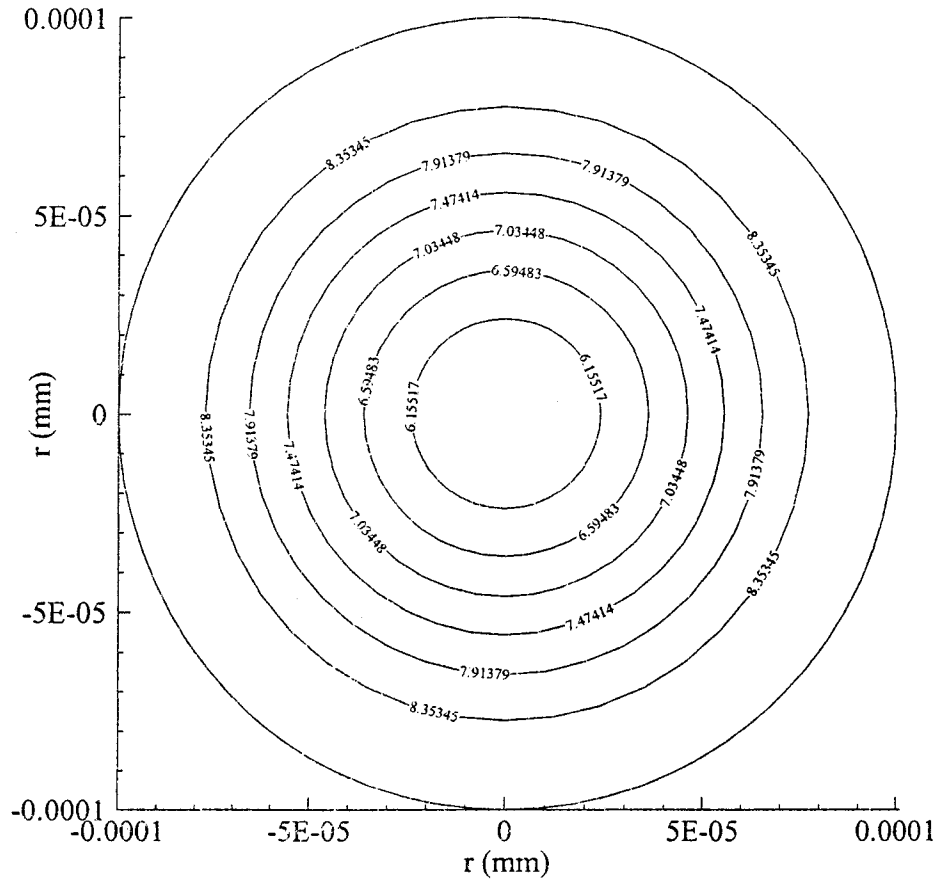


Figure 4.6 Contours of temperature distribution in the $r\theta$ cross-section of the sphere subjected to symmetric pulse laser irradiation on the surface when $t = 1.0$ ps.

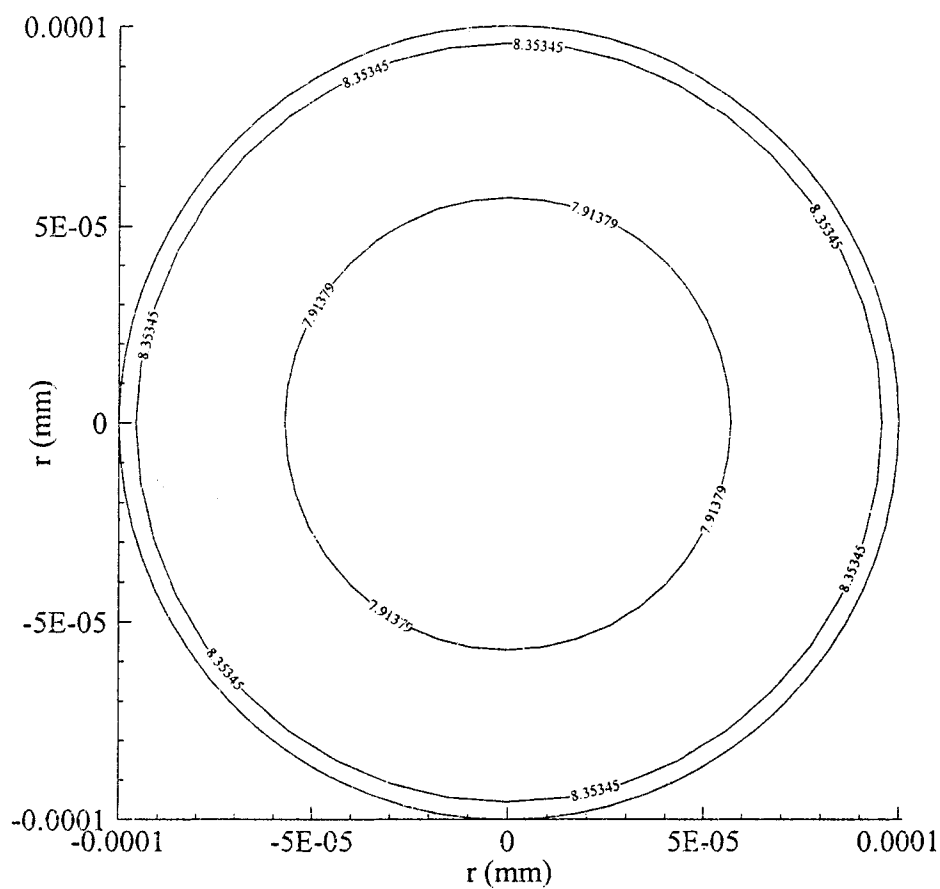


Figure 4.7 Contours of temperature distribution in the $r\theta$ cross-section of the sphere subjected to symmetric pulse laser irradiation on the surface when $t = 2.0$ ps.

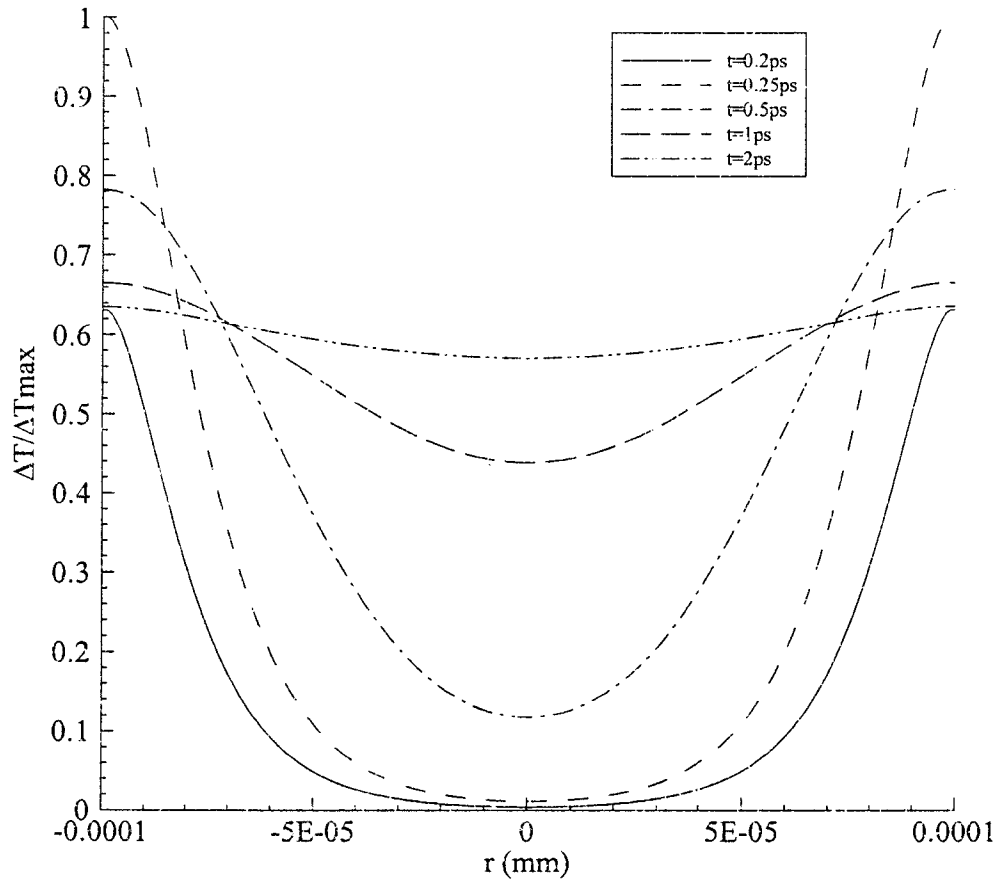


Figure 4.8 Temperature change along r -axis ($\theta = 0$ and π) of the sphere subjected to symmetric pulse laser irradiation on the surface.

4.3 Example with Semi-Sphere Heating

4.3.1 Heat Source

In this example, we assume that the short-pulse laser irradiation is heating on the surface of the semi-sphere from the top ($r = L$, $0 \leq \theta \leq \frac{\pi}{2}$, $0 \leq \varphi \leq 2\pi$) in parallel, as shown in Figure 4.9. The heat source is chosen to be

$$Q(r, \theta, t) = 0.94J \left[\frac{1-R}{t_p \delta} \right] e^{-\frac{L-r}{\delta} - 2.77 \left(\frac{t-2t_p}{t_p} \right)^2} \cos \theta. \quad (4.7)$$

where $J = 13.4 \text{ J/m}^2$, $t_p = 100 \text{ fs}$ ($1 \text{ fs} = 10^{-15} \text{ s}$), $\delta = 15.3 \text{ nm}$ ($1 \text{ nm} = 10^{-9} \text{ m}$), and $R = 0.93$ [Tzou, 1996].

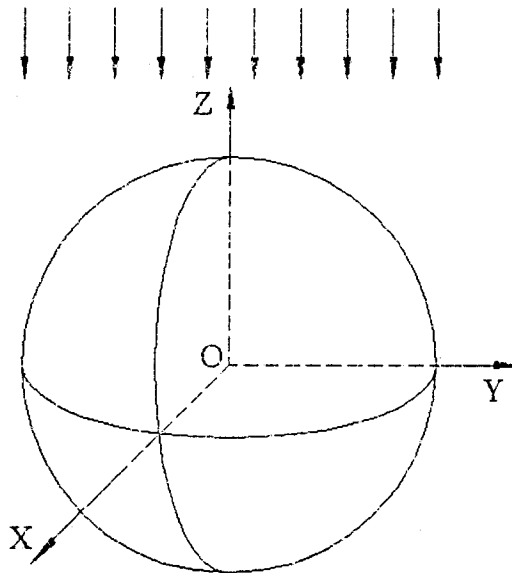


Figure 4.9 The gold sphere subjected to short-pulse laser irradiation on the top half of the surface ($r = L$, $0 \leq \theta \leq \frac{\pi}{2}$, $0 \leq \varphi \leq 2\pi$) in parallel.

4.3.2 Result Analysis

Figure 4.10 shows the temperature change $\left(\frac{\Delta T}{(\Delta T)_{\max}}\right)$ at the top point on the surface ($r = L, \theta = 0$) of the gold sphere with time. The temperature rises rapidly at first and reaches its maximum $(\Delta T)_{\max}$, which is about 12.36 K at time $t = 0.26 \text{ ps}$; then it goes down gradually. The plot is similar to that obtained in [Tzou, 1996]. Also, it can be seen that mesh size has no significant effect on the solution, implying that the scheme is stable.

Figures 4.11 ~ 4.15 show the contours of temperature distributions on the $r\theta$ cross-section ($0 \leq r \leq L, 0 \leq \theta \leq \pi$) at $t = 0.2 \text{ ps}$, 0.25 ps , 0.5 ps , 1.0 ps , and 2.0 ps , respectively. It can be seen that the heat is transferred from top to bottom of the sphere. Compared with the example in the previous section, the heat source in this example is unbalanced and has less power. Therefore, it takes longer time to reach the balance, which has a lower average temperature. Figure 4.11 shows that at time $t = 0.2 \text{ ps}$, the heat is transferred from the top surface to inner area. At time $t = 0.25 \text{ ps}$, as shown in Figure 4.12, the heat is transferred toward inside rapidly and the temperature at the top point of the surface almost reaches its maximum. Figure 4.13 shows that the heat continuously transfers to the bottom at time $t = 0.5 \text{ ps}$. The temperature in the area near the top surface goes down. Meanwhile, the temperature in the area near the bottom goes up slowly. From Figure 4.14 and Figure 4.15, it can be seen that at time $t = 1.0 \text{ ps}$ and 2.0 ps , the temperature distribution becomes more and more uniform.

Figure 4.16 gives the temperature rise along the r -axis of the sphere with $\theta = 0$ and π for different times ($t = 0.2 \text{ ps}$, 0.25 ps , 0.5 ps , 1.0 ps and 2.0 ps). The temperature in

the area near the top surface goes up rapidly at time $t = 0.2 \text{ ps}$, and almost reaches its maximum at time $t = 0.25 \text{ ps}$. Then, at time $t = 0.5 \text{ ps}$, 1.0 ps , 2.0 ps it goes down gradually. The temperature in the area near the bottom continuously goes up at time $t = 0.2 \text{ ps}$, 0.25 ps , 0.5 ps , 1.0 ps and 2.0 ps . The temperature distribution becomes uniform with time.

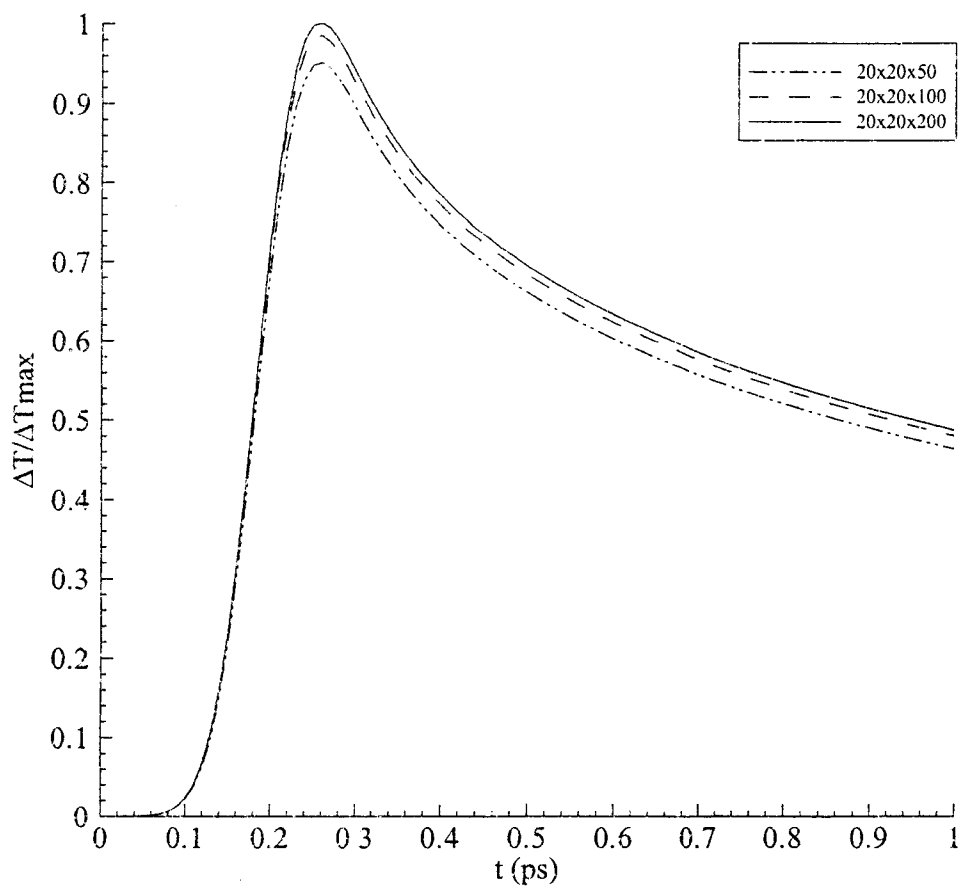


Figure 4.10 Temperature change with time at the top point of the sphere subjected to parallel pulse laser irradiation on the top half of the surface.

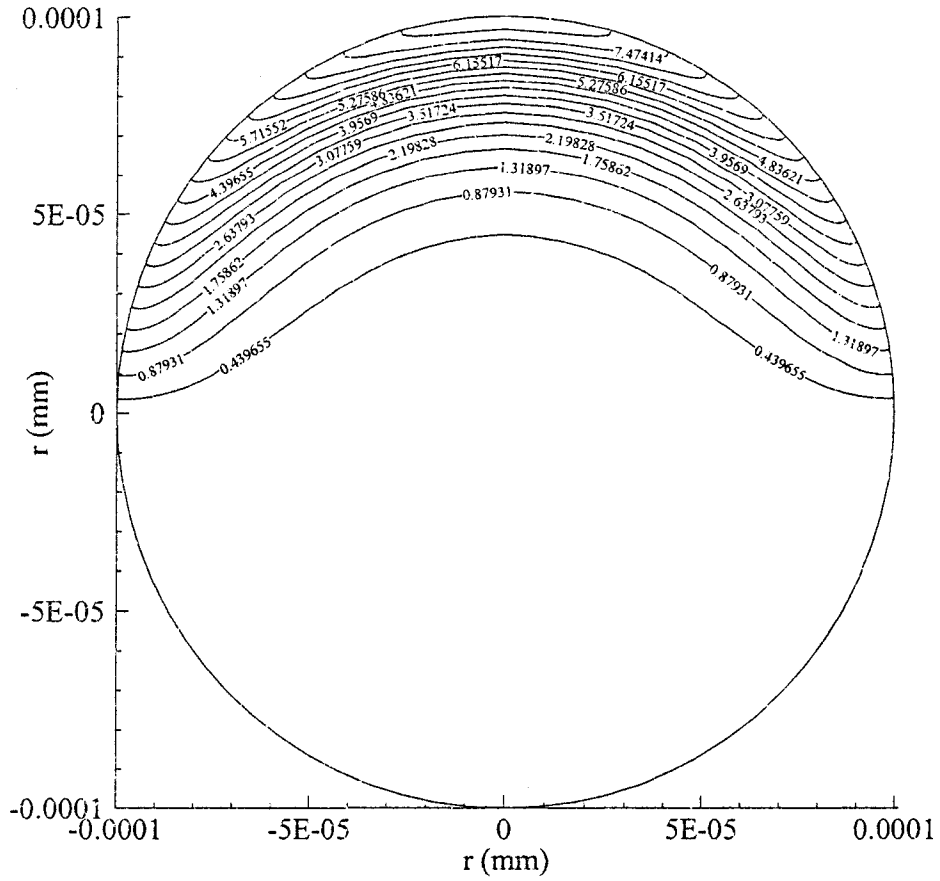


Figure 4.11 Contours of temperature distribution in the $r\theta$ cross-section of the sphere subjected to parallel pulse laser irradiation on the top half of the surface when $t = 0.2 \text{ ps}$.

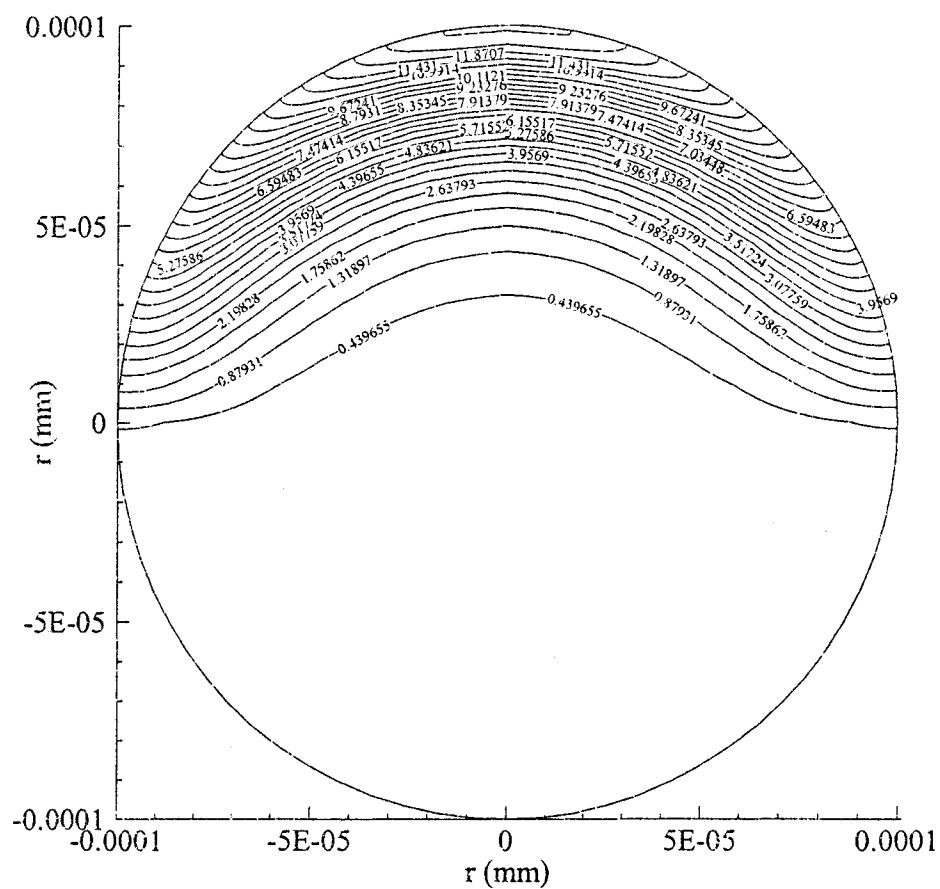


Figure 4.12 Contours of temperature distribution in the $r\theta$ cross-section of the sphere subjected to parallel pulse laser irradiation on the top half of the surface when $t = 0.25 \text{ ps}$.

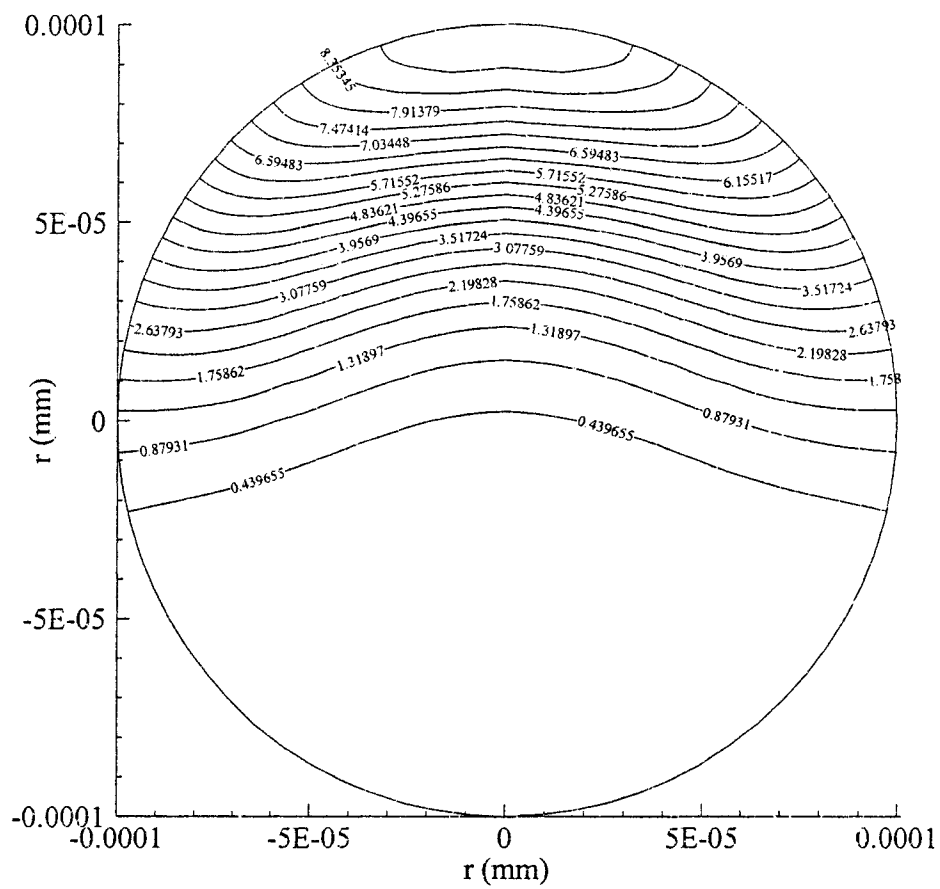


Figure 4.13 Contours of temperature distribution in the $r\theta$ cross-section of the sphere subjected to parallel pulse laser irradiation on the top half of the surface when $t = 0.5 \text{ ps}$.

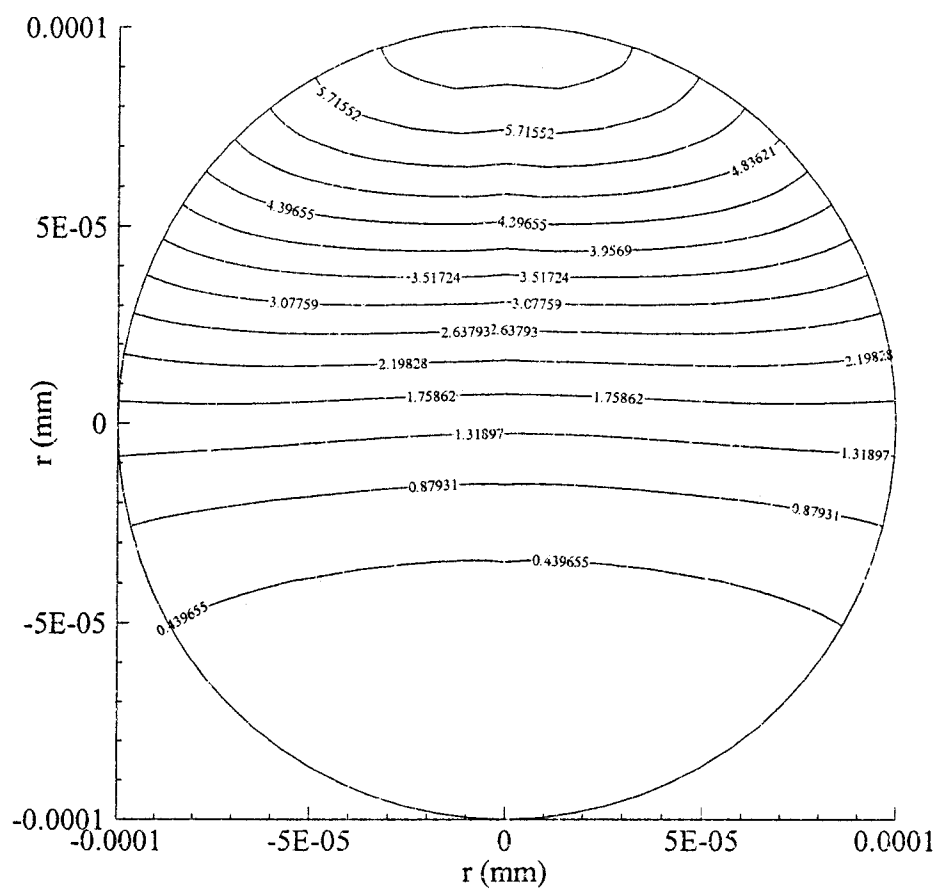


Figure 4.14 Contours of temperature distribution in the $r\theta$ cross-section of the sphere subjected to parallel pulse laser irradiation on the top half of the surface when $t = 1.0 \text{ ps}$.

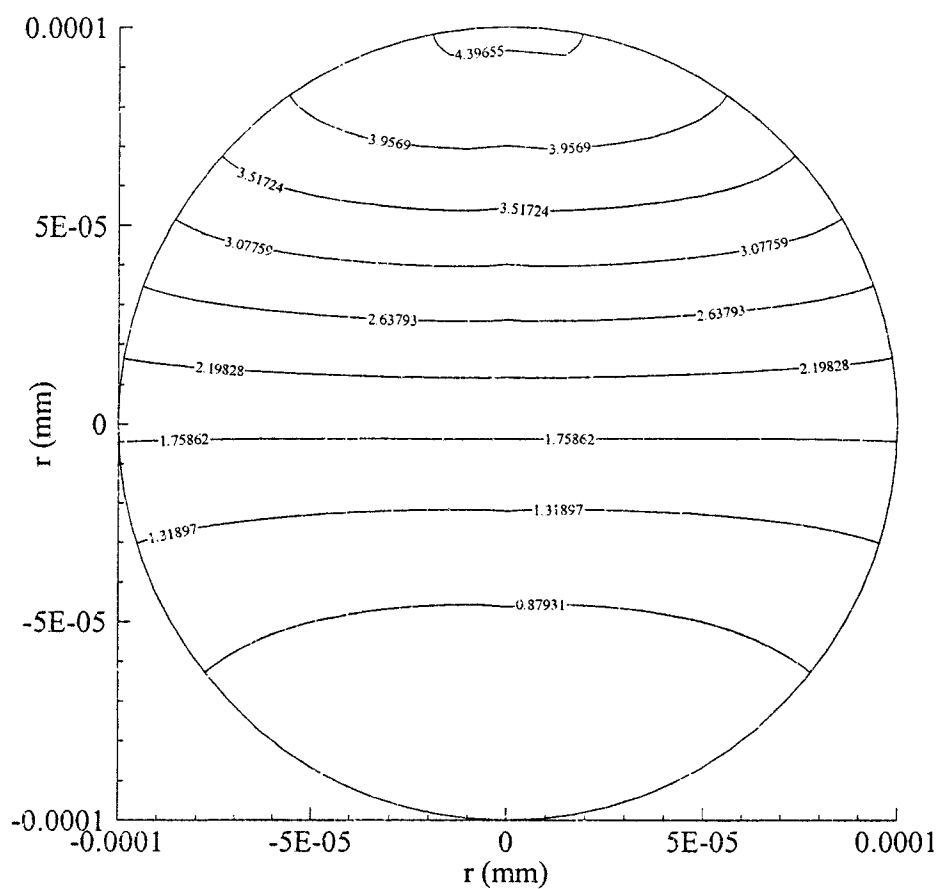


Figure 4.15 Contours of temperature distribution in the $r\theta$ cross-section of the sphere subjected to parallel pulse laser irradiation on the top half of the surface when $t = 2.0 \text{ ps}$.

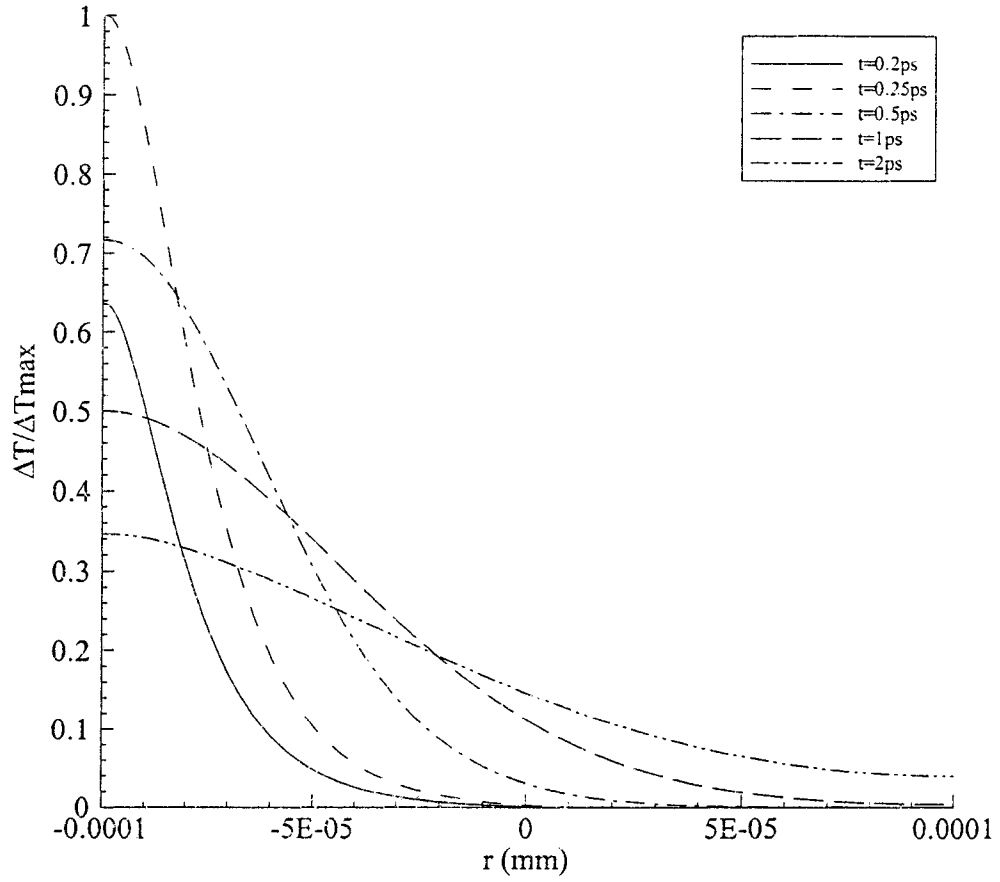


Figure 4.16 Temperature change along r -axis ($\theta = 0$ and π) of the sphere subjected to parallel pulse laser irradiation on the top half of the surface.

4.4 Example with Portion Heating

4.4.1 Heat Source

In this example, we assume that the short-pulse laser irradiation is heating on a portion of the surface of the sphere from the top ($r = L$, $0 \leq \theta \leq \frac{\pi}{4}$, $0 \leq \varphi \leq 2\pi$) in parallel, as shown in Figure 4.17. The heat source is chosen to be

$$Q(r, \theta, t) = 0.94J \left[\frac{1-R}{t_p \delta} \right] e^{-\frac{L-r}{\delta} - 2.77 \left(\frac{t-2t_p}{t_p} \right)^2} \cos \theta. \quad (4.8)$$

where $J = 13.4 \text{ J/m}^2$, $t_p = 100 \text{ fs}$ ($1 \text{ fs} = 10^{-15} \text{ s}$), $\delta = 15.3 \text{ nm}$ ($1 \text{ nm} = 10^{-9} \text{ m}$), and $R = 0.93$ [Tzou, 1996].

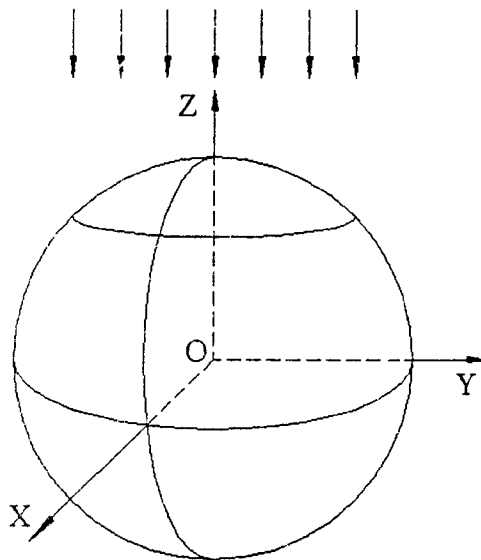


Figure 4.17 The gold sphere subjected to short-pulse laser irradiation on a portion of the surface ($r = L$, $0 \leq \theta \leq \frac{\pi}{4}$, $0 \leq \varphi \leq 2\pi$) in parallel.

4.4.2 Result Analysis

Figure 4.18 shows the temperature change $\left(\frac{\Delta T}{(\Delta T)_{\max}}\right)$ at the top point on the surface ($r = L, \theta = 0$) of the gold sphere with time. The temperature rises rapidly at first and reaches its maximum $(\Delta T)_{\max}$, which is about 12.36 K at time $t = 0.26 \text{ ps}$; then it goes down gradually. The plot is similar to that obtained in [Tzou, 1996]. Also, it can be seen that mesh size has no significant effect on the solution, implying that the scheme is stable.

Figures 4.19 ~ 4.23 show the contours of temperature distributions on the $r\theta$ cross-section ($0 \leq r \leq L, 0 \leq \theta \leq \pi$) at $t = 0.2 \text{ ps}$, 0.25 ps , 0.5 ps , 1.0 ps , and 2.0 ps , respectively. It can be seen that the heat is transferred from top to bottom of the sphere. Compared with the example in the previous sections, the heat source in this example is even more unbalanced and has less power. Therefore, it takes longer time to reach the balance, which has a lower average temperature. Figure 4.19 shows that at time $t = 0.2 \text{ ps}$, the heat is transferred from the top surface to inner area. At time $t = 0.25 \text{ ps}$, as shown in Figure 4.20, the heat is transferred toward inside rapidly and the temperature at the top point of the surface almost reaches its maximum. Figure 4.21 shows that the heat continuously transfers to the bottom at time $t = 0.5 \text{ ps}$. The temperature in the area near the top surface goes down. Meanwhile, the temperature in the area near the bottom goes up slowly. From Figures 4.22 and 4.23, it can be seen that at time $t = 1.0 \text{ ps}$ and 2.0 ps , the temperature distribution becomes more and more uniform.

Figure 4.24 gives the temperature rise along the r -axis with $\theta = 0$ and π for different times ($t = 0.2 \text{ ps}$, 0.25 ps , 0.5 ps , 1.0 ps and 2.0 ps). The temperature in the area

near the top surface goes up rapidly at time $t = 0.2 \text{ ps}$, and almost reaches its maximum at time $t = 0.25 \text{ ps}$. Then, at time $t = 0.5 \text{ ps}$, 1.0 ps , 2.0 ps it goes down gradually. The temperature in the area near the bottom continuously goes up at time $t = 0.2 \text{ ps}$, 0.25 ps , 0.5 ps , 1.0 ps and 2.0 ps . The temperature distribution becomes uniform with time.

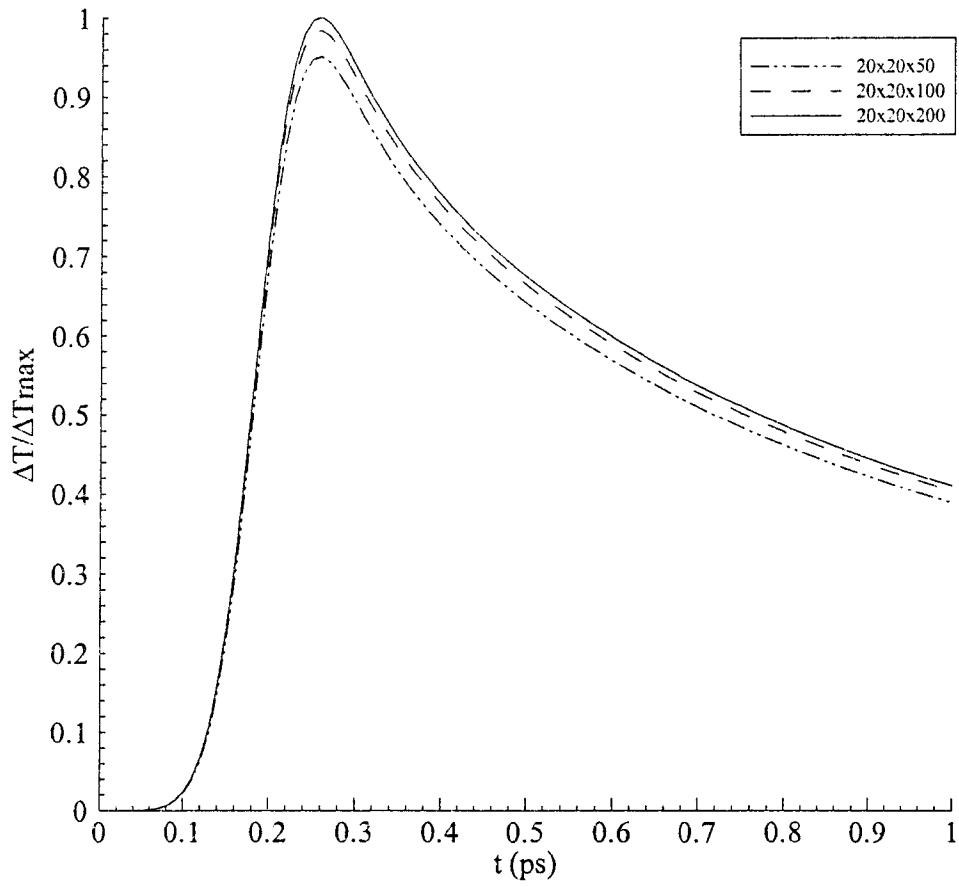


Figure 4.18 Temperature change with time at the top point of the sphere subjected to parallel pulse laser irradiation on a portion of the surface.

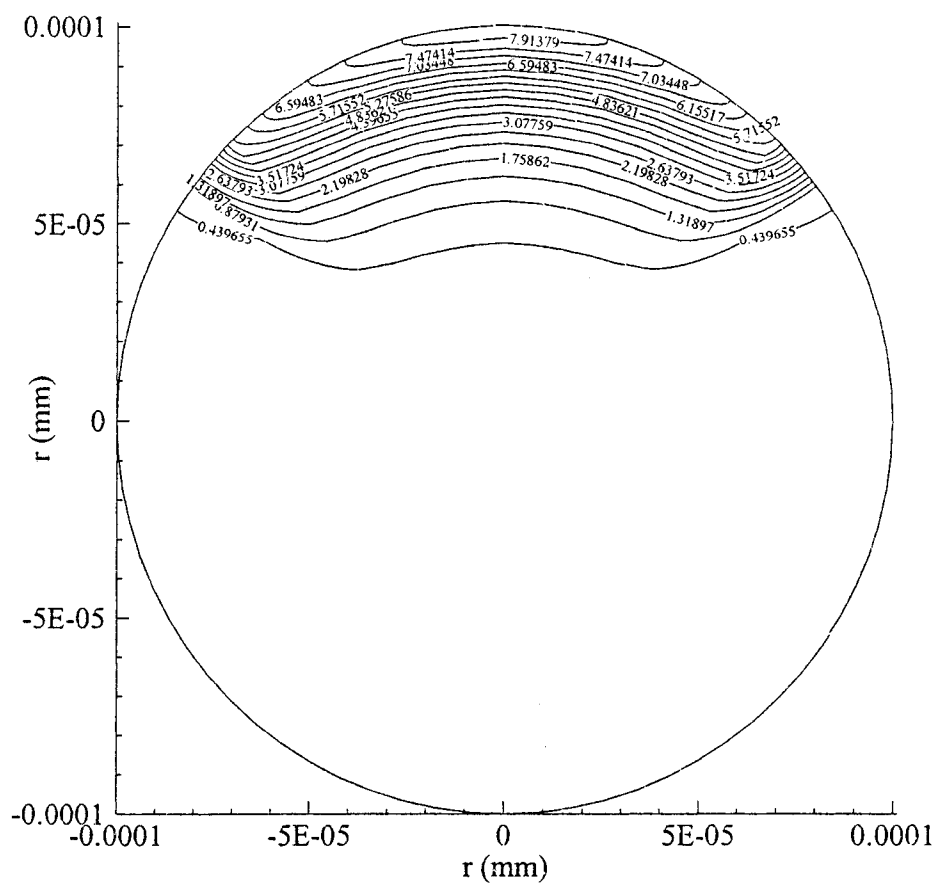


Figure 4.19 Contours of temperature distribution in the $r\theta$ cross-section of the sphere subjected to parallel pulse laser irradiation on a portion of the surface when $t = 0.2 \text{ ps}$.

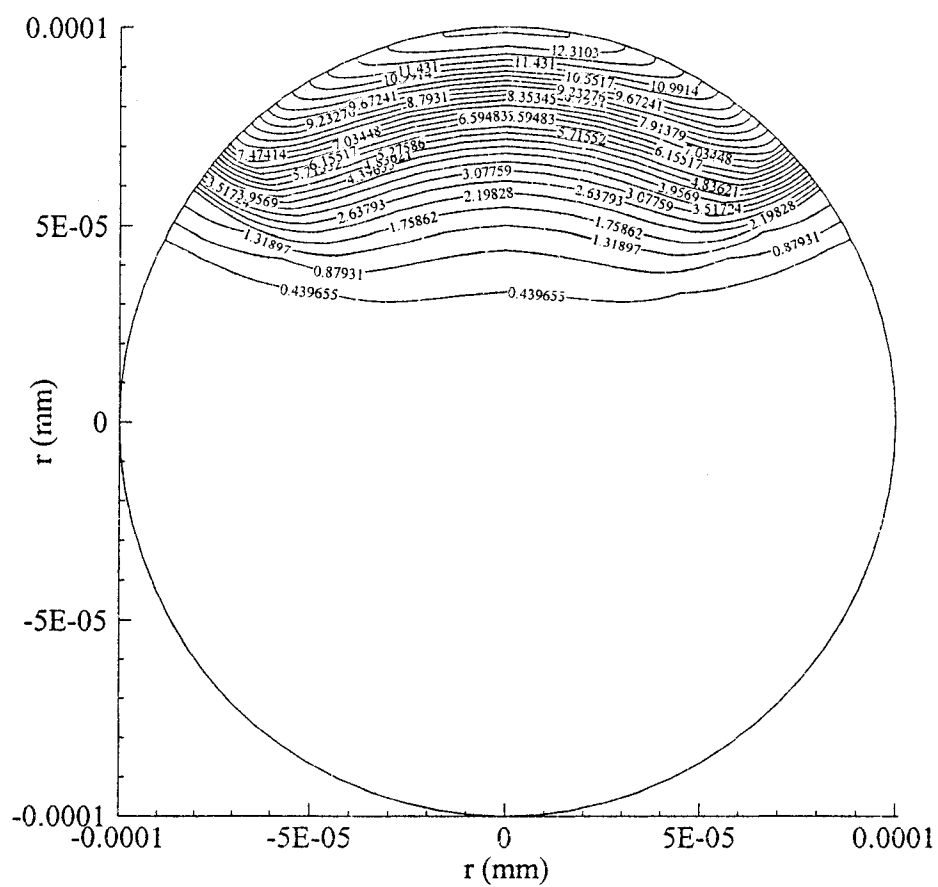


Figure 4.20 Contours of temperature distribution in the $r\theta$ cross-section of the sphere subjected to parallel pulse laser irradiation on a portion of the surface when $t = 0.25 \text{ ps}$.

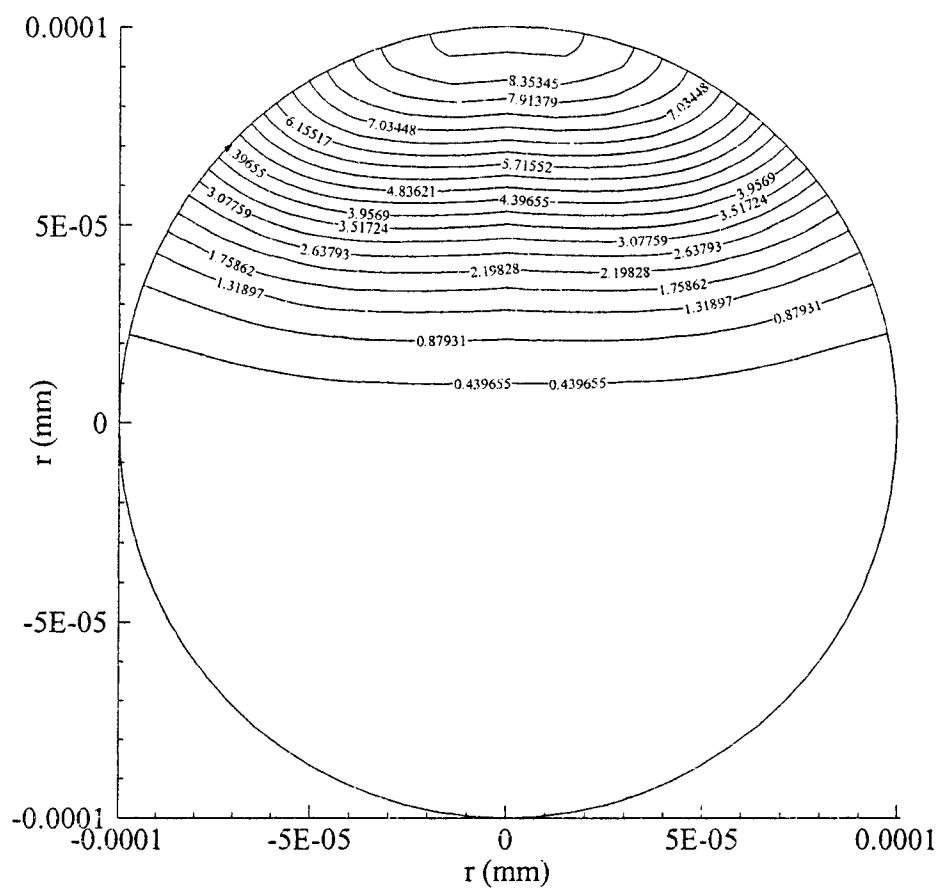


Figure 4.21 Contours of temperature distribution in the $r\theta$ cross-section of the sphere subjected to parallel pulse laser irradiation on a portion of the surface when $t = 0.5 \text{ ps}$.

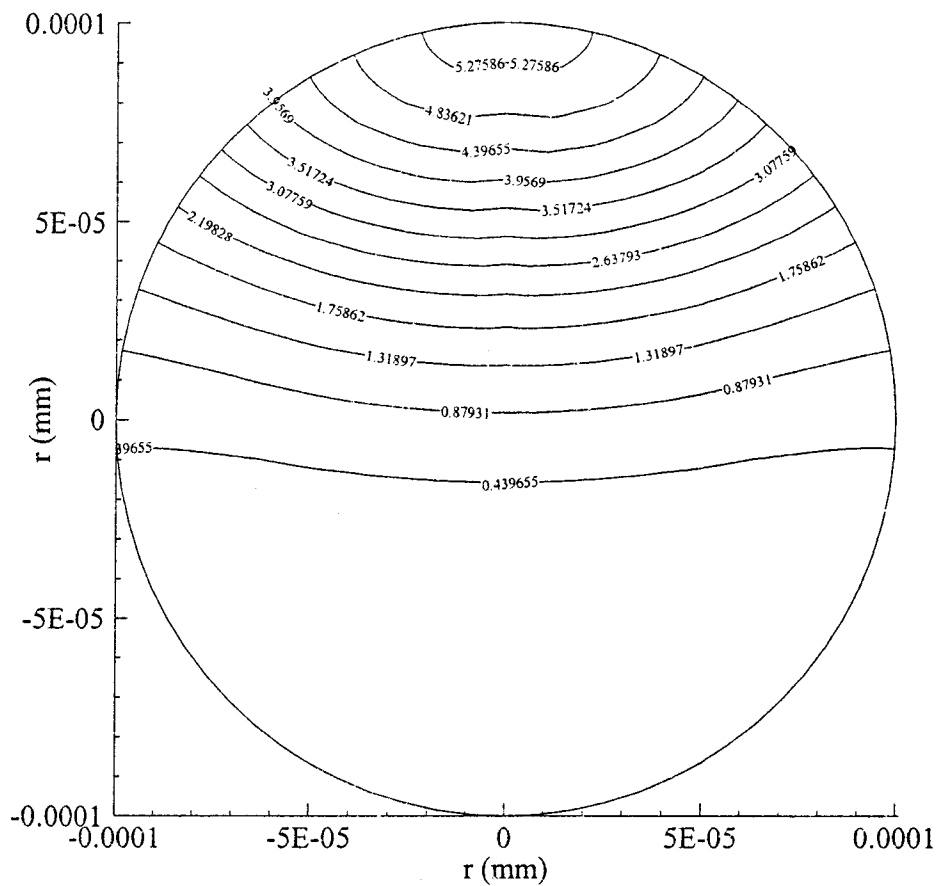


Figure 4.22 Contours of temperature distribution in the $r\theta$ cross-section of the sphere subjected to parallel pulse laser irradiation on a portion of the surface when $t = 1.0$ ps.

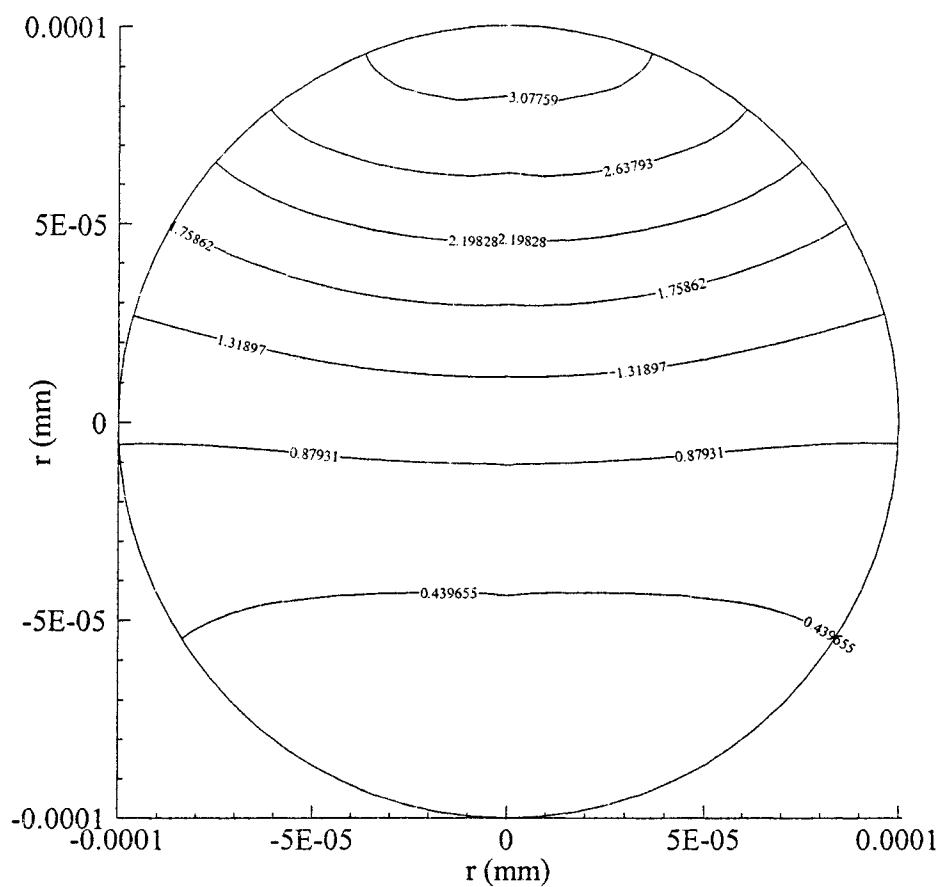


Figure 4.23 Contours of temperature distribution in the $r\theta$ cross-section of the sphere subjected to parallel pulse laser irradiation on a portion of the surface when $t = 2.0$ ps.

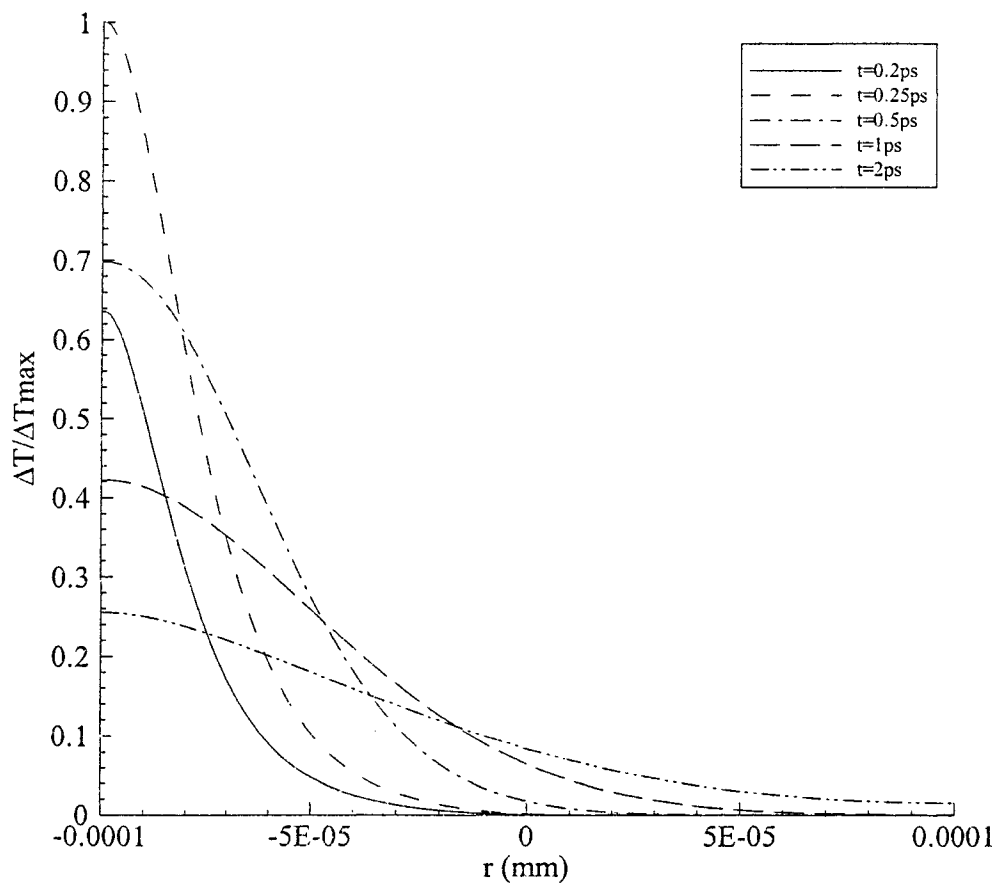


Figure 4.24 Temperature change along r -axis ($\theta = 0$ and π) of the sphere subjected to parallel pulse laser irradiation on a portion of the surface.

CHAPTER 5

CONCLUSION

In this dissertation, we have reviewed the fundamentals of microscale heat transfer and dual-phase-lagging model. The dual-phase-lagging heat conduction equation originates from the first law of thermodynamics and the dual-phase-lagging constitutive relation of heat flux density. It is developed in examining energy transport involving the high-rate heating in which the non-equilibrium thermodynamic transition and the microstructural effect become important associated with shortening of the response time. The high-rate heating is developing rapidly due to the advancement of high-power short-pulse laser technologies. The dual-phase-lagging heat conduction equation forms a generalized, unified equation with the classical parabolic heat conduction equation, the hyperbolic heat conduction equation, and the energy equation in the phonon-electron interaction model as its special case. With the rapid growth of microscale heat conduction of high-rate flux, it has attracted the recent research effort on dual-phase-lagging heat conduction equations.

Based on the fundamental of microscale heat transfer and the dual-phase-lagging model, in this study, we consider the dual-phase-lagging heat transport equation in three-dimensional spherical coordinates and develop a three level finite difference scheme. We have shown that the scheme is unconditionally stable. And then we have developed a

FORTRAN program based on the Gauss-Seidel iterative method to solve the heat transfer in a microsphere subjected to a short-pulse laser. Three numerical examples are illustrated to investigate the temperature rise of a gold sphere irradiated by a short-pulse laser.

The future work of this research may be to develop a numerical method for solving the dual-phase-lagging heat transport equation in a three-dimensional double-layered microsphere, and to develop a numerical method for solving the dual-phase-lagging heat transport equation in a three-dimensional thin film or microsphere with temperature-dependent thermal properties.

APPENDIX

SOURCE CODE OF THE FINITE

DIFFERENCE SCHEME

```

c *****
c
c Title: 3d-microsphere.f
c Author: Lixin Shen
c Date: Sept., 2003
c
c This program investigates the efficiency of the finite difference
c scheme for solving a dual-phase-lagging heat transport equation
c in a three dimensional microsphere.
c
c This program includes the following calculation:
c
c 1)The temperature change at the top point on the surface;
c 2)The temperature distribution in the cross-section;
c 3)The temperature change along r-axis.
c
c Three different heat sources are applied and the calculation is
c processed accordingly. The three heat sources are:
c
c 1)A short-pulse laser heats on the surface of the microsphere
c symmetrically;
c 2)A short-pulse laser heats on the half of the surface of the
c microsphere in parallel;
c 3)A short-pulse laser heats on a portion of the surface of the
c microsphere in parallel.
c
c *****
c
c *****
c *** Matrix definition
c *****
c
c dimension aa1(0:200,0:20,0:20)
c dimension aa2(0:200,0:20,0:20)
c dimension aa3(0:200,0:20,0:20)
c dimension bb1(0:200,0:20,0:20)
c dimension bb2(0:200,0:20,0:20)
c dimension bb3(0:200,0:20,0:20)
c dimension cc1(0:200,0:20,0:20)
c dimension cc2(0:200,0:20,0:20)
c dimension cc3(0:200,0:20,0:20)
c dimension dd1(0:200,0:20,0:20)
c dimension dd2(0:200,0:20,0:20)
c dimension dd3(0:200,0:20,0:20)
c dimension ee1(0:200,0:20,0:20)
c dimension ee2(0:200,0:20,0:20)

```

```

dimension ee3(0:200,0:20,0:20)
dimension ff1(0:200,0:20,0:20)
dimension ff2(0:200,0:20,0:20)
dimension ff3(0:200,0:20,0:20)
dimension gg1(0:200,0:20,0:20)
dimension gg2(0:200,0:20,0:20)
dimension gg3(0:200,0:20,0:20)
dimension hh3(0:200,0:20,0:20)
dimension tn1(0:200,0:20,0:20)
dimension tn2(0:200,0:20,0:20)
dimension tn3(0:200,0:20,0:20)
dimension sq(0:200,0:20,0:20)
dimension x0(0:200,0:20,0:20)

```

```

c *****
c *** Variable definition
c *****

```

```

double precision tt,tq,tk,cp,rl,pl,ql,sj,sr,stp,sd,sa
double precision pc,ss,tpc,cc,t
double precision r,r1,r2,r3,p1,p2,p3,tn1,tn2,tn3
double precision dt,dr,dp,dq
double precision dtrr,dtrr,dtrr,dtrr,dtrr,dtrr,dtrr,dtrr
double precision aa1,aa2,aa3,bb1,bb2,bb3
double precision cc1,cc2,cc3,dd1,dd2,dd3
double precision ee1,ee2,ee3,ff1,ff2,ff3
double precision gg1,gg2,gg3,hh3
double precision x0,sq
double precision pi,xmerr,tol,temp,sum0,sumn,summ

```

```

c *****
c *** Parameter definition
c *****

```

```

pi=3.1415926535897932384626433832795
zero=0.0

```

```

tt=90.0
tq=8.5
tk=3.15d-13
cp=0.00249

```

```

rl=0.0001
pl=pi
ql=2.0*pi

```

```

sj=0.0000134
sr=0.93
stp=0.1
sd=0.0000153
sa=2.77

nt=200
nr=100
np=20
nq=20

ni=2000
tol=1.0e-6

dt=0.01
dr=r1/nr
dp=p1/np
dq=q1/nq

dtrr=dt/(dr*dr)
dttrr=dt*dt/(dr*dr)
dtp=dt/(dp*dp)
dtpp=dt*dt/(dp*dp)
dtqq=dt/(dq*dq)
dttqq=dt*dt/(dq*dq)

pc=1.0/cp
ss=4.0*dt*dt*pc*0.94*sj*(1.0-sr)/(stp*sd)
tpc=tk*pc

c *****
c *** Initial condition
c *****

do k=0,nq-1
do j=0,np
do i=0,nr

tn1(i,j,k)=0.0
tn2(i,j,k)=0.0
tn3(i,j,k)=0.0

enddo
enddo
enddo

```

```

c *****
c *** Coefficient definition
c *****

do k=0,nq-1
do j=1,np-1
do i=1,nr-1

    r1=i*i*dr*dr
    r2=(i+0.5)*(i+0.5)*dr*dr
    r3=(i-0.5)*(i-0.5)*dr*dr
    p1=sin(j*dp)
    p2=sin((j+0.5)*dp)
    p3=sin((j-0.5)*dp)

    aal(i,j,k)=2.0*dt*r1*p1*p1+4.0*r1*p1*p1*tq
$           +tpc*dttrr*p1*p1*(r2+r3)+2.0*tpc*tt*dtrr*p1*p1*(r2+r3)
$           +tpc*dtpp*p1*(p2+p3)+2.0*tpc*tt*dtpp*p1*(p2+p3)
$           +2.0*tpc*dttqq+4.0*tpc*tt*dtqq
    bb1(i,j,k)=-tpc*dttrr*p1*p1*r3-2.0*tpc*tt*dtrr*p1*p1*r3
    cc1(i,j,k)=-tpc*dttrr*p1*p1*r2-2.0*tpc*tt*dtrr*p1*p1*r2
    dd1(i,j,k)=-tpc*dtpp*p1*p3-2.0*tpc*tt*dtpp*p1*p3
    ee1(i,j,k)=-tpc*dtpp*p1*p2-2.0*tpc*tt*dtpp*p1*p2
    ff1(i,j,k)=-tpc*dttqq-2.0*tpc*tt*dtqq
    gg1(i,j,k)=-tpc*dttqq-2.0*tpc*tt*dtqq

    aa2(i,j,k)=8*r1*p1*p1*tq-2.0*tpc*dttrr*p1*p1*(r2+r3)
$           -2.0*tpc*dtpp*p1*(p2+p3)-4.0*tpc*dttqq
    bb2(i,j,k)=2.0*tpc*dttrr*p1*p1*r3
    cc2(i,j,k)=2.0*tpc*dttrr*p1*p1*r2
    dd2(i,j,k)=2.0*tpc*dtpp*p1*p3
    ee2(i,j,k)=2.0*tpc*dtpp*p1*p2
    ff2(i,j,k)=2.0*tpc*dttqq
    gg2(i,j,k)=2.0*tpc*dttqq

    aa3(i,j,k)=2.0*dt*r1*p1*p1-4.0*r1*p1*p1*tq
$           -tpc*dttrr*p1*p1*(r2+r3)+2.0*tpc*tt*dtrr*p1*p1*(r2+r3)
$           -tpc*dtpp*p1*(p2+p3)+2.0*tpc*tt*dtpp*p1*(p2+p3)
$           -2.0*tpc*dttqq+4.0*tpc*tt*dtqq
    bb3(i,j,k)=tpc*dttrr*p1*p1*r3-2.0*tpc*tt*dtrr*p1*p1*r3
    cc3(i,j,k)=tpc*dttrr*p1*p1*r2-2.0*tpc*tt*dtrr*p1*p1*r2
    dd3(i,j,k)=tpc*dtpp*p1*p3-2.0*tpc*tt*dtpp*p1*p3
    ee3(i,j,k)=tpc*dtpp*p1*p2-2.0*tpc*tt*dtpp*p1*p2
    ff3(i,j,k)=tpc*dttqq-2.0*tpc*tt*dtqq
    gg3(i,j,k)=tpc*dttqq-2.0*tpc*tt*dtqq

```

```

enddo
enddo
enddo

open(unit=06,file='3d.dat')

c *****
c *** Iteration and calculation
c *****

do n=1,nt
    t=n*dt

c *****
c *** Heat source
c *****

do k=0,nq-1
do j=1,np-1
do i=1,nr-1

    r=r1-i*dr
    r1=i*i*dr*dr
    p1=sin(j*dp)
    cc=r/sd+sa*(t-2.0*stp)*(t-2.0*stp)/(stp*stp)

c *****
c *** Symmetric heat source
c *****

c          sq(i,j,k)=ss*r1*p1*p1*exp(-cc)
c $          *(1.0-2.0*sa*tq*(t-2.0*stp)/(stp*stp))

c *****
c *** Parallel heat source on semi surface
c *****

c          crd=0.0

c          if (j .le. np/2) then
c              crd=cos(j*dp)
c          endif
c          sq(i,j,k)=crd*ss*r1*p1*p1*exp(-cc)
c $          *(1.0-2.0*sa*tq*(t-2.0*stp)/(stp*stp))

c *****

```

```

c   *** Parallel heat source on a portion of the surface
c   ****
c
c       crd=0.0
c
c       if (j .le. np/4) then
c           crd=cos(j*dp)
c       endif
c       sq(i,j,k)=crd*ss*r1*p1*p1*exp(-cc)
$           *(1.0-2.0*sa*tq*(t-2.0*stp)/(stp*stp))
c
c       enddo
c       enddo
c       enddo
c
c   ****
c   *** Solving the linear system
c   ****
c
c       do k=1,nq-2
c       do j=1,np-1
c       do i=1,nr-1
c
c           hh3(i,j,k)=aa3(i,j,k)*tn1(i,j,k)
$           +bb3(i,j,k)*tn1(i-1,j,k)+cc3(i,j,k)*tn1(i+1,j,k)
$           +dd3(i,j,k)*tn1(i,j-1,k)+ee3(i,j,k)*tn1(i,j+1,k)
$           +ff3(i,j,k)*tn1(i,j,k-1)+gg3(i,j,k)*tn1(i,j,k+1)
$           +aa2(i,j,k)*tn2(i,j,k)
$           +bb2(i,j,k)*tn2(i-1,j,k)+cc2(i,j,k)*tn2(i+1,j,k)
$           +dd2(i,j,k)*tn2(i,j-1,k)+ee2(i,j,k)*tn2(i,j+1,k)
$           +ff2(i,j,k)*tn2(i,j,k-1)+gg2(i,j,k)*tn2(i,j,k+1)
$           +sq(i,j,k)
c           x0(i,j,k)=tn2(i,j,k)
c
c       enddo
c       enddo
c       enddo
c
c       do j=1,np-1
c       do i=1,nr-1
c
c           hh3(i,j,0)=aa3(i,j,0)*tn1(i,j,0)
$           +bb3(i,j,0)*tn1(i-1,j,0)+cc3(i,j,0)*tn1(i+1,j,0)
$           +dd3(i,j,0)*tn1(i,j-1,0)+ee3(i,j,0)*tn1(i,j+1,0)
$           +ff3(i,j,0)*tn1(i,j,nq-1)+gg3(i,j,0)*tn1(i,j,1)
$           +aa2(i,j,0)*tn2(i,j,0)

```

```

$      +bb2(i,j,0)*tn2(i-1,j,0)+cc2(i,j,0)*tn2(i+1,j,0)
$      +dd2(i,j,0)*tn2(i,j-1,0)+ee2(i,j,0)*tn2(i,j+1,0)
$      +ff2(i,j,0)*tn2(i,j,nq-1)+gg2(i,j,0)*tn2(i,j,1)
$      +sq(i,j,0)
      hh3(i,j,nq-1)=aa3(i,j,nq-1)*tn1(i,j,nq-1)
$      +bb3(i,j,nq-1)*tn1(i-1,j,nq-1)+cc3(i,j,nq-1)*tn1(i+1,j,nq-1)
$      +dd3(i,j,nq-1)*tn1(i,j-1,nq-1)+ee3(i,j,nq-1)*tn1(i,j+1,nq-1)
$      +ff3(i,j,nq-1)*tn1(i,j,nq-2)+gg3(i,j,nq-1)*tn1(i,j,0)
$      +aa2(i,j,nq-1)*tn2(i,j,nq-1)
$      +bb2(i,j,nq-1)*tn2(i-1,j,nq-1)+cc2(i,j,nq-1)*tn2(i+1,j,nq-1)
$      +dd2(i,j,nq-1)*tn2(i,j-1,nq-1)+ee2(i,j,nq-1)*tn2(i,j+1,nq-1)
$      +ff2(i,j,nq-1)*tn2(i,j,nq-2)+gg2(i,j,nq-1)*tn2(i,j,0)
$      +sq(i,j,nq-1)
      x0(i,j,0)=tn2(i,j,0)
      x0(i,j,nq-1)=tn2(i,j,nq-1)

      enddo
      enddo

c      *****
c      *** Gauss_Seidel iteration
c      *****

      kk=1

      do while (kk.le.ni)

      xmerr=0.0
      do k=1,nq-2
      do j=1,np-1
      do i=1,nr-1

      tn3(i,j,k)=(-bb1(i,j,k)*tn3(i-1,j,k)-cc1(i,j,k)*x0(i+1,j,k)
$      -dd1(i,j,k)*tn3(i,j-1,k)-ee1(i,j,k)*x0(i,j+1,k)
$      -ff1(i,j,k)*tn3(i,j,k-1)-gg1(i,j,k)*x0(i,j,k+1)
$      +hh3(i,j,k))/aa1(i,j,k)

      temp=abs(tn3(i,j,k)-x0(i,j,k))

      if (xmerr.le.temp) then
          xmerr=temp
      endif

      enddo
      enddo
      enddo

```

```

do j=1,np-1
do i=1,nr-1

      tn3(i,j,0)=(-bb1(i,j,0)*tn3(i-1,j,0)-cc1(i,j,0)*x0(i+1,j,0)
$          -dd1(i,j,0)*tn3(i,j-1,0)-ee1(i,j,0)*x0(i,j+1,0)
$          -ff1(i,j,0)*tn3(i,j,nq-1)-gg1(i,j,0)*x0(i,j,1)
$          +hh3(i,j,0))/aa1(i,j,0)

      temp=abs(tn3(i,j,0)-x0(i,j,0))

      if (xmerr.le.temp) then
        xmerr=temp
      endif

      tn3(i,j,nq-1)=(-bb1(i,j,nq-1)*tn3(i-1,j,nq-1)
$          -cc1(i,j,nq-1)*x0(i+1,j,nq-1)
$          -dd1(i,j,nq-1)*tn3(i,j-1,nq-1)
$          -ee1(i,j,nq-1)*x0(i,j+1,nq-1)
$          -ff1(i,j,nq-1)*tn3(i,j,nq-2)-gg1(i,j,nq-1)*x0(i,j,0)
$          +hh3(i,j,nq-1))/aa1(i,j,nq-1)

      temp=abs(tn3(i,j,nq-1)-x0(i,j,nq-1))

      if (xmerr.le.temp) then
        xmerr=temp
      endif

enddo
enddo

do i=1,nr-1

      sum0=0.0
      sumn=0.0

      do k=0,nq-1
        sum0=sum0+tn3(i,1,k)
        sumn=sumn+tn3(i,np-1,k)
      enddo

      do k=0,nq-1
        tn3(i,0,k)=sum0/nq
        tn3(i,np,k)=sumn/nq
      enddo
enddo

```

```

summ=0.0
do k=0,nq-1
do j=0,np
    summ=summ+tn3(1,j,k)
enddo
enddo

do k=0,nq-1
do j=0,np
    tn3(0,j,k)=summ/(nq*(np+1))
enddo
enddo

do k=0,nq-1
do j=0,np
    tn3(nr,j,k)=tn3(nr-1,j,k)
enddo
enddo

if (xmerr.le.tol) then
    goto 100
endif

do k=0,nq-1
do j=0,np
do i=0,nr
    x0(i,j,k)=tn3(i,j,k)
enddo
enddo
enddo

kk=kk+1
enddo

write (6,112)
112 format ('can not get result')
goto 110

100 ppp=0.0

c *****
c *** Output the temperature at the top point on the surface
c *****

c write (6,13) t, tn3(nr,0,0)

```

```

13  format(e14.4,2x,e14.4)

c  *****
c  *** Output the temperature along r-axis
c  *****

c  if (n.eq.19) then

c  write (6,30)
c 30  format ("TITLE = "3D Micro-Sphere Temperature in a line")
c  write (6,31)
c 31  format ("VARIABLES = "X", "Temperature")

c  write (6,32) 2*nr+2
c 32  format ('ZONE T="t=0.2ps", I=', I5)
c  do i=0,nr
c      write (6,13) -(nr-i)*dr, tn3(nr-i,0,0)
c  enddo
c  do i=0,nr
c      write (6,13) i*dr, tn3(i,np,0)
c  enddo
c  endif

c  if (n.eq.24) then
c  write (6,33) 2*nr+2
c 33  format ('ZONE T="t=0.25ps", I=', I5)
c  do i=0,nr
c      write (6,13) -(nr-i)*dr, tn3(nr-i,0,0)
c  enddo
c  do i=0,nr
c      write (6,13) i*dr, tn3(i,np,0)
c  enddo
c  endif

c  if (n.eq.49) then
c  write (6,34) 2*nr+2
c 34  format ('ZONE T="t=0.5ps", I=', I5)
c  do i=0,nr
c      write (6,13) -(nr-i)*dr, tn3(nr-i,0,0)
c  enddo
c  do i=0,nr
c      write (6,13) i*dr, tn3(i,np,0)
c  enddo
c  endif

c  if (n.eq.99) then

```

```

c      write (6,35) 2*nr+2
c 35   format ('ZONE T="t=1ps", I=', I5)
c      do i=0,nr
c          write (6,13) -(nr-i)*dr, tn3(nr-i,0,0)
c      enddo
c      do i=0,nr
c          write (6,13) i*dr, tn3(i,np,0)
c      enddo
c      endif

c      if (n.eq.199) then
c          write (6,36) 2*nr+2
c 36   format ('ZONE T="t=2ps", I=', I5)
c      do i=0,nr
c          write (6,13) -(nr-i)*dr, tn3(nr-i,0,0)
c      enddo
c      do i=0,nr
c          write (6,13) i*dr, tn3(i,np,0)
c      enddo
c      endif

c      *****
c      *** Output the temperature distribution in the cross-section
c      *****

      if(n.eq.nt-1) then
      write (6,101)
101   format ('TITLE = "3D Contour"')
      write (6,102)
102   format ('VARIABLES = "X", "Y", "Temperature"')
      write (6,103) nr+1, np+np+2
103   format ('ZONE I=', I5, 2X, 'J=', I5, 2X, 'F=POINT')

      do j=0,np
      do i=0,nr
          write (6,19) i*dr*sin(j*dp), i*dr*cos(j*dp), tn3(i,j,nq/4)
      enddo
      enddo

      do j=np,0,-1
      do i=0,nr
          write (6,19) -i*dr*sin(j*dp), i*dr*cos(j*dp), tn3(i,j,nq/4*3)
      enddo
      enddo

      endif

```

```
19  format(3e14.4)

    do k=0,nq-1
    do j=0,np
    do i=0,nr
        tn1(i,j,k)=tn2(i,j,k)
        tn2(i,j,k)=tn3(i,j,k)
    enddo
    enddo
    enddo

    enddo

110 end
```

REFERENCES

- [Al-Nimr 2000] M. K. Al-Nimr and V. S. Arpaci, "The thermal behavior of thin metal films in the hyperbolic two-step model", *International Journal of Heat and Mass Transfer*, Vol. 43, (2000), pp. 2021-2028.
- [Anisimov 1974] S. I. Anisimov, B. L. Kapeliovich, and T. L. Perel'man, "Electron emission from metal surface exposed to ultra-short laser pulse", *Soviet Physics JETP*, Vol. 39, (1974), pp. 375-377.
- [Antaki 1998] P. Antaki, "Solution for non-Fourier dual phase lag heat conduction in a semi-infinite slab with surface heat flux", *International Journal of Heat and Mass Transfer*, Vol. 41, (1998), pp. 2253-2258.
- [Brorson 1990] S. D. Brorson, J. G. Fujimoto, and E. P. Ippen, "Femtosecond electron heat-transport dynamics in thin gold film", *Physical Review Letters*, Vol. 59, (1987), pp. 1962-1965.
- [Brorson 1990] S. D. Brorson, A. Kazeroonian, J. S. Moodera, D. W. Face, T. K. Cheng, E. P. Ippen, M. S. Dresselhaus and G. Dresselhaus, "Femtosecond room temperature measurement of the electron-phonon coupling constant in metallic superconductors", *Physical Review Letters*, Vol. 64, (1990), pp. 2172-2175.
- [Cattaneo 1958] C. Cattaneo, "A form of heat conduction equation which eliminates the paradox of instantaneous propagation", *Compte Rendus*, Vol. 247, (1958), pp. 431-433.
- [Chen 2000] J. K. Chen and J. E. Beraun, "Numerical study of ultrashort laser pulse interactions with metal films", *Numerical Heat Transfer, Part A*, Vol. 40, (2000), pp. 1-20.
- [Chester 1963] M. Chester, "Second sound in solids", *Physical Review*, Vol. 131, (1963), pp. 2013-2015
- [Chiffell 1994] R. J. Chiffell, *On the Wave Behavior and Rate Effect of Thermal and Thermomechanical Waves*, M.S. Thesis, University of New Mexico, Albuquerque, NM, 1994.
- [Dai 1999] W. Dai and R. Nassar, "A finite difference scheme for solving the heat transport equation at the microscale", *Numerical Methods for Partial Differential Equations*, Vol. 15, (1999), pp. 697-708.

- [Dai 2000] W. Dai and R. Nassar, "A compact finite difference scheme for solving a three-dimensional heat transport equation in a thin film", *Numerical Methods for Partial Differential Equations*, Vol. 16, (2000), pp. 441-458.
- [Dai 2001a] W. Dai and R. Nassar, "A finite difference scheme for solving a three-dimensional heat transport equation in a thin film with microscale thickness", *International Journal of Numerical Method in Engineering*, Vol. 50, (2001), pp. 1865-1880.
- [Dai 2001b] W. Dai and R. Nassar, "A compact finite difference scheme for solving a one-dimensional heat transport equation at the microscale", *Journal of Computational and Applied Mathematics*, Vol. 130, (2001), pp. 431-441.
- [Duncan 1994] A. B. Duncan and G. P. Peterson, "Review of microscale heat transfer", *ASME Journal of Applied Mechanics Review*, Vol. 47, (1994), pp. 397-428.
- [Elsayed-Ali 1987] H. E. Elsayed-Ali, T. B. Norris, M. A. Pessot, G. A. Mourou, "Time-resolved observation of electron-phonon relaxation in copper", *Physical Review Letters*, Vol. 58, (1987), pp. 1212-1215.
- [Elsayed-Ali 1991] H. E. Elsayed-Ali, "Femtosecond thermorefectivity and thermotransmissivity of polycrystalline and single-crystalline gold films", *Physical Review B*, Vol. 43, (1991), pp. 4488-4491.
- [Groeneveld 1990] R. H. M. Groeneveld, R. Sprik, M. Wittebrood, and A. Lagendijk, "Ultrafast relaxation of electrons probed by surface plasmons at a thin silver film", *Ultrafast Phenomena VII*, Springer, Berlin, (1990), 368-370.
- [Joseph 1989] D. D. Joseph and L. Preziosi, "Heat waves", *Reviews of Modern Physics*, Vol. 61, (1989), pp. 41-73.
- [Joseph 1990] D. D. Joseph and L. Preziosi, "Addendum to the paper on heat waves", *Reviews of Modern Physics*, Vol. 62, (1990), pp. 375-391.
- [Joshi 1993] A. A. Joshi and A. Majumdar, "Transient ballistic and diffusive phonon heat transport in thin films", *Journal of Applied Physics*, Vol 74, (1993), pp 31-39.
- [Kaganov 1957] M. I. Kaganov, I. M. Lifshitz, and M. V. Tanatarov, "Relaxation between electrons and crystalline Lattices", *Soviet Physics JETP*, Vol 4, (1957), pp. 173-178.
- [Kuipers 1969] L. Kuipers and R. Timman, *Handbook of Mathematics*, Pergamon Press, New York, (1969).

- [Lees 1961] M. Lees, "Alternating direction and semi-explicit difference methods for parabolic partial differential equations", *Numerical Mathematics*, Vol. 3, (1961), pp. 398-412.
- [Lees 1996] M. Lees, "A linear three-level difference scheme for quasilinear parabolic equations", *Mathematics of Computation*, Vol. 20, (1966), pp. 516-522.
- [Lin 1997] C. K. Lin, C. C. Hwang and Y. P. Chang, "The unsteady solution of a unified heat conduction equation", *International Journal of Heat and Mass Transfer*, Vol. 40, (1997), pp. 1716-1719.
- [Özisik 1994] M. N. Özisik and D. Y. Tzou, "On the wave theory in heat conduction", *ASME Journal of Heat Transfer*, Vol. 116, (1994), pp. 526-535.
- [Qui 1992] T. Q. Qiu and C. L. Tien, "Short-pulse laser heating on metals", *International Journal of Heat and Mass Transfer*, Vol. 35, (1992), pp. 719-726.
- [Qiu 1993] T. Q. Qiu and C. L. Tien, "Heat transfer mechanisms during short-pulse laser heating of metals", *ASME Journal of Heat Transfer*, Vol. 115, (1993), pp. 835-841.
- [Qiu 1994] T. Q. Qiu and C. L. Tien, "Femtosecond laser heating of multi-layered metals-I. analysis", *International Journal of Heat and Mass Transfer*, Vol. 37, (1994), pp. 2789-2797.
- [Tien 1994] C. L. Tien and G. Chen, "Challenges in microscale conductive and radiative heat transfer", *ASME Journal of Heat Transfer*, Vol. 116, (1994), pp. 799-807
- [Tang 1999] D. W. Tang and N. Araki, "Wavy, wavelike, diffusive thermal responses of finite rigid slabs to high-speed heating of laser-pulses", *International Journal of Heat and Mass Transfer*, Vol. 42, (1999), pp. 855-860.
- [Tzou 1989a] D. Y. Tzou, "On the thermal shock wave induced by a moving heat source", *ASME Journal of Heat Transfer*, Vol. 111, (1989), pp. 232-238.
- [Tzou 1989b] D. Y. Tzou, "Shock wave formation around a moving heat source in a solid with finite speed of heat propagation", *International Journal of Heat and Mass Transfer*, Vol. 32, (1989), pp. 1979-1987.
- [Tzou 1990a] D. Y. Tzou, "Thermal shock waves induced by a moving crack", *ASME Journal of Heat Transfer*, Vol. 112, (1990), pp.21-27.
- [Tzou 1990b] D. Y. Tzou, "Thermal shock waves induced by a moving crack – a heat flux formulation", *International Journal of Heat and Mass Transfer*, Vol. 33, (1990), pp. 877-885.

- [Tzou 1991a] D. Y. Tzou, "The resonance phenomenon in thermal waves", *International Journal of Engineering Sciences*, Vol. 29, (1991), pp. 1167-1177.
- [Tzou 1991b] D. Y. Tzou, "Resonance of thermal waves under frequency excitations", *ASME HTD*, Vol. 173, (1991), pp. 11-27.
- [Tzou 1992a] D. Y. Tzou, "Thermal shock phenomena under high-rate response in solids", *Annual Review of Heat Transfer*, Hemisphere Publishing Inc., Washington, D.C., (1992), pp. 111-185.
- [Tzou 1992b] D. Y. Tzou, "Thermal resonance under frequency excitations", *ASME Journal of Heat Transfer*, Vol. 114, (1992), pp. 310-316.
- [Tzou 1992c] D. Y. Tzou, "Damping and resonance phenomena of thermal waves", *ASME Journal of Applied Mechanics*, Vol. 59, (1992), pp. 862-867.
- [Tzou 1995a] D. Y. Tzou, "A unified field approach for heat conduction from micro- to macro-scale", *ASME Journal of Heat Transfer*, Vol. 117, (1995), pp. 8-16.
- [Tzou 1995b] D. Y. Tzou, "The generalized lagging response in small-scale and high-rate heating", *International Journal of Heat and Mass Transfer*, Vol. 38, (1995), pp. 3231-3240.
- [Tzou 1995c] D. Y. Tzou, "Experimental support for the lagging response in heat propagation", *AIAA Journal of Thermophysics and Heat Transfer*, Vol. 9, (1995), pp. 686-693.
- [Tzou 1995d] D. Y. Tzou and Y. S. Zhang, "An analytic study on the fast-transient process in small scales", *International Journal of Engineering and Science*. Vol. 33 (1995), pp. 1449-1463.
- [Tzou 1996] D. Y. Tzou, *Macro- To Micro Heat Transfer- The Lagging Behavior*, Taylor & Francis, Washington, DC, (1996).
- [Tzou 2001] D. Y. Tzou and K. S. Chiu, "Temperature-dependent thermal lagging in ultrafast laser heating", *International Journal of Heat and Mass Transfer*, Vol. 44, (2001), pp. 1725-1734.
- [Vernotte 1958] P. Vernotte, "Les paradoxes de la theorie continue de lequation de la chaleur", *Compte Rendus*, Vol. 246, (1958), pp. 3154-3155.
- [Vernotte 1961] P. Vernotte, "Some possible complication in the phenomena of thermal conduction", *Compte Rendus*, Vol. 252, (1961), pp. 2190-2191.
- [Wang 2000] L. Wang and X. Zhou, "Dual-Phase-Lagging Heat Conduction", *Shandong University Press*, Jinan, 2000.

[Wang 2001] L. Wang, M. Xu and X. Zhou, “Well-posedness and solution structure of dual-phase-lagging heat conduction”, *International Journal of Heat and Mass Transfer*, Vol. 44, (2001) pp. 1659-1669.

[Wang 2002] L. Wang and M. Xu, “Well-posedness of dual-phase-lagging heat conduction equation: higher dimensions”, *International Journal of Heat and Mass Transfer*, Vol. 45, (2002), pp. 1165-1171.